Synthesis and Performance Analysis of Ammonium Dinitramide

Asad Rahman

(MSc Chem. Eng.)

Thesis Submitted to The University of Nottingham for Degree of Doctor of Philosophy

ACKNOWLEDGMENTS:

I would like to thank my supervisor Dr. Chin Jitkai and Dr. Khiew Poi Sim for giving me the opportunity to work on this project. I really appreciate the cooperation of Dr. Chin Jitkai, for his guidance, advice and technical expertise, which made the foundation of this thesis. Thank you for always being there to guide throughout the very interesting journey of my life.

I am also thankful to the University of Nottingham for the Dean's Scholarship award, which provided the funding for my PhD studies, as well as the technical support for my experiments. I am also thankful to Mr. Faizal, Mr. Andrew, Ms. Filzah, Ms. Fatihah, Mr. Bob and Ms. Farah for their help and continued patience, especially for allowing to use wet chemistry lab as my second home throughout these 3 years.

I am thankful to Allah Almighty for His blessings, parents for believing in me and my wife Anum, and all my friends for being patient and encouraging.

ABSTRACT:

Ammonium dinitramide as non-corrosive, high performance, and Eco-friendly propellant was first synthesized by Russians in early 1970s, and then independently in early 1990s by Stanford Research International. Since then, there has been increased interest in its synthesis and performance analysis. Therefore, this project was aimed to enhance the study of ADN and explore new areas of its application. This project has 3 objectives where syntheses, prilling, electrolysis of ADN were studied.

In first objective, a new, modified ADN synthesis method was developed. This method was able to synthesize ADN at near-zero temperature by nitration of potassium sulfamate with mixture of nitric acid, sulfuric acid and trifluoroacetic acid. Once synthesized, parametric studies were performed to increase the reaction yield. It was developed by analyzing the existing ADN synthesis methods and their reaction mechanisms.

In the second objective, ADN prilling and sonication was performed via ultrasound treatment and the results were compared with ADN obtained by existing methods. It was necessary to perform prilling i.e. conversion of ADN crystal morphology because, ADN in its raw form have long needle like structure. Secondly, it has low critical humidity level of ADN i.e. 55.2%RH renders practical and handling issue in humid climate. Therefore, an ultrasound based prilling and coating method was developed, where ADN was sonicated in toluene as sonication medium along with surfactants and coating polymers. With this method, it was possible to combine prilling and coating of ADN particles into single step with results comparable to conventional melt prilling method.

In third objective, ADN based liquid monopropellant named FLP-103 was electrolytically decomposed and its performance was analyzed in micro thrusters. In order to decompose ADN by electrolysis, Micro thrusters were fabricated with Polydimethyl siloxane (PDMS) and the experiments were analyzed by video footage, load cell thrust measurement and self-fabricated thrust measurement system. The thrusters were fabricated using

combination of embossing and engraving techniques with PDMS to eliminate leakages and backpressure. Thrust measurement system, based on PDMS made torsion rod was developed as a proof of concept by using low cost sensors LDC-1000 from Texas instruments. Its results were compared with the results obtained by load cell thrust measurement. The results showed that ADN can be successfully decomposed via electrolysis in micro thrusters and electrolysis occurs predominately at cathode.

Synthesis and Performance Analysis of Ammonium Dinitramide

TABLE OF CONTENT

LIST OF FIGURES:

LIST OF TABLES:

LIST OF ABBREVIATIONS:

ADN: Ammonium Dinitramide

CTAB: Citryl Tetramethyl Ammonium Bromide

KDN: Potassium Dinitramide

FLP-103: Name of the fuel based on ADN

TMD: Theoretical Mean Density

TMS: Thrust Measurement System

AS: Ammonium Sulfamate

KS: Potassium Sulfamate

NA: Nitric Acid

SA: Sulfuric Acid

TFA: Trifluoroacetic Acid

NTFB: Nitronium Tetrafluoroborate

AP: Ammonium Perchlorate

RDX: Research Department Formula X (IUPAC name: 1,3,5-Trinitroperhydro-1,3,5-triazine)

PDMS: Polydimethyl siloxane

HTPB: Hydroxyl Terminated Polybutadiene

PS: Polystyrene

TDI: Toulene Diisocyanate

Isp: Specific impulse

K-TFA: Potassium salt of trifluoroacetic acid

KNO3: Potassium nitrate

CLF: Chloroform

Chapter 1. **Overview**

The synthesis and development of ammonium dinitramide (ADN) salt was a result of continuous interest of researchers since 1950's to obtain energetic materials with higher performance attributes than existing hydrazine and perchlorate based propellants. The research was mainly focused on organic nitro and poly nitro groups, attached to carbon atoms, but there were problems associated with compound having central carbons, first, low stability due to steric hindrance, and secondly possibility of nucleophilic attack on central carbon.

The solution to these problems was suggested to create an anionic center in the molecule which can protect two nitronium groups attached to it, i.e. $N(NO_2)_2$ attached to a cationic part, which could be changed to increase stability (Luk'yanov, et al., 1994). Dinitramide ions are similar to nitramides and nitramines, which are unstable in acidic medium due to high anionic charge, and have low energy of formation because of delocalized charge.

In order to synthesize ADN, N,N-dinitro-β-aminopropionitrile, $(NO_2)_2NCH_2CH_2$type molecules for the purpose was selected (Luk'yanov, et al., 1994), where X is a cationic ions which is able to attract electrons from other compounds, and hence facilitates the creation of nucleophilic center at the dinitramide portion, which could be isolated. However, the direction of reaction depends on type of group X. From Figure 1-1, it can be observed that the desired product yield is dependent on electron withdrawing strength of the cationic part in the presence of electron donors.

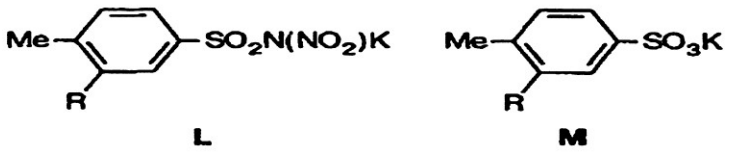

L M

Run	X	R	Yield (%)	
			L	M
1	COMe	H	93	—
2	COMe	NO_2	73	—
3	CHO	NO_2	43	32
4	CN	NO_2	6	82

Figure 1-1 The reactivity and yield is dependent on the stregnth cation. (Luk'yanov, et al., 1994)

ADN in its generic form have long needle shaped morphology, which hinders the higher solid loading (Larson & Wingborg, 2011). Therefore, it is of utmost importance to alter its crystal morphology into low aspect ratio octagonal or spherical shapes. Secondly, the low critical humidity level of ADN i.e. 52%RH renders it unusable in humid climate hence encapsulation with hydrophobic polymer is necessary.

The raw crystal morphology of ADN is unsuitable for application as propellant in both solid grain and melt casting method. Furthermore, the higher hydrophilicity of ADN than AP necessitates encapsulation of processed crystals (Ostmark, et al., 2000). All these factors contribute in reduction of maximum theoretical mean density (TMD) of the solid grain of ADN.

Many methods have been utilized for alteration of particle morphology of energetic materials such as ultrasound assisted crystallization (Bayat & Zeynali, 2011), melt prilling (Heintz, et al., 2009), solvent crystallization (Fuhr, 2008), and spray crystallization (Teipel, 1999). The importance of optimized crystal morphology can be highlighted by its ability to enhance specific impulse by 30% to 50% (Larson & Wingborg, 2011). Modification of crystal morphology by ultrasound for CL-20 has been reported by (Bayat & Zeynali, 2011) and for RDX by (Kim, et al., 2011), but not for ADN. Although ultrasound treatment could induce oxidation reactions for many substrates as reported by (Kuppa & Moholkar, 2010) and (Malani, et al.,

2013). Nevertheless, ADN does not undergo decomposition or oxidative reactions in absence of base (Qadir, et al., 2003).

Electrolytic decomposition of ionic liquid propellant, such as hydroxyl ammonium nitrate (HAN), was reported by (Wu & Yetter, 2009). However, it has not been reported for any other propellants thus far. Furthermore, there are no reports of ADN usage in micro thrusters. Therefore, in this study, electrolytic decomposition and performance in micro thrusters was extended to ADN based liquid monopropellants. Although spark and resistive ignition of ADN monopropellants was reported by (Larson, et al., 2005), it was slightly different from the electrolysis, as it employed ultra-high voltage and current to produce detonation, rather than gradual decomposition which is required by propellants. In order to conduct experiments for electrolytic decomposition, PDMS based Micro thrusters and open chambers were employed to initiate decomposition of ADN based liquid fuel in it. And, the thrust generated by these micro thrusters was detected by load cells, and self-fabricated thrust measurement system. The results from these two thrust detection systems were also compared, and the propagation of electrolysis was also analyzed.

1.1 Project scope

There were 3 main proposed objectives for the project:

1. Improvement in ADN synthesis method where it could be synthesized at near zero temperature using easily available chemicals and raw materials.
2. Modification of ADN crystal morphology and polymeric coating to produce spherical particles with reduced hygroscopicity.
3. Analysis of ADN based liquid monopropellant under electrolytic decomposition and its performance as a fuel in micro thrusters.

1.2 Project outline

1.2.1 Improved ADN synthesis methods:

Although there are several methods available for ADN synthesis, it employed expensive nitronium salts, or used ultra-low temperature reaction conditions that make it infeasible for large-scale production. In ADN synthesis, the most important step is synthesis of dinitramide anion, which can attach to different cations by ion exchange reactions immediately after synthesis. Therefore, in this project, attempts to produce ADN using different approaches and chemical routes to achieve ADN synthesis were carried out with aim of either the reaction has higher yield, i.e> 50-60% or at least increase the reaction temperature to near zero level, which could be feasible for large-scale production. The attempts including nitration of calcium sulfamate, sodium sulfamate, potassium sulfamate, nitro urea, and urea nitrate. Furthermore, several compositions of nitrating acid mixture were tested. Ultimately, addition of trifluoroacetic acid in nitrating acid mixture for nitration of potassium sulfamate was found to yield trace amounts i.e. 1-2wt. % of KDN, which is an important intermediate product for ADN synthesis. Therefore, further efforts to develop new synthesis method were focused in this method, and several optimization runs were performed, including different acid compositions, reaction mediums, reaction time and catalysts. By the end of this project, KDN yield was increased up to 5wt. % with use of powdered silica gel as catalyst. Detailed discussion on ADN synthesis method is presented in Chapter 3.

1.2.2 Modification of ADN crystal morphology and polymeric encapsulation:

Two major methods have been reported for alteration of ADN crystal, and both employs melting of ADN during the process. In melt-prilling, ADN was melted in hot paraffin oil under agitation to obtain spherical particles, and in Spray-prilling, molten ADN was sprayed through nozzles into cooling chambers to obtain spherical particles. However, ADN has been reported to degrade via decomposition in molten phase (Andreev, et al., 2000). Therefore, in this project, alternate method has been proposed which not only operates at lower temperature to avoid ADN melting, but combines polymeric coating into a single step process.

In this series of experiments, the crystal morphology modification and Polymeric coating of ADN was performed. ADN used in these experiments was synthesized in-house by nitration of potassium sulfamate by sulfuric acid catalyzed nitric acid at -45^{o}C (Nazeri, et al., 2008). The polymeric coating of ADN requires completely dry ADN, which is impossible in humid Malaysian environment because average relative humidity is always above 80%RH, where as critical humidity limit of ADN is 55.2%RH. It was possible to dry ADN in dry chambers but it will start absorbing moisture during experimental conditions. Therefore, a method which can combine both crystal morphology modification and polymeric encapsulation into a single step process was investigated. Furthermore, ADN is prone to super cooling, where it exists in liquid phase below freezing point, which ruled out improvement in melt prilling method. However, melt prilling was performed few times to obtain melt prilled ADN samples for comparison purposes (Teipel, et al., 2000).

Therefore, application of ultrasound was investigated on ADN, and subsequent processing method was developed and presented in Chapter 4.

1.2.3 Electrolytic decomposition of ADN based liquid monopropellant:

Electrolytic decomposition of FLP-103, an ADN-based liquid monopropellant was investigated. The decomposition phenomenon was investigated by video footages and by thrust measurement via load cell and dedicated thrust measurement system (TMS).

Thrust measurement stand (TMS) was developed as prove of concept for low cost, yet sensitive thrust measurement system to detect micro newton forces generated by micro thrusters. These systems are important for performance analysis of propellants. There are several methods of TMS fabrication and calibration, as discussed in later sections. Among them, torsion rod offers ease of fabrication, calibration, and it could be used with different types of sensors, hence offering wide range of possibilities (Chen & Pan, 2011; Huh & Sejin, 2014; Koizumi, et al., 2004; Yan, et al., 2009). The TMS fabricated and calibrated in these experiments consisted of polydimethyl siloxane (PDMS)

based torsion rod of 6mm diameter, and 26cm long aluminum plate. Two opposite magnets were attached to one side of the aluminum plate to exert restoring force, and to maintain the center position of the aluminum plate with respect to induction sensor. The other side of the aluminum plate acts as receiver of force applied by the Micro thruster. It was calibrated by attaching a string and the string was bent 90° by a sliding pulley. One the other end of the string, a small tray was hanged, where pre-weighted aluminum chips were added as idle weights to calibrate the system by detecting deflection of aluminum plate per milligram weight. The results showed that the TMS was capable of successfully detecting micro newton force generated by micro thrusters.

Micro thrusters employed for thrust measurement experiments were built by PDMS. The design of Micro thrusters was optimized to reduce backpressure by incorporating different channel widths and 6, 90° bents. In addition, fuel leakage was eliminated by making a combination of engraved and embossed design, which fitted into each other to offer lateral support around fuel lines and combustion chamber. Analysis of electrolysis of FLP-103 revealed that the decomposition process initiated in liquid phase and proceeded predominately at cathode, with almost no activity at anode terminal. The details of electrolytic decomposition of FLP-103 are given in Chapter 5.

Chapter 2. **Literature review**

2.1 Introduction:

In this chapter, review of ADN synthesis, nitration methods, polymer coating, electrolytic decomposition, and thrust measurement systems in given in detail. This chapter is subdivided into 4 sections, each for ADN synthesis, polymeric coating and prilling, electrolytic decomposition and thrust measurement stand.

2.2 Nitration reactions:

Nitration reaction is one of the oldest reactions known to alchemist as early as 17th century, where picric acid was obtained by reacting nitric acid with wool and silk (Urbanski, 1964). In 1833, Branconnot obtained nitric esters cellulose and starch by reacting nitric acid with plant fibers and starch at low temperatures. In 1834, benzene was nitrated to nitrobenzene. Currently nitration is the most widely applied substitution reaction. Nitration proceeds by three mechanisms (Figure 2-1) , as direct nitration or introduction of nitro group into unsaturated compound having double bonds or by indirect methods consisting of single and double substitution reactions (Urbanski, 1964).

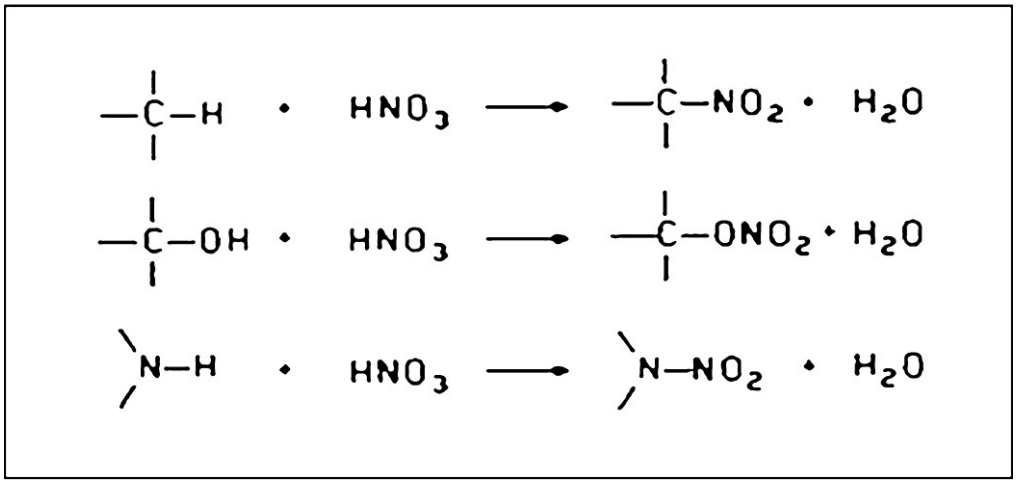

Figure 2-1 Examples of Direct Nitration, O-Nitration and C-nitration respectively. (Olah, et al., 1988)

Nitrating agents are often consisting of mixture of two compounds, the source of nitro group and catalyst for generation of nitro groups. However, stable nitronium salts like nitronium tetra fluoroborate (NTFB) and di-nitrogen

pentoxides were used in direct nitration of both organic and inorganic compounds in inert reaction mediums (Olah, et al., 1982). The selection of suitable nitration catalyst or solvent had been divided into two types: fast and slow, by Hughes, Ingold and Reed (Tedder, 1955). The slow category consists of catalysts like dioxane, acetic acid, acetonitrile, nitromethane, and acetic anhydride. The fast category consists of sulfuric acid, trifluoroacetic acid, super-acids and magic acids, like 1:1 mixture of antimony penta fluoride and fluorosulfuric acid by (Olah, et al., 1982).

Nitration with respect to structure and attachment of nitro group is classified as C-nitration, where the nitro group attaches to the main carbon chain, as it happens in tri-nitro-toluene (TNT). N-nitration, where nitro group attaches to activated or deactivated amides or imide groups of the substrate as in ammonium dinitramide, and lastly O-nitration, where nitro group attaches to oxygen atom of the substrate as it happens in nitro-glycerol or nitro-cellulose (Olah & Squire, 1991).

The nitration reactions are further divided as ionic, radical and free radical reactions, which mostly depends on the type of nitrating agent used and the type of nitro-group generated by nitrating mixture (Olah, et al., 1989).

2.2.1 Ionic nitration:

In ionic nitration, there are two types of reaction propagation, electrophilic nitration reactions consisting of nitronium ions, and nucleophilic nitration reactions consisting of displacement reactions of nitrite ions with suitable leaving groups (Olah, et al., 1988).

2.2.2 Protic acid catalyzed nitration:

This reaction, also known as electrophilic nitration reactions, in which nitrating agent consists of nitric acid or its derivatives, with acid catalyst which may comprise of sulfuric acid or other strong acids where nitronium ions (NO_2^+) was generated as the primary reactive agent. The general formula as $NO_2 - X$; where X was nucleophile and its electronegativity is considered directly proportional to the strength of reactive nitrating agent, and it was

defined as $NO_2 - {}^{+}OH_2 > NO_2 - Cl > NO_2 - NO_3 > NO_2 - O(CO)CH_3 > NO_2 - OH > NO_2 - OCH_3$ (Olah & Squire, 1991). In this reaction, the electron deficiency of anionic part of the molecule plays an important role. Moreover, the concentration and chemical purity of the system increases the yield of final product. In nitric acid-sulfuric acid nitrating system, the strength, and the reactivity of the system decreases with time due to formation of water molecules during the reaction between sulfuric acid and nitric acid. Over the years, several nitrating system based on Protic acids have been reported in literature (Olah, et al., 1989), but their effectiveness was only confined to particular type of compounds. (Olah, et al., 1989) Suggested the use of fluorosulfuric acid and nitric acid to eliminate the problem of water generation, because the water produced reacts with fluorosulfuric acid to yield sulfuric acid and hydrogen fluoride. The nitrating system suggested by (Olah, et al., 1989) is efficient in number of highly unreactive species including deactivated aromatics.

2.2.3 Nitric acid and sulfuric acid:

Nitration by mixture of nitric acid and sulfuric was by far the most commonly used nitrating system, due to its high reactivity, wide application, isomer control and most importantly industrial availability of the nitrating agent. There are several factors, which affect the efficiency of nitrating mixture, including acid composition, temperature, and excess of nitric acid. The composition of nitrating agent plays a significant role because concentration of nitric acid was often used in slight excess in order to maintain system reactivity. In selection of acid composition, another significant aspect that should be considered was formation of water molecules during acid catalysis of nitric acid (Urbanski, 1964), which as a result decreases reactivity and concentration of nitronium ions via dilution. The concentration of nitronium ions was not only dependent on the concentration of nitric acid, but also the temperature and concentration of sulfuric acid (Ross, et al., 1983). The nitronium ion concentration increases with the concentration of sulfuric acid and decrease in temperature. At above 93wt. % concentration level, sulfuric acid can convert the nitric acid completely into nitronium ions. The use of

oleum is limited to highly deactivated substrates; otherwise, it can cause sulfonation and oxidation of reactive substrates (Olah, et al., 1988).

2.2.4 Nitric acid and triflouroacetic acid:

Trifluoroacetic acid is much stronger acid than acetic acid and can be used as an acid catalyst, although its usage is limited to few reactions, it promotes the generation of nitronium ions by first forming trifluroacetyl nitrate which then gives nitronium ions (Olah, et al., 1988).

$$CF_3(CO)_2OH + HNO_3 \xrightarrow{WATER} NO_2^+CF_3CO_2^- \leftrightarrow \quad CF_3CO(O)NO_2$$

Another worth mentioning nitrating mixture consists of trifluoroacetic acid anhydrate and ammonium nitrate. Trifluoroacetic acid has been known to be 1000 times stronger than acetic acid, and comparable to nitric acid. Due to the presence of fluorine in its structure, it acts as a strong electrophile, and acts as condensing agent for several aromatic reactions (Tedder, 1955). Another nitrating mixture consists of trifluoroacetic acid and nitrate salt (Olah & Squire, 1991). In this combination, nitration depends on the solubility of nitrate salt. Therefore, ammonium nitrate having good solubility in a number of solvents, gives successful results. The propagation of nitrating system was given as:

$$CF_3(CO)_2O + NH_4NO_3 \xrightarrow{yields} CF_3C(O)ONO_2 + CF_3C(O)ONH_4$$

$$CF_3C(O)ONO_2 \xrightarrow{yields} NO_2^+ + CF_3COO^-$$

Trifluoroacetic acid catalyzed nitrating in combination with transition metal nitrates was used for nitration of activated aromatics (Olah, et al., 1988).

2.2.5 Safety considerations:

The chemistry of nitration consists of hazardous materials, and requires extreme caution while performing them in order to prevent accident, for example spilling of chemicals, skin, and eye contact with the chemicals, inhalation of fumes and accidental fire or explosion (Liu, 2014).

In case of ADN synthesis, all the above scenarios are possible but can be avoided by using proper personnel safety equipment, performing experiments in enclosed fume hood and most importantly good laboratory practices. During Prilling process, molten ADN is considered one of the most dangerous steps due to instability of ADN in molten state, but it can be taken care of by using open vessels to avoid pressure built-up and proper temperature control methods. The storage of the chemicals used should be according the protocols and synthesized samples of ADN do not possess any danger under normal lab conditions due to stable nature, which increases manifold in misty environment, which also eliminates the static charge ignition issue. ADN in its generic form is very stable compound, it can only be detonated under extreme conditions, which includes critical mass diameter of 25mm under highly dense conditions, and even after that requires high activation energy (Ostmark, et al., 2002). In case of explosion, its detonation velocity is very low hence less danger (Larson & Wingborg, 2011). In addition, storage of ADN should be done in light body materials to avoid pressure built-up due to any accidental condition, which will eliminate the danger.

During the course of experiments, the nitration step is considered to be the most hazardous because of liberation of toxic fumes, use of very low temperature, and heat evolved during neutralization process which if not controlled properly could lead to exothermic decomposition of reaction mixture and generate large amount toxic dark brown NO_2 fumes.

According material safety data, inhalation or digestion of ADN can cause irritation to mucous membrane of respiratory organ, blood damage (anaemia) and epileptic convulsions and unconscious, LD50 (oral rat) is 823mg/kg, and LD50 (dermal rabbit) is greater than 2000mg/kg. However, ADN is to be non-carcinogenic and noncorrosive. It is also nonirritant to skin (Larson & Wingborg, 2011).

2.3 Reaction mechanisms of ADN synthesis:

According to (Luk'yanov, et al., 1994), dinitramide anions (DNA) would be instable in acidic medium like nitramides and nitramines. And this hypothesis

lead to assumption that DNA could be synthesized by reaction of N,N dinitramines (Figure 2-2) or nitrosulfamides (Figure 2-3) with bases. This assumption was first tested with nitrosulfamides compound marked as 2 in Figure 2-3 due to safety considerations. In Figure 2-3, the preference of reaction pathway A, which is a precursor to dinitramide salts was depended on the type of molecule at position X.

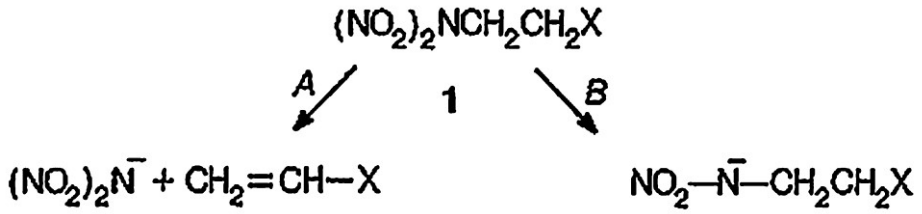

Figure 2-2 The reaction of compound 1 could go in direction of compound A or B, depending on the X. (Luk'yanov, et al., 1994)

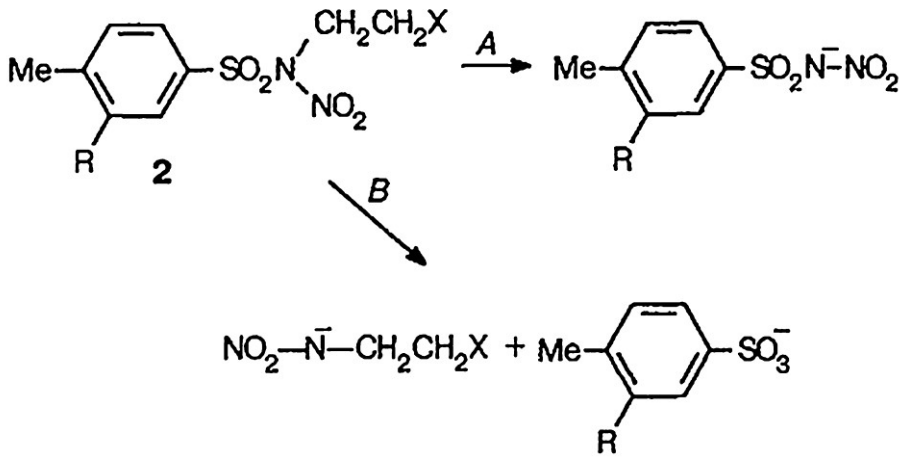

Figure 2-3 Reaction pathway of Nitrosulfamides with bases to form dinitramide precursor (pathaway A). (Luk'yanov, et al., 1994)

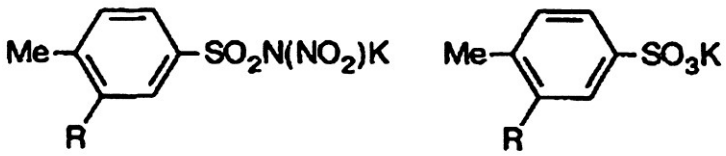

L M

Run	X	R	Yield (%)	
			L	M
1	COMe	H	93	—
2	COMe	NO_2	73	—
3	CHO	NO_2	43	32
4	CN	NO_2	6	82

Figure 2-4 Comparitive Reaction yield of the reaction of compound 2 (as shown previosuly Figure 2-3) with different substituents, which are marked as X and R. (Luk'yanov, et al., 1994)

In Figure 2-4, the results of electrophilicity of sulfur atom of compound 2 (Figure 2-3) are presented, which according to (Luk'yanov, et al., 1994) are more electrophilic then nitrogen atom of compound 1 (Figure 2-2). With the help of this comparative study, it was confirmed that CN group as X is the least reactive and hence safe to perform further reactions of compound 1. The compound 1 was then converted to compound 1a as shown in Figure 2-3, where X=CN, via nitration method. The resultant compound 1a was then reacted with potassium hydroxide in ethanol solution to produce potassium dinitramide (KDN) as shown in equation below (Luk'yanov, et al., 1994). Alternatively, the use of ammonia instead of potassium hydroxide directly gives ADN.

$$(O_2N)_2NCH_2CH_2CN + KOH \rightarrow KN(NO_2)_2 + CH_2 = CH - CN$$

Once the first stable dinitramide salt (KDN) was synthesized, it could be converted to other derivatives of dinitramide, such as ADN.

The reaction of KDN to ADN is straight forward, and is performed by reaction of KDN with ammonium sulfate in water at 40~50ºC followed by filtration to obtain ADN (Nazeri, et al., 2008).

Other derivatives of dinitramide are prepared by conversion of ADN or KDN into dinitramide acid as shown in equation below, where "M" represents cation such as potassium or ammonium (Luk'yanov, et al., 1994).

$$MN(NO_2)_2 + HCl \rightarrow HN(NO_2)_2 + MCl$$

The resultant dinitramide acid ($HN(NO_2)_2$) from equation above is then reacted with suitable base to obtain desired dinitramide salt.

In this work, synthesis method for potassium dinitramide (KDN) which is a stable and important intermediate product for synthesis of ADN is reported. This method utilizes sulfuric acid (SA), nitric acid (NA) and trifluoroacetic acid (TFA). Importance of synthesizing ADN via KDN intermediate has been suggested to give better yields as investigated by (Golofit, et al., 2010) and (Nazeri, et al., 2008). Several dinitramide salt synthesis methods are available in literature. This includes the use of very expensive nitronium salts to mixed acid nitrating agents (Bottaro, et al., 1997; Langlet, et al., 1999). The brief overview of different ADN synthesis method is given in the Table 2-1 below (Langlet, et al., 1999).

Table 2-1 Comparision of different ADN synthesis routes (Venkatachalam, et al., 2004)

S. no.	Starting material	Nitrating agent	Reaction temperature	Yield (wt. %)
1	$Me_3Si(CH_2)_2NCO$	NO_2BF_4 /HNO_3	<0 ºC	25%
2	NH_2NO_2	NO_2BF_4	-20 ºC	60%
		N_2O_5	-20 ºC	<1%
		NO_2HS_2O	-40 ºC	53%
3	NH_4COONH_2	NO_2BF_4	0 ºC	15%
4	NH_3	NO_2BF_4	-78 ºC	25%
		N_2O_5	-78 ºC	15%
		NO_2HS_2O	-78 ºC	15%
5	NH_2COONH_2	NO_2BF_4	-40 ºC	20%
6	$NH_2COOC_2H_5$	N_2O_5	-48 ºC	70%
		NO_2BF_4	-60 ºC	60%
7	$HN(CH_2CH_2COOEt)_2$	NO_2BF_4	<0 ºC	31%
8	$HN(CH_2CH_2CN)_2$	NO_2BF_4	-10 ºC	60%
9	$NH_2SO_3NH_4$	HNO_3 /H_2SO_4	-45 ºC	60%

In dinitramide synthesis, the reaction yield is highly dependent on reactivity of electrophilic and nucleophilic regents. For example, in ADN synthesis by nitration with nitronium salts proposed in (Bottaro, et al., 1997; Suzuki, et al., 1997), yield of ADN ranges from 15wt. % to 90wt. % at -78^{0}C to - 10^{0}C in

10-120 minutes depending on substrate and reaction time. The dependence of yield is due to reactivity of the substrate and the nitrating agent. For example, in nitration of Ammonia by dinitrogen pentaoxide (NO_2NO_3) and by Nitronium tetra fluoroborate (BF_4NO_2) (NTFB) gives 15wt. % and 25wt. % of yield at -78^{0}C and 120 minutes of reaction time respectively (Luk'yanov, et al., 1994; Schmitt, et al., 1994). Similarly, in nitration of Nitramide (NH_2NO_2) by NO_2NO_3 and NTFB, the reaction yield of 60wt. % (Venkatachalam, et al., 2004) and 95wt. % (Bottaro, et al., 1997) obtained respectively. The relatively low yield from NO_2NO_3 is attributed to comparatively low reactivity of NO_2NO_3 as compared to NTFB (Table 2-2). It is because NTFB is stronger nitrating agent as compared to NO_2NO_3, and nitramide is more reactive substrate as compared to ammonia. Comparison of nitration of KS and AS with NA/SA is also shown in Table 2-2, where KS is more reactive as compared to AS.

Table 2-2 Comparision of Ammonia and nitramide nitration by NTFB and NO_2NO_3.

Nitrating Agent	Substrate	Yield (wt.%)
NTFB	Ammonia	25
	Nitramide	90
NO_2NO_3	Ammonia	15
	Nitramide	60
Nitric acid and Sulfuric acid mixture (NA/SA)	Potassium sulfamate (KS)	60
	Ammonium sulfamate (AS)	40

In addition to the strength of nitrating agents, the reaction yield also depend on other reaction parameters for example temperature, reaction time and mixing as discussed by (Golofit, et al., 2010) and (Nazeri, et al., 2008). Among nitrating agents, only NTFB can react with Nitramide to produce dinitramide salts at above -20^{0}C (Venkatachalam, et al., 2004). However, apart from expensive NTFB, synthesis of nitramide salt is a laborious process in which

nitration of urea or sodium sulfamate at -10^{0}C to -15^{0}C is required (Lobanova, et al., 2010).

In nitration of potassium sulfamate, and ammonia sulfamate by mixed acid gives 60wt. % and 40wt. % of yield respectively at -45^{0}C (Nazeri, et al., 2008)(Table 2-2). It suggests that the presence of potassium ion may have increased its reactivity, given that the reaction conditions were reported to be similar for both potassium and ammonium salts of sulfamate (Nazeri, et al., 2008).

2.4 Experimental procedures for Ammonium Dinitramide synthesis:

There are several experimental procedures for synthesis of ADN, which are discussed in this sections in detail. ADN can be synthesized by several methods with varying degree of reaction yield based on starting materials, method, and temperature employed for synthesis. However, majority of methods utilizes expensive nitronium salts as nitrating agents except in nitration of potassium sulfamate, which is performed by mixed acid nitration (Larson & Wingborg, 2011). It is of utmost importance to study the existing methods to understand reaction mechanism behind these synthesis methods, so that, a work on improvement can be performed. Among the synthesis methods, selected few, which has been used for ADN synthesis for research purposes, are discussed in the next sections.

2.4.1 ADN via Nitramide:

ADN is synthesized by nitration of nitramide with mixed acid, NTFB or NO_3NO_2 in inert solvent as medium of reaction. The reaction conditions for this particular method varies widely depending on nitration time, temperature, nitrating agent, ratio of nitrating agent to substrate and inert solvent.

In this procedure, substrate i.e. nitramide was synthesized by nitration of urea (10g) with mixed acid nitrating mixture consisting of oleum (35g) and nitric acid (35g) at 0^{0}C for 40min. After 40min, it is quenched by ice-water mixture (300g) and extracted with ethyl acetate (100ml*4) and conditioned at 20^{0}C for 2hr followed by evaporation in vacuum to obtain 15.5g of nitramide

(Lobanova, et al., 2010). Further purification was performed by dissolution in ether and precipitation with n-hexane (400ml) to obtain precipitate of byproducts, which was filtered and removed. Further purification by mixture of dichloroethane and 2-propanol in 9:1 ratio by part give 13g nitramide (Lobanova, et al., 2010).

Once nitramide was synthesized, it was nitrated by either NTFB, NO_3NO_2 or with nitric acid-sulfuric acid at sub-zero temperatures to produce ADN (Langlet, et al., 1999). Synthesis of dinitramide salts from nitramide by mixed acid nitrating mixture is similar to the nitration of potassium sulfamate (Langlet, et al., 1999). However, Nitration with NTFB or NO_3NO_2 requires organic solvent like methyl cyanide, dichloromethane or ethyl acetate as medium of reaction (Lobanova, et al., 2002).

2.4.2 Free radical nitration:

In this type of reaction, stable free radical compounds of nitronium ions were used, including nitronium tetrafluoroborate (NO_2BF_4)(NTFB) and dinitrogen pentaoxide(NO_2NO_3). They give above average results for many substrates, including ammonia, aromatics, urea derivatives, and other highly unreactive compounds. In these nitrating agents, especially for NTFB, the high reactivity of tetrafluoroborate ion is due to its extremely strong Nucleophillic properties, activating the substrate by nitronium ion.

2.4.2.1 ADN synthesis via nitration of Ammonium salts of N-nitrourethane:

ADN was synthesized by nitration of N'N'-dinitro derivatives of organic amides by NTFB. Ammonium salts of N-nitrourethane was first nitrated by sulfuric acid and potassium nitrate mixture followed by treatment with ammonia to N'N'-dinitro derivative of organic amides, which was then nitrated by NTFB to produce N,N-dinitro-urethane. This N,N-urethane was then converted into ADN by action of ammonia. In this procedure, using methyl cyanide as solvent, the highest reported yield was 74% at -40^{0}C, in reaction time of 25 minutes (Luk'yanov, et al., 1996).

2.4.2.2 ADN synthesis via Nitration of Ammonia:

ADN was synthesized by nitration of ammonia at -78^{0}C by NTFB or NO_3NO_2 (Schmitt, et al., 1994). In this method, nitrating agent NO_3NO_2 (12.3g) was suspended in dichloromethane at -78^{0}C and dry anhydrous ammonia (6g) was bubbled through the suspension in 30min. After bubbling of ammonia, the mixture was agitated for 120min at -78^{0}C to obtain ADN. Reaction yield: 15%.

2.4.2.3 ADN synthesis via nitration of Ethyl Carbamate:

ADN was synthesized by nitration of ethyl carbamate with (NO_3NO_2) at -48^{0}C (Stern, et al., 1998). The procedure starts with preparation of substrate.

The substrate ethyl N-Nitrocarbamae, was prepared by addition of fuming nitric acid, 389.3g into 1135.2g acetic acid anhydrate at 0^{0}C under N_2 environment. It is heated to 25^{0}C in 15minutes and stirred for 30mins. Then cooled down to 0^{0}C followed by addition of 500g ethyl carbamate in 70minutes to avoid temperature raise above 10^{0}C. After stirring for 2 hours at 0^{0}C before heading back to room temperature and subsequently vacuum evaporation to obtain yellow crystals. These crystals are washed with 500ml CCl_4 twice and dried in vacuum. The dried crystals of ethyl N-nitrocarbamate 503g are bubbled with anhydrous ammonia in a mixture 1625ml CH_2Cl_2 and 825ml dry CH_3OH at 9^{0}C under N_2 environment. The mixture is filtered to collect solid particles which are dried in vacuum to obtain 563g ammonium ethyl N-nitrocarbamate as colorless crystals.

After preparation of substrate, nitrating agent consisting of 866.5g nitrogen pentaoxide (N_2O_5) 14.9wt. % in CH_2Cl_2 was prepared. In another mixture containing 164g ammonium ethyl N-nitrocarbamate in 1640ml CH_2Cl_2 was prepared and cooled to -48^{0}C. Both mixtures are combined together without exceeding -35^{0}C under N_2 environment. The end of the reaction is marked with liberation of brown fumes and mixture turns yellow. Now, anhydrous ammonia is bubble through the solution to obtain ADN and ammonium nitrate mixture. ADN can be separated and purified according to purification methods.

2.4.2.4 ADN synthesis via nitration of Nitrourea:

ADN was synthesized by nitration of nitro urea with nitronium tetrafluoroborate at -30^{0}C for 3.5hrs (Suzuki, et al., 1997). In this method, the substrate i.e. Nitro urea was prepared by nitration of urea (14g) by 50g of 33wt.% nitric acid for 10min to obtain water insoluble urea nitrate (23.8g). The dried urea nitrate (23.8g) was very slowly added to sulfuric acid 96wt.% (84ml) at -5~0^{0}C under strong agitation and conditioned for 30min. After conditioning, the mixture was poured into ice-water mixture (300g) to obtain crystals of nitro urea. The crystals were separated by filtration, and washed with very cold water to remove residual sulfuric acid.

The nitro urea (3.8g) was suspended in acetonitrile (80ml) at -30^{0}C and NTFB (6.1g) was added into the suspension. After 3.5hr of conditioning, it was neutralized by dry ammonia to obtain precipitation. The precipitates were collected by filtration and purified by ethyl acetate to obtain ADN crystals (20wt. % yield).

2.4.2.5 ADN synthesis via nitration of ammonium N-nitoethane:

ADN was synthesized by nitration of N-nitroethane derivatives with dinitrogen pentaoxide (NO_3NO_2) at -78^{0}C (Schmitt, et al., 1995). Several substrates have been reported in the patent (Schmitt, et al., 1995) for the synthesis of ADN. Among one of the method, nitration of ammonium N-nitoethane was carried out by freshly synthesized dinitrogen pentaoxide (NO_3NO_2). It was prepared by ozone treatment of (N_2O_4) at -78^{0}C in dichloromethane until the solution turns blue and temperature reaches -30^{0}C. In another beaker, ammonium N-nitroethane was suspended in dichloromethane (200ml) and cooled down to -50^{0}C. Now both mixtures were combined and stirred for 1hr and its temperature was increased to 30^{0}C. Once the temperature was 30^{0}C, ammonia gas was passed through the solution until pH 10 was reached. The solution was then purified by filtration and followed by addition of acetonitrile and second filtration. ADN was then precipitated by addition of chloroform ($CHCl_3$) to obtain 60wt. % yield.

2.4.3 Nucleophilic Nitration:

This type of nitration occurs by displacement of suitable leaving group by nitrite ions. In the synthesis of ADN by this method, the byproducts were often consists of nitrites if the temperature control was inadequate.

2.4.3.1 ADN synthesis via nitration of sulfamic acid salts:

ADN was synthesized by nitration of salts of sulfamic acid with mixed acid nitrating mixture. The mixed acid nitrating mixture consists of nitric acid and sulfuric acid, where the composition of the components could vary depending on the requirement. These requirements comprises of nitro ion concentration, freezing point of the mixture and amount of water generated during the reaction. In the synthesis route described by (Langlet, et al., 1999), first potassium sulfamate was synthesized by reacting potassium hydroxide (44g) dissolved in water (50ml) with sulfamic acid (70.35g) dissolved in water (50ml). The combined mixture was precipitated by addition of ethanol (70ml) and it was filtered to obtain potassium sulfamate. Potassium sulfamate was washed again with ethanol and dried at 70^0C.

Mixed acid nitration mixture was prepared by addition of sulfuric acid 96wt. % (16ml) into fuming red nitric acid (45ml) under constant cooling and agitation. Once the temperature of mixed acids reaches -45^0C, gradual addition of potassium sulfamate (17g) was performed, and stirred for 25min. After 25min, the entire mixture was poured on to a mixture of crush ice and water (300g) to terminate the nitration process by dilution. Now the diluted solution is neutralized by 30wt. % solution of potassium hydroxide until pH 8 was achieved.

After neutralization, the mixture was evaporated to dryness under vacuum conditions at 60^0C. The dried powder was twice extracted by acetone (200ml) and concentrated in vacuum. The concentrated acetone solution was precipitated by 2-propanol (approx. 100ml) to obtain precipitation of byproducts which were removed via filtration. Now the 2-propanol mixture

was precipitated by n-hexane (100ml) to obtain crystals of ADN (3~9g) which could be collected via filtration or evaporation of n-hexane.

Several optimization studies based on this reaction method have been performed due to its utility of commercial chemicals at relatively less harsh conditions and comparatively better yield (Oliveira, et al., 2012) (Golofit, et al., 2010) (Nazeri, et al., 2008). Optimized method reported by (Golofit, et al., 2010) uses potassium sulfamate to sulfuric acid and nitric acid ratio as 1:1.6:8.6. The nitration time and temperature was reported as 30min and -40^0C respectively. Another optimization of the reaction was reported by (Nazeri, et al., 2008), which includes 25minutes nitration time at -40^0C, and sulfuric acid to nitric acid ratio as 1:3.5. The optimization perform by (Oliveira, et al., 2012) suggests the use of 40ml fuming nitric acid, 20ml sulfuric acid at -35ºC for 90minutes.

If dilatation of nitrating mixture with ice-water mixture was avoided and the mixture was directly neutralized, it could significantly decrease the energy cost of evaporation in the purification stages at the cost of reduction in yield by 3wt. %. However, it elongates the presence of dinitramide ion in acidic medium and prolonged low temperature operation since neutralization is an exothermic reaction (Golofit, et al., 2010). Reaction mechanism of nitration of sulfamic acid derivative is shown:

$$H_2NSO_3^- \xrightarrow{HNO_3/H_2SO_4} {}^-N<_{NO_2}^{NO_2}$$

In this process, filtration process should be performed very carefully because possibility of degradation of ADN into ammonium nitrates (commercial fertilizer). (Oliveira, et al., 2012).

This process of ADN synthesis was the most viable method in among all discussed because of easily available and inexpensive chemicals. Additionally, reaction temperature was comparatively higher than other processes.

2.4.4 Separation of ADN from reaction mixture:

Once ADN synthesized, the next big challenge was to separate ADN from the reaction mixture consisting of large amount of byproducts. In literature, three methods were proposed for separation of ADN obtained by nitration of Ammonium or Potassium sulfamate from its reaction mixture.

2.4.4.1 Solvent extraction:

The most widely applied method for separation of ADN from reaction mixture was solvent extraction. The solubility of ADN in different solvents has been measured as water 357%, Methanol 86.9%, Butyl acetate 0.18%, N-heptane 0.005%, and for Dichloromethane 0.003% at 20^0C. (Larson & Wingborg, 2011). Therefore, several combinations of solvent extraction can be employed. In general procedure, dry powder of neutralized product was extracted by acetone or 2-propanol followed by filtration to remove byproducts, then the solution was concentrated in a rotary evaporator at reduced pressure. The concentrated liquid was then poured into ether or n-hexane to obtain precipitation of ADN. Any precipitation formed during concentration should be filtered. Alternatively, ADN can be extracted from neutralized mixture by isopropanol (Malesa, et al., 1999), followed by concentration and addition to ethyl acetate. After addition of ethyl acetate, the mixture was cooled down and maintained at -18ºC for 16 hours to obtain crystals of ADN. Another method consists of dissolving ADN in boiling n-butanol followed by concentration and addition of chloroform to obtain precipitation of ADN (Schmitt, et al., 1995). Another method for extraction of ADN obtained from nitration of ammonium sulfamate, described in thesis of G.Santhosh (Santhosh, et al., 2010, pp. 83-123) uses hot isopropanol for extracting ADN from reaction mixture followed by drying to obtain ADN and then extraction by ethyl acetate to obtain pure ADN. An overview of these extraction methods was shown in Figure 2-5.

The general method for extraction of KDN from the reaction mixture, can be simplified as first extraction by acetone 10ml per gram of KDN, followed by concentration of extracts, and addition of 2-propanol to precipitate further impurities, and evaporation to dryness to obtain KDN. At this point, KDN is usually converted to ADN via ion-exchange and further purification can be

performed by dissolving ADN in ethyl acetate followed by filtration to remove byproducts and then drying.

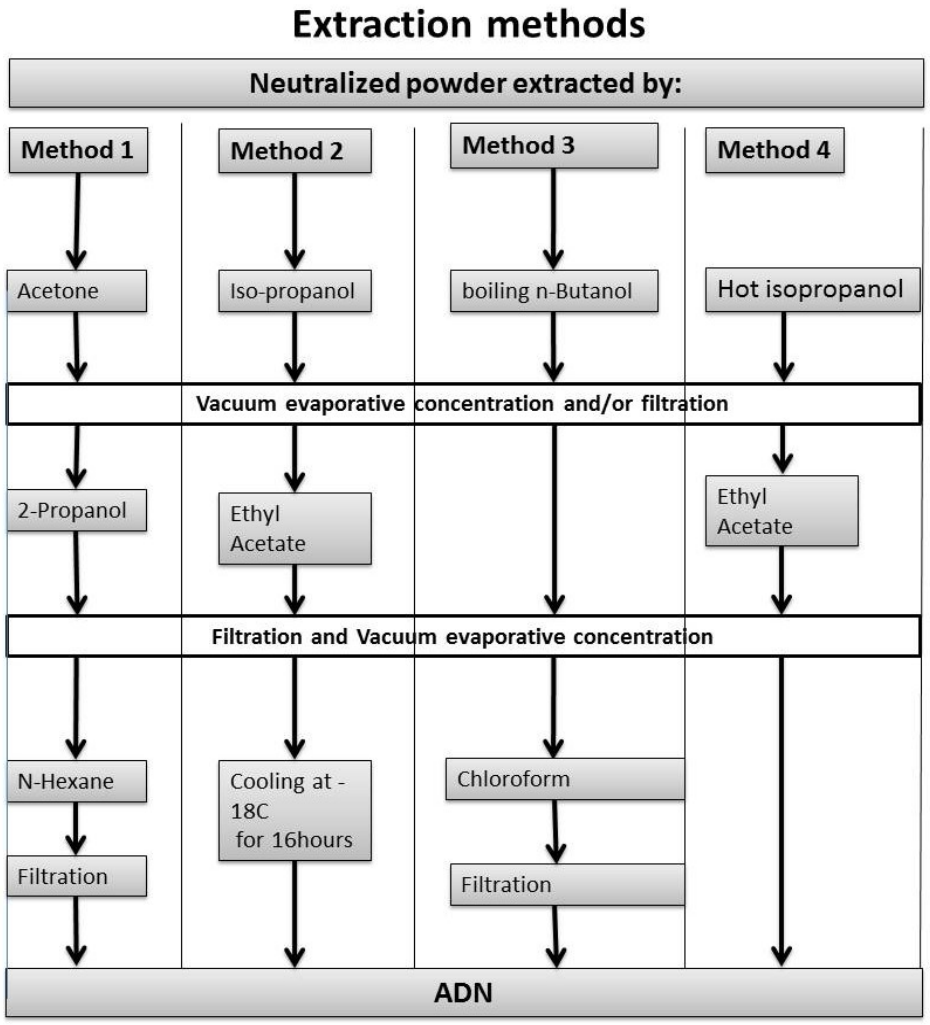

Figure 2-5 Summary of different ADN extraction methods (Schmitt, et al., 1995; Malesa, et al., 1999; Santhosh, et al., 2010)

2.4.4.2 Adsorption-Desorption method:

In this method, the neutralized solution obtained from nitration of ammonium sulfamate was passed through columns of activated charcoal or silica gel to adsorb ADN from solution, followed by filtration and elution by hot water (Santosh, et al., 2003). Although this method gives good efficiency of ADN recovery, large amount of water for ADN elution was a setback. It was due to very high polarity of both water and ADN, which makes removing water from ADN solutions difficult. ADN drying process usually takes 24 hours under

vacuum at 50-60C, which consequently causes the decomposition of ADN into ammonium nitrate, or alternatively, it will again require the use of solvents to decrease the system polarity for convenient drying of the sample.

2.4.4.3 Guanylurea dinitramide formation:

In this method, ammonium sulfamate was nitrated by nitric acid-sulfuric acid system and then instead of neutralization by ammonia, it was poured into 10wt. % cyanoguindine solution to directly obtain water insoluble guanylurea dinitramide, which can then be easily filtered from reaction mixture. The obtained guanlyurea dinitramide was then converted into KDN by reaction with potassium hydroxide in ethanol-water mixture followed by ion-exchange reaction with ammonium sulfate to obtain ADN. (Vorder & Skifs, 2011).

2.4.5 Environmental impact of nitration reactions:

The major concern with the use of acid catalyzed nitrating agents is environmental impact. After the reaction, the mixture of spent acids was diluted by addition of water hence increasing the cost of regeneration. In case of ADN, ammonia was used to neutralize the acids to ammonium sulfate and ammonium nitrate mixture which is a highly exothermic reaction, thus requires dilutions as a way of cooling. Another problem associated with electrophilic nitration was the yield of reaction, which varies greatly with different substrate and type of nitrating agent used, hence more diversified problem to tackle. Additionally, majority of nitration reactions were very slow, where time limit ranges from few minutes to several hours.

The solution to these nitration problems was suggested by numerous researchers, which includes the use of solid acid catalyzes (Choudary, et al., 2004) (Riego, et al., 1996), and microwave assisted nitration (Bose, et al., 2006) (Lidstrom, et al., 2001). However in case of ammonium Dinitramide, the use of solid acid catalyst by Choudary et al. Consisting of sulfuric acid impregnated clay only gave maximum yield between 10-20%. Furthermore, preparation of the catalyst was lengthy and laborious process. Moreover, the use of microwave assisted nitration of energetic materials have been reported

by (Saikia, et al., 2012) for several energetic materials except ADN, but the large scale use of such methods might be a potential hazard.

Another environment friendly method for recovery of spent acid suggested (Vorder & Skifs, 2011) was to first synthesize guandine dinitramide by addition of cyanoguidine in nitration mixture instead of ammonia. The insoluble resultant product can then be filtered while spent acids can be regenerated. The process not only eliminates the neutralization step but also a solvent free method.

2.5 Crystal structure of ADN:

ADN is an anion of dinitramite acid with delocalized negative charge which resonates over 7 atoms. It is stable in mild acidic medium but readily decompose in strong acidic medium due to protonation of oxygen atom or central nitrogen atom. It has small hydrogen bond length which further increases its hygroscopic nature. Among several dinitramide compounds, ammonium salts are most stable as compared to alkyl dinitramides because the dinitramide ions have strong electronegativity and induces electron deficiency in alkyl group by steric hindrance (Cui, et al., 2010), leading to the formation of unstable covalent bond. While, in case ammonium dinitramide, apart from dinitramide ion, ammonium ion also possess strong electronegativity and acts as electronegativity force balancing, which leads to the formation of much stable ionic bond in ADN (Bottaro, et al., 1997).

A detailed study conducted (Cui, et al., 2010) has presented the crystal structure of ADN, as shown Figure 2-6. In comparison to ammonium perchlorate (AP), hydrogen bond length in ADN is short, signifying the strength of hydrogen bonding present in ADN. In ADN, each NH_4^+ is surrounded by six anions of $N(NO_2)_2^-$. This level of hydrogen bonding happens due to the small size (volume) of these ions, hence eliminating the "Static hindrance effect". And also due to arrangement of ions, i.e., first, molecules are connected by first three hydrogen bonds, while the fourth molecule is joined by a long hydrogen bond. It is classified as two-fold three-dimensional inter-propagation networks. This structural network offers good

utilization of space within molecular structures, allowing them to be closely packed and shorter hydrogen bonds.

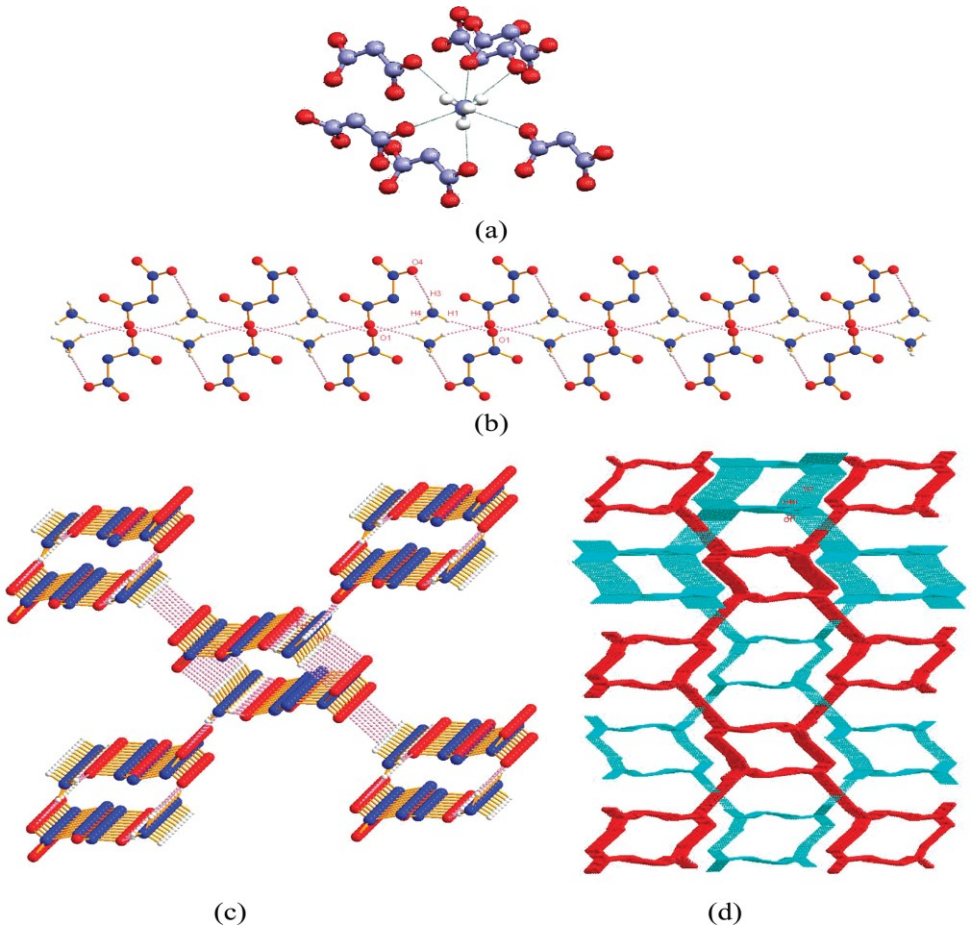

Figure 2-6 Hydrogen-bonding interactions among ADN, showing that the chain is formed along the c axis. (Cui, et al., 2010)

Higher Hygroscopicity (Wingborg, 2006) of ADN than AP is due to hydrogen bonded water molecules on the structure of ADN (Cui, et al., 2010). Hygroscopicity is defined as the ability of a material to absorb moisture/water from surroundings under ambient condition.

Hygroscopicity of ADN is dependent on the hydrogen bonding present in its structure. FTIR spectra analysis confirms the presence of inter-molecular hydrogen bonding among ADN and water molecules in addition to intra-molecular hydrogen bonding of ADN (Cui, et al., 2010). The presence of water in a molecule has been categorized into two types, unbound and bounded. During comparative examination of ADN and AP crystals having 5% moisture, AP has only unbound water molecules mainly on the surface of

the crystal and hence can be removed at 40^0C. However, in case of ADN, water molecules were mainly present in the crystal of ADN, and the hydrogen bonding was strong enough to survive 80^0C, near to the melting point of ADN. ADN not only has very high hygroscopicity but its critical relative humidity i.e. 55.2% is lower than that of AP.

The moisture in the ADN prevents its normal use due to formation of cake. The performance of a propellant depends on its crystalline structure due to the fact that it contributes towards the volumetric loading in the burning chamber, and free flow properties. ADN exists naturally in the form of needle like (monoclinic structure) with very high aspect ratio, ranging from 1:10 to 1:100 or more, therefore, several methods have been devised to alter crystalline structure of energetic materials, including prilling process, spray atomization etc. Some of them have been successfully applied to ADN as well (Teipel, 1999).

The nature of crystal structure in solid propellants is significant, because it determines the density of propellant and most importantly the density at which it can be loaded into the motor. The specific impulse, thrust of the rocket motor, and burn rate are influenced by the crystal structure. With spherical structure, and small median size distribution, very high solid loading can be achieved.

The moisture uptake of solid propellant should be less than 1%, and moisture uptake compassions performed by (Santhosh, et al., 2010) and (Cui, et al., 2010) reveals the moisture content in ADN continues to increase until it becomes liquid phase, in contrast to AP where moisture content uptake stop after reaching saturation level. Therefore, Additional processes are required to induce hydrophobicity in ADN including Prilling and coating with hydrophobic polymers. Studies conducted by (Wingborg, 2006) reported critical humidity of ADN to be 55.1% at 25°C and solubility in water as 78.1% at 20°C.

2.6 ADN prilling and particle size alteration:

As discussed in earlier sections, the particle structure of as-synthesized ADN is unsuitable for application in both solid grain and melt casting method. Furthermore, higher moisture absorption tendency of ADN than AP necessitates encapsulation of processed crystals (Ostmark, et al., 2000). All these factors contribute to reduction of maximum theoretical mean density (TMD) of the solid grain of ADN.

A solid propellant consists of oxidizers such as ADN and AP etc, fuel and binder system where TMD of up to 95~97wt. % is desirable (Hahma, et al., 2010). However, in solid grain casting of as-synthesized ADN, the long needle shaped structure with high aspect ratio hinders the close packing necessary for higher TMD. Furthermore, the higher moisture absorption of ADN (Ramaswamy, 2000) and lower critical humidity level (52%RH) than AP signifies the importance of encapsulating (Heintz, et al., 2009) with hydrophobic polymers such as hydroxyl terminated polybutadiene (HTPB), polystyrene (PS), polyacrylate (PA) etc. The moisture absorption of ADN at 65%RH is 6wt. % as reported by (Cui, et al., 2010). However, no specifications were given for particle size, sample layout geometry, and surface area under testing conditions.

On the other hand, the melt casting of ADN possesses several drawbacks like volumetric expansion in melt phase and the hazardous nature of the process because ADN starts to decompose slowly in molten condition, generate nitrous oxides, (Hahma, et al., 2010; Ostmark, et al., 2002) and these evolving gases creates cavities and fractures during solidification into final grain. During solidification, volumetric shrinkage up to 14% creates foam on the surface of ADN grain (Hahma, et al., 2010).

Many methods have been utilized for the alteration of particle structure of energetic materials such as ultrasound assisted crystallization (Bayat & Zeynali, 2011), melt prilling (Heintz, et al., 2009), solvent crystallization (Fuhr, 2008), and spray crystallization (Teipel, 1999). The importance of optimized crystal structure can be highlighted by its ability to enhance specific impulse by 30% to 50% (Larson & Wingborg, 2011). Modification of crystal structure by ultrasound for RDX has been reported by (Bayat & Zeynali,

2011) and (Kim, et al., 2011), but not for ADN. Although ultrasound treatment could induce oxidation reactions for many substrates as reported by (Kuppa & Moholkar, 2010) and (Malani, et al., 2013) nevertheless ADN does not undergo decomposition or oxidative reactions in absence of base (Qadir, et al., 2003).

2.6.1 Melt prilling:

Several experimental setups have been reported for ADN prilling, such as spray tower, disperse phase prilling, and cooling tower. In spray tower prilling (Highsmith, et al., 2000) molten ADN sprayed from nozzles into the tower consisting of hot and cold sections to provide uniform solidification of spherical ADN particle. In disperse phase prilling, solid ADN is melt in hot non-polar continuous phase, such as Paraffin oil, and stirred until it disperses and then it is slowly cooled down to obtain spherical ADN particles (Teipel, et al., 2000) (Ramaswamy, 2000).

In these methods, the mean particle size of spherical ADN ranges from 40 to few hundred microns depending upon the type of prilling. Spray-prilling-tower offers better size control due to different mesh size nozzles, hence more suitable for different applications. On the other hand, size control is difficult in emulsion prilling as it depends on several factors, including rate of agitation, type of agitator, agitator to vessel size ratio, type of vessel i.e. baffles and the type and quantity of additives used (Teipel, et al., 2000).

In all prilling methods, it was mandatory to melt ADN, which tends to decompose into ammonium nitrate in molten state (Highsmith, et al., 2000). Therefore, several stabilizers has been tested for molten stability, among them, magnesium oxide (Hahma, et al., 2010), urea (Highsmith, et al., 2000), hexamine (hexamethylenetetramine) and many other additives (Ciaramitaro & Reed, 2000). Usually, these stabilizers act as chelates i.e. a compound that reacts with by-products, hence reducing further degradation and gas evolution. In case of magnesium oxide, it acts as a cation-exchanging stabilizer.

In addition to melt stabilizers, agglomeration inhibitors, for example silicon dioxide and fumed Silica or Cab-O-Sil, are used. These additives acts as

emulsification aid and stabilizes the phase boundary regions. Additionally, they alter the flow characteristics of continuous phase, and tend to decrease viscosity. (Teipel, et al., 2000)

A general procedure for disperse phase prilling has been described as:

- 100ml paraffin oil was heated to 90-95ºC with careful temperature control.
- Once the desired temperature was achieved, 10g ADN and ca.05 to 5% additives like Cab-O-Sil and urea was slowly added to the paraffin oil.
- The ADN particles were stirred until all the ADN was melted and there was no ADN left at the bottom of the beaker.
- After stirring, and melting ADN, the mixture was to cool down to room temperature under continuous stirring.
- Once cooled, ADN particles were collected by filtration and washed with non-polar solvent such as hexane to remove access paraffin oil.
- Then, depending on the requirement, prilled ADN particles were coated with desired polymer by dissolving polymer into solvent, which is non-solvent for ADN. Then, ADN particles were added and polymer-solvent mixture was evaporated to obtain coated ADN particles.

2.6.1.1 Spray atomization in Prilling tower:

In spray-atomized prilling, molten ADN sprays from nozzles and solidified into spherical shape while passing though cooling regions of the spray-atomization chamber. The pressure and diameter of nozzle controls the spherical droplets size (Larson & Wingborg, 2011). The growth of crystal during solidification process was further controlled by the direction of flow of cooling fluid. In case of prilling tower, crystalline dendritic growth started from higher temperature gradient to lower temperature gradient, while in case of oil-immersion (disperse phase prilling), it follows the spiral growth due to gradually cooling vortex of paraffin oil by the action of stirrer.

Different methods of prilling causes considerable differences in its properties and significant impact on localized rate of burning which can be observed at

highest level of magnification, such as fluctuation of thrust and rate of burning leading to thrust hiccups. Prills obtained from Prilling tower have smooth edges and surface, as compared to prills obtained by oil-immersion. In case of oil-immersion prilling, the purity level is high while it has bulky structure due to multi-crystalline structure as compared to prills tower method which produces single crystalline structures, smooth up to atomic level (Ramaswamy, 2000). However, in prills tower method, fumed silica contaminates the ADN particles which is released as sweat during combustion.

2.6.1.2 Ultrasound assisted crystallization:

The field of ultrasound assisted chemical synthesis and development of Nano-particles is well established. It has been used for recrystallization of several energetic materials including CL-20 (Bayat & Zeynali, 2011). In this method, solvent containing energetic material was atomized via ultrasound radiations, and a stream of droplets was generated. The stream of atomized solvent was then transferred to non-solvent, where these solvent particles precipitate to forms micro to Nano size particles of energetic materials.

2.6.1.3 Coating:

There are several methods available to introduce hydrophobicity in ADN and most of them have been derived from processing techniques available for other energetic materials. Fluidized bed coating for large-scale coating of ADN is suitable (Heintz, et al., 2009). On the lab scale, ADN particles are coated by solvent coating method. For the selection of coating material, there are several options depending on the requirement, however; the coating material should be compatible with ADN and hydrophobic in order decrease hydrophilicity of ADN.

2.7 Physical properties of ADN:

2.7.1 Density:

High solid density of the energetic materials is crucial to improve efficient propellant properties, and it is compared as percentage of TMD. There are

several factors that contribute to the high solid propellant loading, such as crystal structure, packing method, trapped air or gaseous bubbles, foaming etc. Although ADN has high density, needle shape structure and foaming during solidification hinders solid loading percentage. There are several methods to overcome these issues, which includes prilling, melt casting, vacuum casting, hydraulic press etc (Hahma, et al., 2010).

The density of ADN determined by X-ray diffraction has been reported to be 1.8139gm/cm^3 at 25C without phase transition in temperature range of -150^{0}C to +80^{0}C (Ostmark, et al., 2000). The temperature dependent density of ADN in temperature range of -150^{0}C to 80^{0}C ranges from 1.855 to 1.79gm/cm^3 as shown in the Figure 2-7. The absence of crystalline phase change in ADN indicates its usefulness as oxidizer, because most often the phase changes are associated with change in density too, which tends to create cracks in the cured solid motors leading to catastrophic failures.

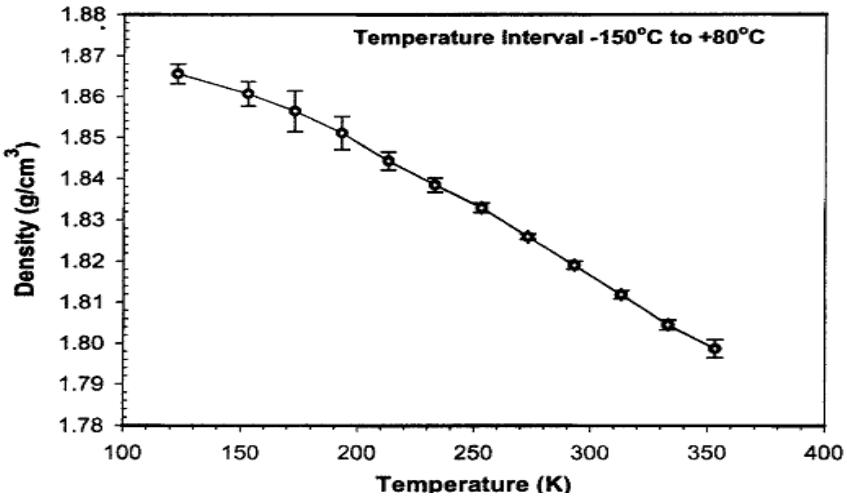

Figure 2-7 : ADN density profile over temperature range of 100K to 350K, indicating no phase transition. (OSTMARK, H et al., 2000)

In molten state, density of ADN decreases as much as 14%, which tends to create cavities during re-solidification, therefore, extreme care and suitable method for slow solidification was required to achieve acceptable solid loading density. In molten state, the generation of fumes, also decreases the density and causes foam formation upon solidification.

In order to increase melt stability of ADN based propellants, several stabilizers have been suggested such as Urea for prilled ADN (Highsmith, et al., 2000), and magnesium oxide for melt casting of ADN (Hahma, et al., 2010). The addition of magnesium oxide converts ADN into magnesium dinitramide to prevent degradation. Therefore, it provides limited pot-life for processing the molten ADN; however, magnesium oxide cannot be used in higher quantity as it reduces the ballistic properties of ADN.

2.7.2 Phase diagram:

Phase diagram for ADN have been reported by (Russel, et al., 1996). The phase diagram (Figure 2-8) of ADN indicates its melting point to be as low as 55^0C for 70/30 mole% mixture of ADN and AN. Another phase diagram (Figure 2-9) for ADN-water solutions has been reported by (Wingborg, 2006) which could be highly significant in determining the properties of liquid propellants based on ADN.

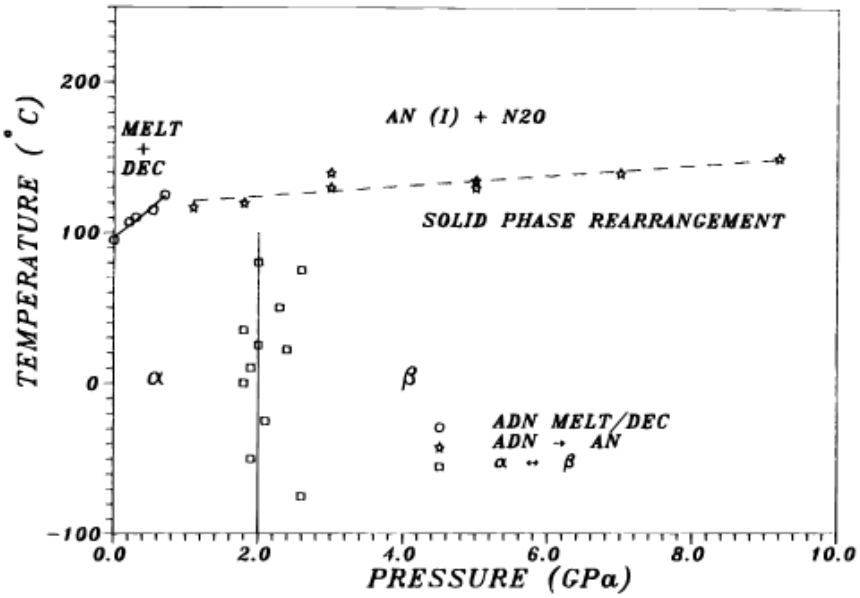

Figure 2-8 Phase diagram of ADN, obtained from (RUSSEL, T P et al., 1996)

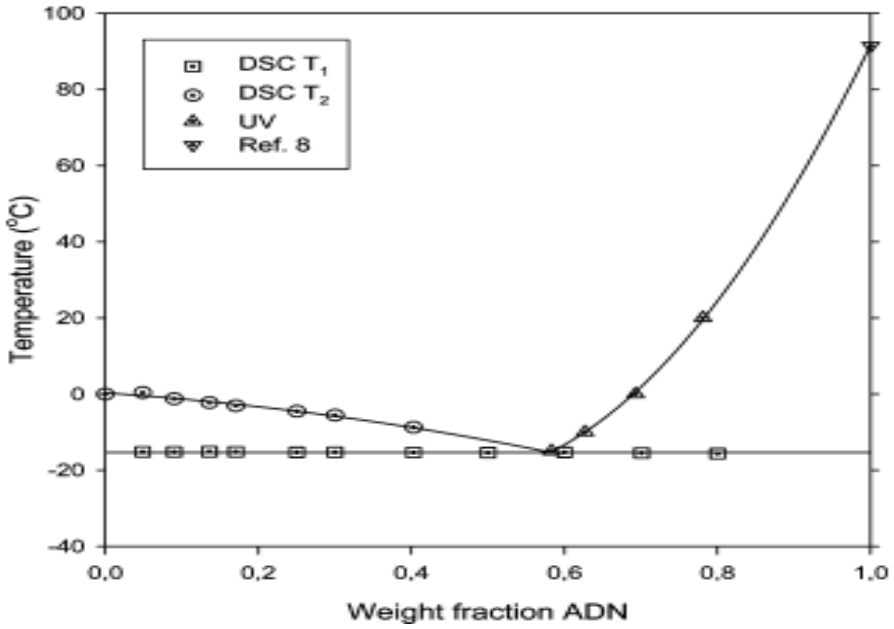

Figure 2-9 ADN-Water phase diagram (Wingborg, 2006)

2.7.3 Oxygen balance:

Oxygen balance of an energetic material determines its degree of oxidation without considering atmospheric oxygen. If oxygen balance was negative, combustion will be incomplete. In case of positive oxygen balance, the combustion will be not only complete but it can also oxidize additional fuel, leading to enhanced combustion.

In a combustion chamber of solid rocket motor, ammonium perchlorate, ammonium dinitramide, nitro-cellulose, nitro-glycerin etc., acts as source of oxygen which in turn used by fast burning fuel to produce thrust. The entire exothermic reaction becomes self-sustaining. The term is a significant parameter to characterize different oxidizers and most significantly, used to formulate different propellant compositions, with final oxygen balance to be positive +1% to ensure efficient and complete burning. The formula for calculating oxygen balance of energetic compound with a general formula of $C_aH_bN_cO_d$ is shown below.

$$OB\% = \frac{d - 2a - \frac{b}{2}}{molecular\ mass\ of\ explosive(M)} * 1600$$

Where d is number of oxygen atoms, a is number of carbon atoms and b is number of hydrogen atoms.

The oxygen balance of ADN calculated to be +25.8%.

$$OB_{ADN}\% = \frac{4 - 2 * 0 - \frac{4}{2}}{124} * 1600 = 25.8\%$$

2.7.4 Sensitivity:

The term Sensitivity in energetic materials means the ease to initiate decomposition by either rapid deflagration or detonation or slow decomposition over time. Its opposite term "insensitivity or insensitive" describes the resistance or difficultly to initiate decomposition in energetic materials. The classification is based on the sensitivity of energetic materials. As a generalized rule of thumb, all primary energetic materials such as mercury fulminate, lead azide etc. are highly sensitive and that is why they are used as detonators. Secondary energetic materials such as ammonium nitrate, RDX, TNT etc. are moderately sensitive and hence used as explosives in military and civilian applications. Tertiary energetic materials are insensitive, such as ADN and AP and used as rocket propellants. There are several types of sensitivities by which an energetic material may suffer from, including radiation, heat, friction, impact, spark and shock sensitivities (Agarwal, 2010, p. 19). The quantitative value of sensitivities of specific material is significantly depended on several factors, including impact and friction at high temperature, moisture content etc.

Radiation sensitivity in this case is referring to the sensitivity of energetic material to radiations other than infrared or heat radiations. Ammonium dinitramide suffers ultraviolet sensitivity and should be protected by storing in materials opaque to UV radiations (Venkatachalam, et al., 2004). UV sensitivity of ADN despite having resonating electrons arises from its simple linear structure. Although, delocalization of electrons reduces UV sensitivity but lack of ring structure also plays an important part in it (Mireles, 2016).

The overall sensitivity of ADN increases with increase in impurities, the most common ADN impurity is ammonium nitrate, which decreases its melting point as described by (Jones, et al., 2005)

Impact sensitivity of the energetic materials is characterized by a 2kg drop weight by BAM-drop weight apparatus, in term of Joules. According to standard by Bureau of explosives (B.E) impact test, 3.6Kg mass was dropped from height of 102mm on about 10mg of sample, the result is recorded in the event of sound, flame or smoke. If the material gives 5 out 10 positive tests for any of the event, it is classified as sensitive to impact. The impact sensitivity of the material is inversely proportional to the particle size (Jones, et al., 2005) but increases with the uniformity of the crystal structure. Prilled ADN has been reported to be twice impact insensitive to RDX (Ostmark, et al., 2000).

The sensitivity of ADN has been determined to be 31cm for raw ADN and 59cm for prilled ADN (Ostmark, et al., 2000). B.E test identifies it as impact sensitive, for positive event results for at least 5 times or more, and BAM-Fall-hammer energy has been given as 4J for both prilled and powdered ADN (Jones, et al., 2005). On the basis of these results ADN could be considered safe for bulk transport.

Shock sensitivity determines the ease at which an energetic material's detonation susceptibility by acoustic, pressure, or thermal shock wave (Agarwal, 2010, p. 20) occurs. It also determines the type of primer (detonator) would work efficiently for initiation of energetic material. ADN has been classified as tertiary energetic material because it is insensitive to shock, and requires an explosive train for initiation. According to (Ostmark, et al., 2000), the shock sensitivity of ADN determined by bullet impact test is in the range of 309-316m/s. Compared to TNT value of same test, which is 364-405m/s, indicating that ADN is more sensitive than TNT.

Friction and spark sensitivity of energetic materials plays a significant role in determination of safety parameters. Friction and spark sensitivity for ADN has been reported to be >35Kp (Hahma, et al., 2010) (Ostmark, et al., 2000)and 0.4j respectively (Venkatachalam, et al., 2004). The electrostatic sensitivity (ESD) of energetic materials having limiting values less than 25mj, are

sensitive to ESD. In case of ADN, the average value of four tests is reported to be 156mj (Jones, et al., 2005), which makes in insensitive to ESD, and similar to that of RDX and AP.

Critical diameter is the property, which elaborates the minimum specific conditions required to initiate detonation in an energetic material, including density and volume. Below critical dimensions and density, it is not possible to initiate detonation but rather deflagration in energetic materials. The critical diameter for ADN is between 25mm to 40mm (Ostmark, et al., 2002).

2.8 Combustion and thermal decomposition Analysis of ADN and ADN based propellants:

Heat of formation of ADN is -148KJ/mole (Larson & Wingborg, 2011), which makes it an excellent choice for potential oxidizer. The performance of ADN as an oxidizer depends on several intrinsic and extrinsic factors, like purity, crystalline structure, compatibility with binder system, rate of burning, temperature/rate of decomposition, type of burning, specific impulse and composite composition.

Solid propellants are required to have sufficiently high burning rate and self-sustaining burning at elevated pressures. The rate of burning depends on several factors, including area of confinement, area of the burning surface and composition of low explosives (Agarwal, 2010, p. 8). Burning rate for solid propellants can be determined by experiments and further extrapolated by using equation i.e. $r = ap^n$; where 'p' is chamber pressure in MPa, 'n' is pressure exponent, R^{2a} is linear correlation coefficient and 'a' is burning rate constant, the values for these constant for ADN has been reported as $a = 9.2, n = 0.49, R^{2a} = 0.993$ (Larson & Wingborg, 2011).

Figure 2-10 shows burning rate of ADN and Glycidal Azide Polymer composite in pressure range of 1 to 20MPa (Larson & Wingborg, 2011). At 7MPa, which is common in most rocket motors, ADN burns at 24mm/s.

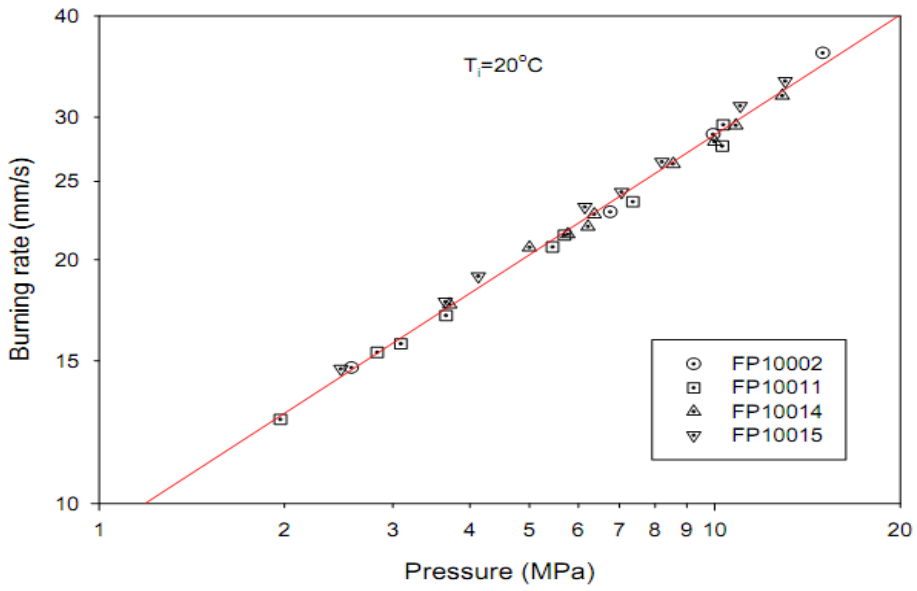

Figure 2-10 ADN/GAP (70/30) burn rate (Larson & Wingborg, 2011)

ADN starts to burn rapidly at microscopic level and quickly expands to the entire body of ADN. The rate of progression is dependent on particle size distribution, uneven particle size distribution leads to the uneven thrust buildup. Solid fuels are seldom used in their pure form for combustion as the combustion mixture consist of auxiliaries like polymer matrix, binders, cross linkers, and stabilizers, and often makes up to 10~20% or more of fuel mass. Among all these auxiliaries, polymer matrix and binder have largest share, and hence significantly affects the rate of burning. The rate of combustion of polymer matrix is inversely proportional to stable burning rate (Ramaswamy, 2000). With ADN, polyglycidylazide polymer (GAP) is used as a binder because of its compatibility, improved performance and good ballistic properties in combination with ADN. (Larson & Wingborg, 2011). The use of these auxiliary materials also facilitates the flow and viscosity of ADN during ballistic testing.

Furthermore, addition of aluminum tends to increase the burning temperature while reducing the flow property due to multiphase flow. According to tests conducted by (Larson & Wingborg, 2011), addition of aluminum increases the specific impulse of ADN. In Figure 2-11, a comparison of different compositions of ADN is given with liquid bi-propellant NTO/MMH.

Propellant	Mixture	I_{sp}(s)	ρ (g/cm³)	ρI_{sp} (gs/cm³)
ADN/GAP	70/30	301	1.61	485
ADN/GAP	80/20	313	1.67	523
ADN/Al/GAP	70/10/20	327	1.73	566
ADN/Al/GAP	65/15/20	332	1.76	584
ADN/Al/GAP	60/20/20	335	1.78	596
NTO/MMH	2/1	340	1.19	405

Figure 2-11: comparison of different compositions of ADN with liquid bi-propellant (Larson & Wingborg, 2011)

A detailed analysis of thermal decomposition of ADN in moderate temperature-slow heating and high temperature-fast heating was performed by (Vyazovkin & Wight, 1997). The surface heating and/or laser ignition technique was used for ignition of ADN samples under controlled environment. A representation of ADN decomposition excluding water molecules is given as:

$$NH_4N(NO_2)_2 \xrightarrow{yields} N_2O + NH_4 \quad (1)$$

$$NH_4N(NO_2)_2 \xrightarrow{yields} NO_2 + NH_4NNO_3 \quad (2)$$

$$NNO_2^- \xrightarrow{yields} NO^- + NO \quad (3)$$

$$NH_4N(NO_2)_2 \xrightarrow{yields} NO_2 + NO + NH_4NO \quad (4)$$

Eq.1 and Eq.2 shows decomposition of ADN, which is identical for both test conditions mentioned earlier, with a slight difference of intermediate products. Eq.3 show the intermediate decomposition of NNO_2^- which leads to the formation of NO_2 and N_2O . Furthermore NO is only formed at 50^0C above the temperature at which NO_2 and N_2O are detected. Further explanation is given (Vyazovkin & Wight, 1997).

Several ADN-based solid and liquid propellants have been developed and reported in the literature. Among them, several fuels and additives were used to obtain desired properties. However, ADN-based composite requires careful selection of fuels to avoid compatibility issues (Landsem, et al., 2012).

As it has been discussed earlier, in practical application of ADN, apart from hygroscopesity and needle like crystalline structure, its material compatibility further limits its usage. Prilling and subsequent polymer coating of the ADN particles resolve these issues. The polymers used for coating are often same as the ones used as fuel component, like GAP and HTPB (Heintz, et al., 2009).

Some of the reported ADN based propellant compositions are compiled in the Table 2-3 below.

Table 2-3 Compilation of ADN based solid and Liquid propellants.

Name	ADN (wt. %)	Fuel, (wt. %)	Metal (wt. %)	Others (wt. %)	Additive (wt. %)	Isp (N.s/Kg	Reference
HP-1	0	HTPB,13	Al, 18	AP, 64	5	2519	(Pang, et al., 2013)
HP-2	10			AP, 54		2531	
HP-3	15			AP, 49		2540	
HP-4	20			AP, 44		2551	
AL/ADN/GAP	60	GAP,24	Al,16		-	2248	(Gettwert, et al., 2015)
ADN/HMX/GAP	58.5	GAP,25.5	-	HMX,11.5	4.5	2237	
ADN/FOX12/GAP	50	25.6	-	FOX12, 20	4.4	2099	
FLP-103[1]	63.4	Methanol, 11.2	-	H2O, 25.4	-	2492	(Wingborg, et al., 2004)
FLP-106[2]	58.7	F6, 11.5	-	H2O, 23.9		2492	(Wingborg, 2011)
LMP-103S[3]	62	Methanol, 18	-	NH3, 20	-		
Propellant A	45	Gap,25.2	-	29.8	-	2334	(Landsem, et al., 2010)
Propellant B	45	GAP, 23.4	-	31.6	-	2312	

[1] Liquid monopropellant
[2] Liquid monopropellant
[3] Liquid monopropellant

Propellant C	45	-	-	55	-	2048	

2.9 Compatibility:

Ammonium dinitramide has known to have compatibility problems with several components of propellant components, including isocyanates which are used primarily as cross linker in ammonium perchlorate based propellant systems (Landsem, et al., 2010), other incompatible materials include rust, iron, copper, nickel, silver metal and their alloys, and cyanoacrylate glue, and polyacetal. Therefore, isocyanates-free curing agents were required for ADN, which may include Bisphenol A Bis(Propargyl Ether) as reported by (Jensen, et al., 2010). The compatible materials for ADN includes stainless steel, aluminum, magnesium, gold, polyethylene without dyestuff, PTFE, RDX, HMX, zinc oxide, magnesium oxide, Dow Slygard 170 two-component silicon resin, and Plexiglas (Hahma, et al., 2010).

2.10 ADN and microfluidics:

Rapid development of the micro satellites have promoted MEMS thrusters as a low cost solution for number of maneuvering requirements of the satellites such as attitude control (Wu & Lin, 2010), navigation (Huh & Sejin, 2014), and multiple powered phases (Zhang, et al., 2005; Yetter, et al., 2007; Ru, et al., 2014). These thrust requirements of the micro satellites depends on their weight and on the type of maneuvering required which can be achieved by installation of an array of MEMS thrusters (Huh & Sejin, 2014). In general, Micro thruster systems are divided into two categories, chemical and electrical propulsion systems. The chemical propulsion system is further divided into solid and liquid propellant systems such as cold gas, vaporizing liquid (Cheah & Low, 2015), bi-propellant (Wu & Lin, 2010) , monopropellant (Huh & Sejin, 2014) and composite solid fuels (Rossi, et al., 2005). Liquid propellant based MEMS thrusters offer variable thrust and multiple ignitions as compared to solid fuel based MEMS thrusters. The materials used for MEMS thrusters' fabrication are ceramics, metals and silicon oxides. The application of Polydimethylsiloxane (PDMS) as the fabrication material offers ease of

fabrication, transparency (Takahashi, 2006) and wide range of material compatibility (Koh, et al., 2013). Although higher thermal conductivity of PDMS often causes heat losses (Cheah & Low, 2015) but it was used as a way to demonstrate applicability of ADN based mono-propellants as potential fuel for MEMS thrusters under electrolytic conditions.

The ignition of MEMS thrusters can be achieved by thermal conduction heating (Kundu, et al., 2012), electrolytic decomposition, spark ignition, and catalytic ignition (Wu & Yetter, 2009). The ignition method selection depends on the type of fuel, such as thermal heating which is suitable for both liquid and solid fuels, while catalytic, spark and electrolytic ignition works only for liquid fuels. In thermal conduction method, the propellant was heated to its decomposition temperature, however higher thermal losses at micro scale due to increased surface-to-volume ratio make it undesirable (Wu & Yetter, 2009). Another disadvantage of conduction heating is its susceptibility to higher energy requirement as compared to resistive heating where energy is supplied directly to propellant (Larsson, et al., 2005). The catalytic ignition has lower ignition temperature but it is prone to loss of catalytic activity with repeated usage (Huh & Sejin, 2014). On the other hand, electrolytic ignition offers an attractive alternate to obtain ignition and subsequently propellant decomposition at relatively low temperature with minimal usage of input power (Koh, et al., 2013). Electrolytic decomposition of ionic liquid mono-propellants can be considered as a hybrid of both chemical and electrical propulsion systems. The basic idea in this mechanism is a passage of electric current through the ionic liquid fuel in combustion chamber resulting in electrolysis (Koh, et al., 2013) and resistive heating (Larson, et al., 2005) that decomposes ionic liquid fuel.

After mission requirements, selection of appropriate fuel for MEMS thrusters is based on material compatibility, application, and ignition methods. In liquid fuels, cold gas vaporizing gives very low impulse (Janson, et al., 1999), hypergolic fuels requires separate pressurized vessels which ultimately increases the overall weight (Kundu, et al., 2012) and bi-propellant mixture of ethanol-hydrogen peroxide requires storage at subzero temperatures to avoid auto decomposition (Huh & Sejin, 2014).

2.10.1 Fabrication methods for MEMS thrusters:

Fabrication of microfluidic devices in general and micro thrusters in particular can be performed by several methods like hot embossing, imprinting, injection molding, laser ablation, soft lithography and X-Ray lithography. Each fabrication method has limitations with respect to size, cost, and durability.

One such method consisted of laser jet printer to create pattern of micro channels on a glossy photo paper, covered with water soluble starch. Then the print tonner was transferred to brass sheet, under heat and pressure applied by household iron. The paper was peeled off by dissolving into water and brass was submerged into ammonium persulfate. The depth of the etched pattern on brass was controlled by duration of immersion of brass in ammonium persulfate. After 1 hour, the brass was removed from the etching chemical, followed by application of PDMS layer onto it. After settling of PDMS, it was then bonded to the glass substrate. In this case, the geometry of micro channels was controlled by pixels of printer line and printer quality (Easly, et al., 2009).

In another method AutoCad patterns are printed on vinyl sheets. These patterns were transferred to glass slides as molds, and then PDMS is poured to obtain final MEMS thrusters (Cheah & Jit Kai, 2013).

2.11 Thrust measurement:

The measurement of thrust generated by MEMS thrusters is in the range of micro newton to milli-newton, and requires dedicated thrust measurement system. The dedication system is required to accommodate the MEMS thrusters properly, and to avoid vibrations, external interference and interference from condensing exhaust gases. There have been several methods and thrust measurement systems reported in the literature, including vertical Pendulum (Packan, et al., 2007; Rossi, et al., 2005; Rossi, et al., 2006; Orieux, et al., 2002), Counter balance Pendulum (Hughes & Oldfield, 2004), micro-force transducers (Wu & Yetter, 2009), high sensitivity laboratory balance (Kundu, et al., 2012) and horizontal torsion balance (Cheah & Low, 2015).

There are two major components of the thrust measurement systems, i.e. physical configuration, and measurement sensor. The physical configuration represents the physical attributes of the setup and in general, the configuration details such as Vertical pendulum (Orieux, et al., 2002) (Figure 2-12), counter balance Pendulum (Figure 2-13) (Hughes & Oldfield, 2004), Torsional balance (Figure 2-14) (Koizumi, et al., 2004), location of the sensor, location and orientation of micro thruster, and vibration-dampening methods. The vibration dampening reduces the noise in recorded data.

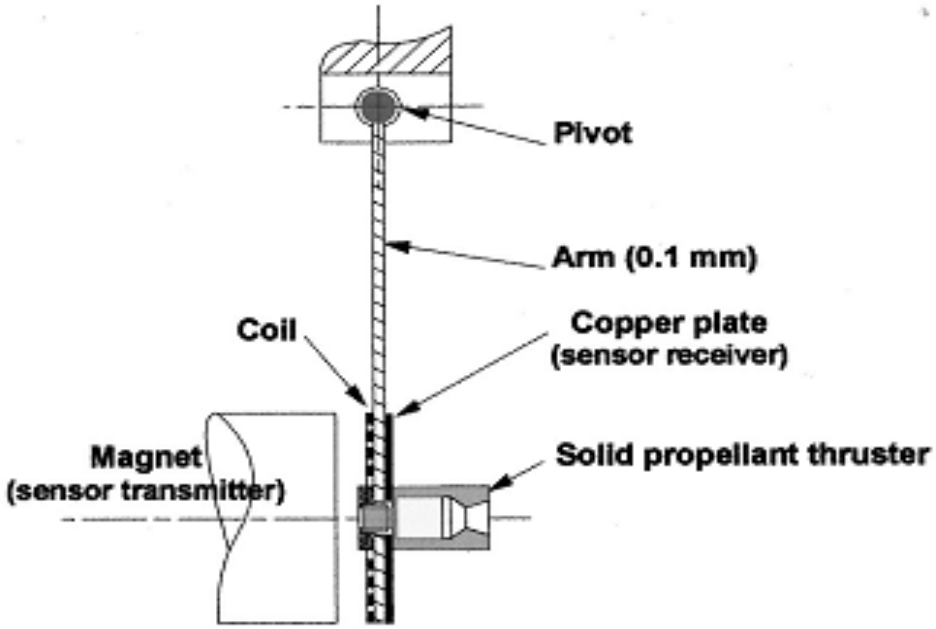

Figure 2-12 Thrust stand setup based on vertical pendulum configuration with induction current sensor (Orieux, et al., 2002)

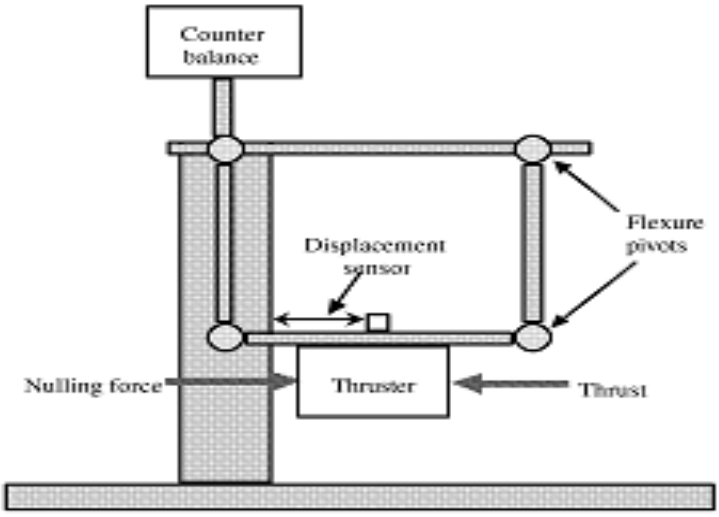

Figure 2-13 Thrust measurement system based on counter balance pendulum and linear displacement force sensor (Hughes & Oldfield, 2004)

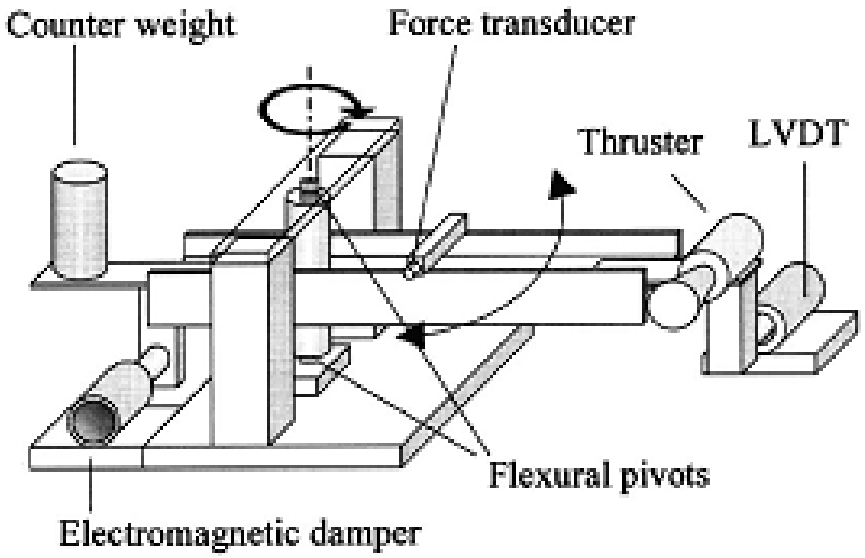

Figure 2-14 thrust measurement system based on torsional balance and LVDT sensor (Koizumi, et al., 2004)

Within each physical configuration, there is a possibility to use different type of measurement sensors, based on cost, accuracy requirement and calibration methods. The commonly used sensors include, micro-force transducers (Wu & Yetter, 2009), which is commonly known as load-cell and high sensitivity laboratory balance (Kundu, et al., 2012), linear displacement sensor (Hughes & Oldfield, 2004), linear variable differential transducer (LVDT) (Koizumi, et al., 2004), induction current sensors (Rossi, et al., 2005; Rossi, et al., 2006) and actuating sensors (Chen & Pan, 2011).

Among all these systems, micro-force transducers and high sensitivity laboratory balance offers the relatively easy experimental setup as shown in (Figure 2-15). The biggest advantage of such systems is the factory calibration, which significantly reduces the error margin in the results. However, they may suffer from low sensitivity or low sampling rate. For example, the high sensitivity laboratory balance used by (Kundu, et al., 2012) managed to record data at 8.6Hz.

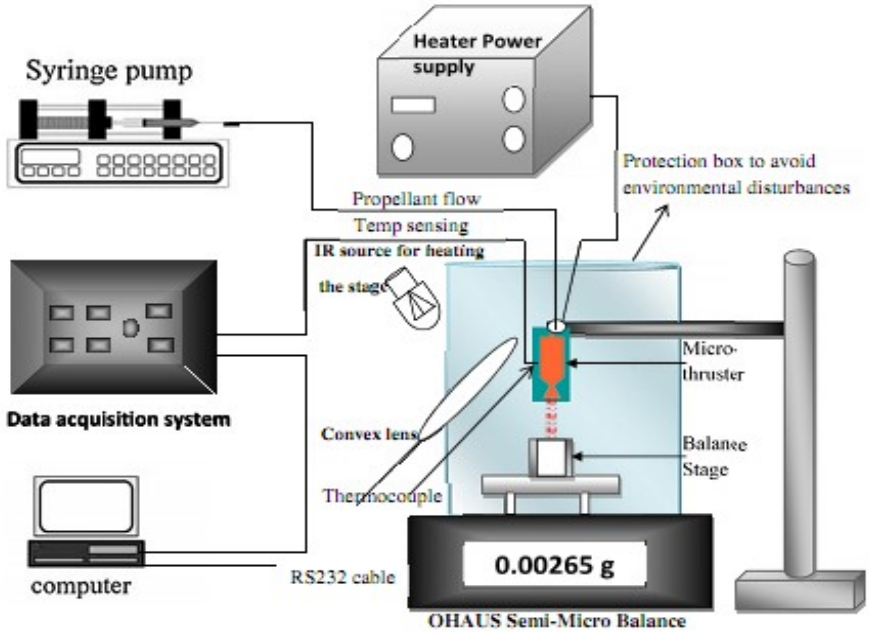

Figure 2-15 high sensitivity balance based thrust measurement system (Kundu, et al., 2012)

The pendulum and torsional balance type thrust stands were difficult and costly to fabricate. They also required self-calibration with known error margins. However, the data recording and sensitivity was dependent on the performance of sensor as well as sensitivity of the stand. The calibration of the sensors with respect to micro or milli newton force is performed by dead weights (Orieux, et al., 2002) and (or) electrostatic fins (Yan, et al., 2009) to generate known force.

In some systems, the force on the thruster measurement system was applied by opposite direction of the Micro thruster by virtue of its physical movement, as shown in (Figure 2-12, Figure 2-13, and Figure 2-14). However, in some cases (Figure 2-15), force was applied on the thrust measurement system by exhaust gas plume from the MEMS thruster. The direct application of exhaust on the thrust measurement system may cause condensation of water due to rapid expansion on the thrust measurement system (Kundu, et al., 2012). Another issue was the distance between the nozzle exit and the location of thrust measurement system at which the force is applied may cause significant variation in the results. Wu & Lin, suggested 2mm as the optimum distance

between nozzle exit and sensor where loses in thrust were negligible (Wu & Lin, 2010).

2.12 Conclusions:

There are several methods available for synthesis of ADN but they either use very expensive or novelty chemicals such as NTFB[4] or NO_2NO_3 or in case of commercial chemicals such as NA and SA, use ultralow temperatures (below -45°C). If novelty and expensive nitration agents are used for synthesis of ADN, then it is possible to obtain ADN at near-zero temperature, but they not only use novelty nitrating agents, but requires either non-commercially available substrates, such as nitramide (NH_2NO_2) or hazardous chemicals like Nitro Urea. In case of nitration of sulfamate salts such as potassium sulfamate with commercially available NA and SA at ultralow temperature, material and operating cost becomes one of the factors against large scale production, however it still remains the most suitable method for producing ADN in both lab or industrial scale as compared to all other available methods. Therefore, it was decided to further investigate the ADN synthesis method consisting of potassium sulfamate nitration with NA and SA. The main target was to investigate the reaction mechanism and to synthesis ADN at near-zero temperature as a step toward industrial feasibility. In addition, once synthesized at near-zero temperature, further studies and optimizations can be performed to increase the reaction yield, which could make near-zero temperature synthesis method feasible as compared to ultralow temperature method.

Therefore, as first step of this objective, the reaction mechanisms of ADN synthesis were studied. It was observed that, synthesis of ADN not only depends on the reactivity or strength of nitrating agent, but it is also depended on the reactivity of substrate. Furthermore, the substrate should have unhindered nucleophilic reaction site where positively charged nitronium ion can bond. Dinitramide formation requires harsh reaction conditions and reactivity because, dinitramide formation is a double nitration process or,

[4] 625rm/5g from Sigma Aldrich

further nitration of nitrated substance at same reaction site. Therefore, the said nucleophilic reaction should not face steric hindrance after first nitration. At this stage of second nitration, which proceeds after first nitration, the reactivity of reaction site decreases by virtue of donating electrons to first positive nitronium ion. At the same time, water and nitrate ions are also generated during the reaction. The nitrate ions (NO_3^-) comes directly from NA, and are also a source of nitronium ions.

This decreased reactivity at reaction site of substrate, possibly leads to formation of byproducts where other highly reactive electrophiles such as potassium or H^+ ions reacts with nitrate ions to produce potassium nitrate, hence reducing the amount of nitronium ions. While considering this entire scenario, it was predicted that, what if there are other strong nucleophiles in the system, which could react with byproduct-electrophile potassium ion. Furthermore, it was also considered that, the addition of such nucleophile can also decrease the rate of reaction by producing intermediate products, because rate of nitration reaction is temperature dependent. Therefore, the basic idea of using TFA as additional chemical in the system came from the above mentioned hypothesis. In case of TFA, which consists of small molecule with 3 fluorine atoms attached to carbon atom, it was expected to have enough nucleophilic strength to protect nitrate and nitronium ions from reacting with potassium, thus leading to ADN formation at near-zero temperature.

In summary, several conditions are required to produce ADN at near zero temperature. First, potassium nitrate is the largest byproduct in this reaction and the only source of nitrate ions is nitric acid. Therefore, a comparable strength nucleophile should be present in the system to counter formation of potassium nitrate and hence increase availability of nitrate and nitrite ions towards formation of dinitramidic acid. Secondly, since dinitramidic acids and salts decomposes in concentrated sulfuric acid at all temperatures, particularly at higher temperature, the dinitramide ion need to be protected in this reaction condition. Hence, trifluoroacetic acid (CF_3COOH, TFA) (Brown & Wirkkala, 1966) could be introduced into the system, which has similar strength as that of nitric acid (Olah, et al., 1989, p. 21) and reported to be suitable nitration catalyst for acid sensitive compounds (Tedder, 1955) and it also serves the

purpose of strong nucleophile. Furthermore, the use of alumina (Santacesaria, et al., 1977) and silica gel (Riego, et al., 1996) has been reported to assist in nitration reactions by means of conjugate acid behavior; therefore, they could be used as additives to identify their effect on reaction yield.

Secondly, in conventional melt prilling, ADN is prone to decomposition due to its melt state instability. Therefore, in prilling and particle size modification of ADN particle and subsequent coating, there are several areas for investigation such as possibility of exploring ultrasound of ADN particles, which could avoid melting of ADN, hence preventing decomposition. Furthermore, the results of ultrasound treatment of RDX and CL-20 as reported in literature were promising and it was possible to obtain similar results for ADN particles. Therefore, ultrasound treatment method was extended to ADN and the results were compared with existing data.

Furthermore, the ionic nature of ADN solutions can be exploited to induce low temperature, low energy consuming decomposition via electrolysis in micro thrusters. In addition, PDMS can be explored to develop torsion rod based Thrust measurement systems, using off-the-shelve electronic sensors. It was expected that the new thrust measurement system would be able to detect force generated by the micro thrusters. However, their calibration will be challenging. In the field of MEMS thrusters, several fuels were reported with exception of ADN based monopropellants. Therefore, in this project, an ADN based monopropellant named FLP-103 was used in PDMS based micro thrusters and its performance was characterized.

Chapter 3. **Ammonium Dinitramide Synthesis**

3.1 Introduction:

In this chapter, ADN synthesis methods are discussed in details. ADN synthesis can be initiated by using Potassium sulfamate (KS) or ammonium sulfamate (AS) as nitration substrate. However, synthesis of ADN from KS was suggested to give more yields (Vyazovkin & Wight, 1997) (Nazeri, et al., 2008) as compared to AS route. During KS route, Potassium dinitramide is first prepared as an intermediate product. The intermediate, KDN is then converted into ADN by ion exchange reaction with ammonium sulfate. In the conversion process, KDN reacts with ammonium sulfate to produce ADN, Potassium sulfate and ammonia gas.

The reaction yield results presented in this chapter were calculated for KDN obtained by nitration of KS. Because, conversion of KDN to ADN is a straightforward ion exchange reaction, and the parameter alteration and characterization of reaction conditions are performed during dinitramide synthesis. The KDN was synthesized according to methods 1 and 2 respectively. However, ADN or KDN produced by Method 1, i.e. Ultra-low temperature nitration, was used for reference purpose in these experimental series. The parameters in these experiments were examined in progressive manner. Therefore, first, nitrating acid composition was identified, then nitrating acid to substrate ratio, and then effect of additives. It was performed progressively to reduce the number for experimental combinations.

3.2 Dinitramide Synthesis experiments and Analytical methods:

3.2.1 Materials and Chemicals:

All the chemicals used in this study were of analytical grade and used without further purification unless stated otherwise. Fuming nitric acid (100%), Sulfuric acid (95~98%), Sulfamic Acid (99%), Dicyanodiamide (99%), Ammonium Sulfamate (99%), Potassium hydroxide (85%), Acetone, 2-propanol, n-hexane, Dichloromethane, Dichloroethane, Acetonitrile, Ethanol,

Methanol and Urea, were all purchased from Merck Chemicals. Triflouroacetic acid (99%) was purchased from Fischer Chemicals. Silica Gel (C0707) was purchased from Bendosen Chemicals and grounded in centrifugal mill to 100µm sieve before it was used in experiments. Alumina powder (CR30) was purchased from Absco Materials, UK. Deionized water was obtained from Mili-Q Plus system (Millipore filtration system). Potassium sulfamate was prepared by neutralization of sulfamic acid with potassium hydroxide (Langlet, et al., 1999). Guanylurea sulfate was synthesized by reaction of sulfuric acid with dicyanodiamide followed by drying in vacuum at 60^0C (Roberts, 1951).

Ultralow temperature, -45 to -50^0C was achieved by adding liquid nitrogen onto the dichloromethane in a Dewar vessel. Near zero temperature was achieved by mixture of ice water and salt mixture for -5 to +5^0C range. Reaction vessel temperature was continuously monitored by digital thermometer. Mechanical agitation was performed by Fisher 16W overhead stirrer.

3.2.2 Method 1: Ultralow Temperature Synthesis:

These experiments were initiated by preparation of mixed acid nitration mixture by addition of 60ml nitric acid and 40ml sulfuric acid into a glass beaker. The mixture was cooled down to -45^0C by cooling liquid in Dewar vessel. After achieving required temperature, 20g of potassium sulfamate was gradually added while the reaction mixture was stirred at 700RPM for 25min. Then, the reaction mixture was poured into 600g of ice-water mixture and immediately neutralized by potassium hydroxide. The neutralized mixture was dried in a rotary evaporator. The dried powder was extracted with 200ml acetone followed by concentrated to ¼ of original volume via rotary evaporator and then 200ml 2-propanol was added to precipitate impurities. The impurities were removed by filter paper and the liquid extract was poured into 200ml n-hexane. The solvent mixture was then evaporated in vacuum to obtain crystals of potassium dinitramide (KDN).

The obtained KDN was converted to ADN by ion exchange with ammonium sulfate in deionized water. Further purified by repetition of same acetone, 2-propanol, n-hexane sequence to obtain 70- 80wt% pure ADN. Finally it was extracted by ethyl acetate and precipitated by n-hexane or Dichloromethane to obtain 99-99.8wt% of pure ADN. The ADN and KDN produced by this method were used for comparison of results with near zero temperature KDN and it was used in prilling and electrolytic decomposition experiments (Langlet, et al., 1999). The sample calculations of purity determination are shown in

Table 0-2 and Table 0-3 in the appendix of this chapter.

3.2.2 Method 2: Near-zero Temperature Synthesis:

A typical experiment was initiated by preparation of mixed acid nitration mixture consisting of 20ml nitric acid, 20ml sulfuric acid, and 5ml trifluoroacetic acid (TFA), followed by addition of 20g alumina. Once the reaction mixture was cooled to -5 to 5^0C, 5g potassium sulfamate was added gradually and reaction was agitated at 250 to 500RPM for 10min. After 10min, the reaction mixture was poured on to 300g mixture of ice-water followed by neutralization with potassium hydroxide. The neutralized mixture was evaporated to dried powder in rotary evaporator. The dried neutralized powder was extracted by acetone 100ml and concentrated in rotary evaporator. The acetone concentrate was added to 100ml 2-propanol and concentrated again in the evaporator. 2-propanol concentrates were added to 100 n-hexane to obtain KDN sample with purity ranging from 2- 5wt. % which gives KDN yield in range of 3 to 6wt% with respect to potassium sulfamate.

3.2.3 Ultraviolet spectroscopy:

Ultraviolet spectroscope (UV-vis) (Spectra 40, Perkin Elmer,) was used for determination of the concentration of the samples at scanning rate of 240nm/min in 190nm to 600nm range. The UV spectrometer was factory calibrated and used without further calibration. The UV-vis spectroscopy operating based on Beer Lambda law, which states that the intensity of electromagnetic light of a given wavelength transmitted through a sample, is

inversely proportional to sample thickness and concentration (Atkins & Paula, 2010, p. 491) and is given as:

$$T = \frac{I}{I_o}$$

Where I and I_o, represents intensity of electromagnetic light before and after passing through respectively. Moreover, the log of it, gives absorbency value as shown below.

$$A = \text{Log}\left(\frac{I}{I_o}\right) = \varepsilon \text{lc}$$

Where, ε,l and c represents molar absorbency constant, length of the sample path, and spectroscopic concentration of the sample. From the above equation, spectroscopic concentration of the samples can be determined and compared with experimental concentration of the sample, to calculate sample purity and mass content based on total sample weight and yield of the reaction based on reactant quantity.

Dinitramide salts shows cation characteristic peaks at 212nm (Bottaro, et al., 1997), to 223nm (Luk'yanov & Tartakovsky, 2000) and anionic peak at 284nm (Bottaro, et al., 1997; Nazeri, et al., 2008; Bottaro, et al., 1997). The Table 3-1 shows the literature values for molar absorbency constant for dinitramide peak i.e. 284nm.

Table 3-1 Literature reported values of Molar absorbency constant for 284nm peak.

Wavelength (nm)	**Molar absorbency constant (L.mole^{-1}.cm^{-1})**	**Reference**
284	5207	(Bottaro, et al., 1997)
	5329 L.mole^{-1}.cm^{-1}	(Nazeri, et al., 2008)
	5627 L.mole^{-1}.cm^{-1}	(Shlyapochnikov, et al., 1994)
	5640 L.mole^{-1}.cm^{-1}	(Santhosh, et al., 2002)

In dinitramide salts, anionic spectroscopic peak at 284nm is preferred for concentration analysis because the cationic peak, i.e. 212~223nm coincides with the molar absorbency peaks of possible byproducts and impurities, which could be present in the sample as impurity and may lead to false data. The Table 3-2 shows some of the possible coinciding peaks (Dean, 1998, p. 7.19; Szilagyi, et al., 2009).

Table 3-2 UV peaks of possible byproducts and impurities

Ions	**Structure**	**Molar absorbency peak (nm)**
Nitrite	$-ONO$	220~230
Nitro	$-NO_2$	210
Amine	$-NH_2$	195
Iron (+2/+3)	Fe^{-2}, Fe^{-3}	190~230

The solutions for UV-vis were prepared by dissolving weighted amount of experimental samples in 500ml DI water and then poured into 1cm wide quartz UV-vis cuvette and scanned in the range of 190 to 600nm range at 240nm/min scanning rate.

The spectroscopic concentration was then calculated by plugging molar absorbency value (A) into:

$$A = \text{Log}\left(\frac{I}{I_o}\right) = \varepsilon \text{lc}$$

$$\text{c} = conc\ obtained\ by\ UV = \text{A}/\varepsilon\text{l}$$

The obtained spectroscopic concentration value was then plugged into the equation shown below:

$$Yield = \left(\frac{\left(\frac{solution\ conc}{conc\ obtained\ by\ UV}\right) * sample\ weight}{substrate\ used}\right) * 100$$

Where, “solution conc.” represents the concentration of KDN sample whose absorbency was to be determined by UV. “Sample weight” represents the total

weight of KDN sample obtained at the end of experiment. “Substrate used” is the weight of KS used in the experiment. “Conc. Obtained by UV” is the concentration obtained by UV spectrometer using the formula: $c = A/\varepsilon l$, where A: absorbency, ε= molar absorbency constant, l: length of the UV cuvette.

In these calculations, sample weight is the most important factor and leftover or stuck samples in the beaker can significantly affect the value of reaction yield. Therefore, samples were weighted while they were in the flasks to obtain cumulative weight reading, and then the weight of the flask was deducted to obtain actual sample weight.

The final product of near-zero temperature experiments (method 2) was in few milligrams per experiment, therefore, attempts to purify into pure KDN and subsequently into ADN, would have resulted in erroneous results due to losses in purification and extraction. Therefore, weight of the final sample of each experiment, which consisted of potassium trifluoroacetate (K-TFA), potassium nitrate, potassium sulfate, and KDN, was measured and then its concentration was measured by Uv-spectrometer. Then the absorbency from the UV-spectrometer was plugged into equation, given below, to obtain purity and yield.

$$yield = \left(\frac{\left(\frac{solution\ conc}{conc\ obtained\ by\ UV} \right) * sample\ weight}{substrate\ used} \right) * 100$$

In this equation, the ADN absorption constant value, 5640 $L.mole^{-1}.cm^{-1}$ given by (Santhosh, et al., 2002) was used. Since this value, is only meant for dinitramide anion; therefore, it is applicable for both ADN and KDN, by changing the molar weights accordingly. Therefore, in weight percentage, the value of absorption constant was converted into 45.48$L.g^{-1}.cm^{-1}$ for KDN, and 38.89$L.g^{-1}.cm^{-1}$ for ADN by dividing the 5640 by molar weight of respective dinitramide salt to obtain results directly as weight percentage. The value given by Santosh (Santhosh, et al., 2002) was used because it was the highest value and would give lowest yield result because it has inverse relation with

concentration. Furthermore, results from other constant values were within ±0.3wt. % range.

In order to confirm the effectiveness of this conversion of units for directly obtaining the results in weight percentage, samples obtained by ultralow temperature nitration (method 1), which is literature reported method, were purified, and their purity was calculated in both molar and weight percentage units as shown in appendix. Furthermore, the current method for determination of reaction yield in impure form is a well-established method as reported by (Nazeri, et al., 2008), where 1ml of the nitration mixture sample was diluted into 1000ml water for Uv-spectroscopy. In order to further confirm the method, and effectiveness of UV spectroscopy, pure samples from ultralow temperature experiments were tested in UV for purity and then in DSC-TGA to confirm its melting point, which was in literature reported range of 92~95^{o}C.

3.3 Experimental results:

Table 3-3 shows the compiled results obtained by near zero temperature experiments unless stated otherwise. In addition, sample calculation for reaction yield is shown in appendix (Table 0-1). Furthermore, all the experiments were repeated 3 times for ensure reproducibility, however, the experiments which gave less than 1wt. % yield in first attempt were not repeated.

Table 3-3 Experiments and their details

Exp. Name	**Substrate**	**NA (ml)**	**SA (ml)**	**TFA (ml)**	**Additive/ comments**	**Nitration time (min)**	**Yield (wt %)**
A-1	KS, 5g	15	15	5	0	2	**2.18** **1.25** **2.2**
A-2	KS, 5g	20	20	5	0	2	**2.33**

							1.4 **1.03**
A-3	KS, 5g	25	25	5	0	2	**2.1** **2.3** **1.35**
A-4	KS, 5g	30	30	5	0	2	**1.9** **0.6** **2.7**
A-5	KS, 5g	35	35	5	0	2	**2.3**
B-1	KS,17g	45	27	10	50ml DCE[5]	2	**0.3**
B-2	KS,8g	25	10	5	40ml DCE+40 ml DCM[6]	0	**0**
B-3	KS,11g	30	12	0	DCE 30ml	8	**0**
B-4	NS,12g	40	20	10	DCE 10ml+CYN	10	**0.2**
B-5	KS,17g	45	27	10	CLF[7] 50ml	10	**0.16**
B-6	NS, 12g	40	20	0	-40C, DCE 10ml	10	**1.5**

[5] Dichloroethane
[6] dichloromethane
[7] Chloroform

B-7	KS, 17g	45	27	10	DCE 50ml + C[8] 20gm	5	**0**
B-8	KS, 17g	45	27	10	KCl[9] 11gm, DCE 50ml	10	**0**
B-9	KS,17g	45	27	10	KNO_3[10], 17gm	5	**0.17**
C-1	KS, 5g	20	20	5	Al_2O_3, 5gm	2	**2.44**
							2.8
							3.6
C-2	KS, 5g	20	20	5	Al_2O_3, 10gm	2	**1.5**
							3.1
							4
C-3	KS, 5g	20	20	5	Al_2O_3, 15gm	2	**3.7**
							2.7
							3.32
C-4	KS, 5g	20	20	5	Al_2O_3, 20gm	2	**1**
							3.2
							2.41
D-1	KS, 5g	20	20	5	Al_2O_3, 20gm	2	**1**
							3.2
							2.41
D-2	KS, 5g	20	20	5	Al_2O_3, 20gm	5	**4.5**
							1.13
							1.92
D-3	KS, 5g	20	20	5	Al_2O_3,	10	**5.8**

[8] Charcoal
[9] Potassium chloride
[10] Potassium nitrate

					20gm		**1.45**
							1.32
D-4	KS, 5g	20	20	5	Al_2O_3, 20gm	15	**1.98**
							0
							1.02
	KS, 5g	20	20	5	Al_2O_3, 20gm	20	**0.97**
							0
E-1	KS, 5g	20	20	5	SiO_2, 20gm	2	**5.3**
	KS, 5g	20	20	5	SiO_2, 20gm	5	**2.74**
							3.86
E-2	KS, 5g	20	20	5	SiO_2, 20gm	10	**9**
							2.34
							3.2
E-3	KS, 5g	20	20	5	SiO_2, 20gm	15	**2.58**
							1.84
							2.02
F-1	KS, 5g	20	20	5	SiO_2, 40gm	10	**1.12**
	KS, 5g	20	20	5	SiO_2, 40gm	10	**1.32**
Acetic acid	KS, 8.5g	27	15		CH_3COOH, 20,	30	**0**
L1, L2	KS, 17g	45	27	10		15	**0**
L3	KS, 17g	45	27	10		10	**0**
L4	KS, 17g	45	27	10		30	**<0.1**
urea	Nitrourea, 8g	32	16	10		5	**0**

3.4 Results and discussion:

In these experiments, selected parameters for investigation were nitrating acid to substrate ratio, effect of solvents and additives, and their effect on yield of

dinitramide salts were studied. These parameters were selected because physical conditions of the reaction plays a significant role in nitration reactions, as demonstrated by several authors, where they managed to obtain varying degree of ADN yield only by changing the reaction time, reaction temperature, and composition of nitrating mixtures (Nazeri, et al., 2008) (Oliveira, et al., 2012). Moreover, ADN synthesis by catalytic nitration was also demonstrated (Choudary, et al., 2004). In ADN synthesis by NTFB and NO_2NO_3, reaction medium such as DCM, DCE etc were required.

Within these reaction parameters, hundreds of thousands of different combinations were possible. Therefore, the numbers of tested parameters were restricted to minimum due to large number of permutation combinations as shown in Table 3-4, and only those experiments which produced more than 1wt. % yield in the first attempt were repeated. In addition, they were selected in progressive manner by first determining compositions for NA to SA ratios for a given substrate weight (nitrating mixture composition), then for substrate to each nitrating mixture composition, then nitration time for each one of them and so on. Furthermore, minimum and maximum limit for each parameter was selected with input from literature reported values.

Table 3-4 Possible number of combinations

	NA (ml)	SA (ml)	TFA (ml)	Alumina (g)	Time (min)	Temperature (°C)	Substrate (g)
	15	5	1	1	1	0	5
	20	10	2	2	2	1	10
	25	15	3	3	3	2	15
	30	20	4	4	4	3	20
		25	5	5	5	4	
		30	6	6	6	5	
			7	…	…		
			8	…	…		
			9	…	…		
			10	20	15		
total	4	6	10	20	15	6	4
Total number of combinations				=4*6*10*20*15*6*4			**=432000**

As it can be observed in Table 3-4, there are more than 400 thousand different combinations possible. Therefore, the parameters tested were based on literature reported combinations and in a range close to it.

3.4.1 Composition of Nitrating mixture and the ratio of nitrating mixture to substrate:

In the first step, suitable nitrating mixture composition was determined. The nitrating mixture compositions given by (Nazeri, et al., 2008), (Golofit, et al., 2010) were tested. However, results were abysmal and produced less than 1wt. % KDN as shown L1-L4 series in Table 3-3. Since composition of nitrating mixture, its ratio to substrate and nitration time are interconnected with each other, ratio of composition in nitrating mixture was fixed at 1:1 by volume. In addition, experiments also repeated with different TFA quantity and absence of SA. Experimental result shows increment in TFA and/or absence of SA had insignificant effect on the yield of KDN. The absence of SA failed to produce dinitramide, and different quantities of TFA resulted in almost same results as 5ml TFA. Therefore, quantity of TFA was also fixed at 5ml and henceforth, all other experiments used nitrating mixture composition of 20ml NA, 20ml SA and 5ml TFA.

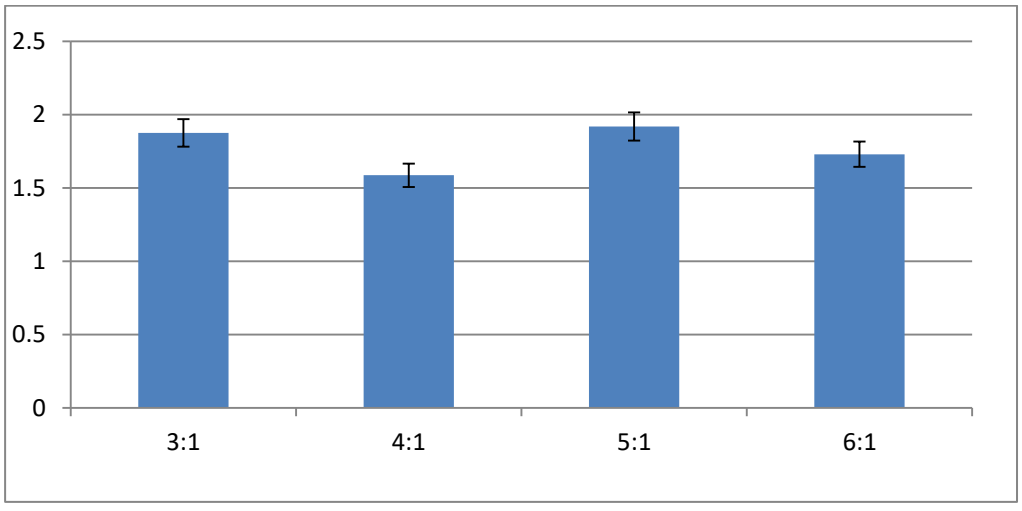

Figure 3-1 Effect of nitrating mixture to substrate ratio

After fixing nitrating mixture composition, its ratio to substrate was determined. The ratio of nitrating mixture to substrate was driven by quantity

of NA as reported by (Nazeri, et al., 2008) (Golofit, et al., 2010). Therefore, experiments were performed for nitrating mixture to substrate in the range of 3:1 to 6:1, as shown in Figure 3-1.

Since, the reaction yield was within ±0.3wt % range for each substrate to nitrating mixture ratio, and according to literature, nitrating acid mixture to substrate ratio is between 3:1 to 4:1 range because increase in quantity of nitronium ions in the system allows better mixing without significantly increasing the viscosity. Ratios higher than 4:1 were abandoned for conservation of the expensive nitrating acid mixture. Therefore, substrate to nitrating mixture ratio of 4:1 was selected and all the other experiments were carried out at this ratio. In order to eliminate decomposition of dinitramide ions by sulfuric acid at higher concentrations, all experiments were conducted at 2min nitration time unless stated otherwise.

3.4.2 Effect of reaction medium:

Dinitramide ion synthesis is a highly exothermic reaction. Improper heat dissipation causes decrease in reaction yield due to localized overheating. Therefore, in order to dilute the reaction mixture and to provide heat dissipation, inert solvents (Table 3-3. Series B1-B9) were tested as potential catalyst for the reaction such as, chloroform, dichloromethane (DCM) and dichloroethane (DCE), as shown in Figure 3-2.

Most solvents used were immiscible with nitrating mixture and hence decreased the reaction yield. Furthermore, the addition of potassium nitrate (KNO_3) had no effect on yield. These experiments were performed only once because each of these experiments produced less than 1wt. % ADN.

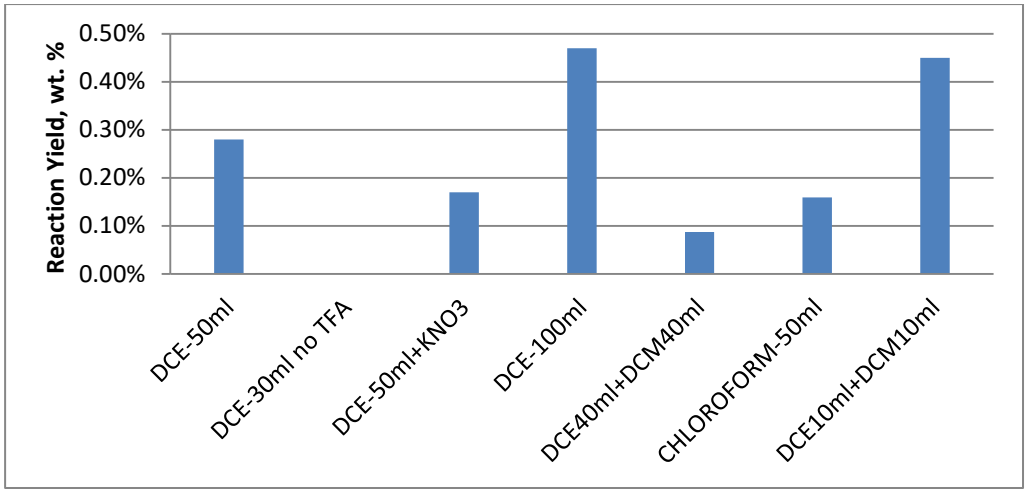

Figure 3-2 Effect of reaction medium on the yield.

3.4.3 Effect of additives:

In highly concentrated non-aqueous nitration reactions, the rate is dependent on effective collision between molecules and active reaction sites (Luk'yanov, et al., 1994). Addition of TFA into the nitrating mixture successfully synthesized dinitramide salt near-zero temperature in low yield <2%.

3.4.3.1 Effect of Alumina:

Low yield were due to increased rate of reaction and decomposition of KDN simultaneously in the acid mixture (Bottaro, et al., 1993). Therefore, Alumina (Table 3-3. Series C1-C4, D1-D4) was used as rate modifying additive because of their compatibilities with nitrating mixtures (Riego, et al., 1996) and the effects as a conjugate base under acidic conditions (Sarvari, et al., 2010). The addition of alumina slightly increased the KDN yield as shown in Figure 3-3 and Figure 3-4.

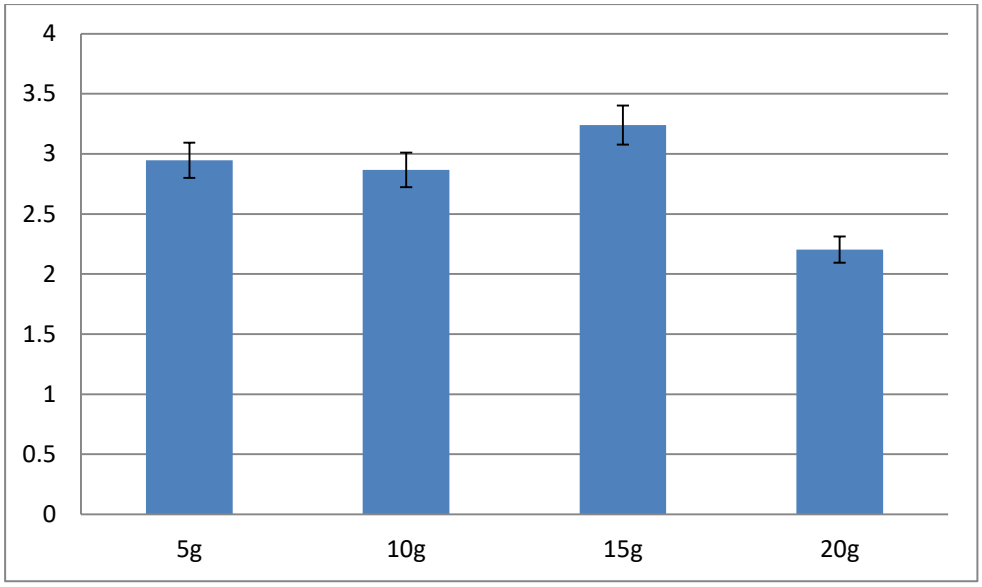

Figure 3-3 Effect of Alumina on reaction yield

In order to identify the role of alumina, another series of experiments was performed where the weight of alumina was kept constant at 20g while the nitration time was different. 20g alumina was selected because it had lowest yield and highest amount of Alumina in 2-min nitration reactions as shown in Figure 3-4 . 20g Alumina was selected under the assumption that, if alumina were indeed acting as rate modifier in the reaction, then increased time with maximum quantity would increase the reaction yield. The increment in nitration time increased the KDN yield from 2.2% to 2.8% at 10min, shows the impact of additive as a rate modifier. The decrease in reaction yield after 10min was attributed to decomposition in the reaction mixture.

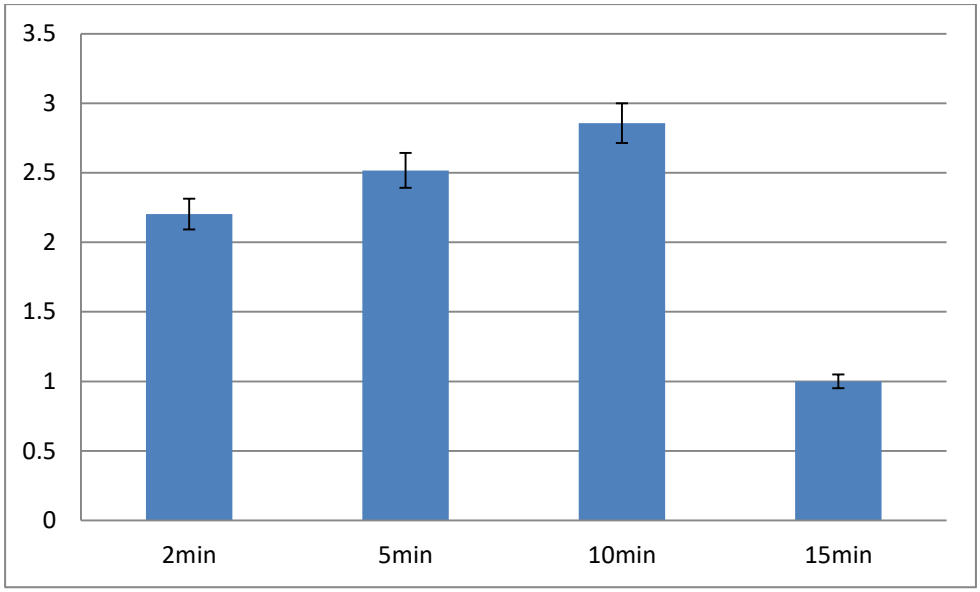

Figure 3-4 Effect of 20g alumina on reaction yield

3.4.3.2 Effect of silica gel:

From the results from alumina addition, another series of experiments was performed where silica gel was used instead of Alumina. The results are shown in Figure 3-5. Similar to alumina, the reaction yield decreased after 10min nitration as expected due to decomposition of KDN by sulfuric acid.

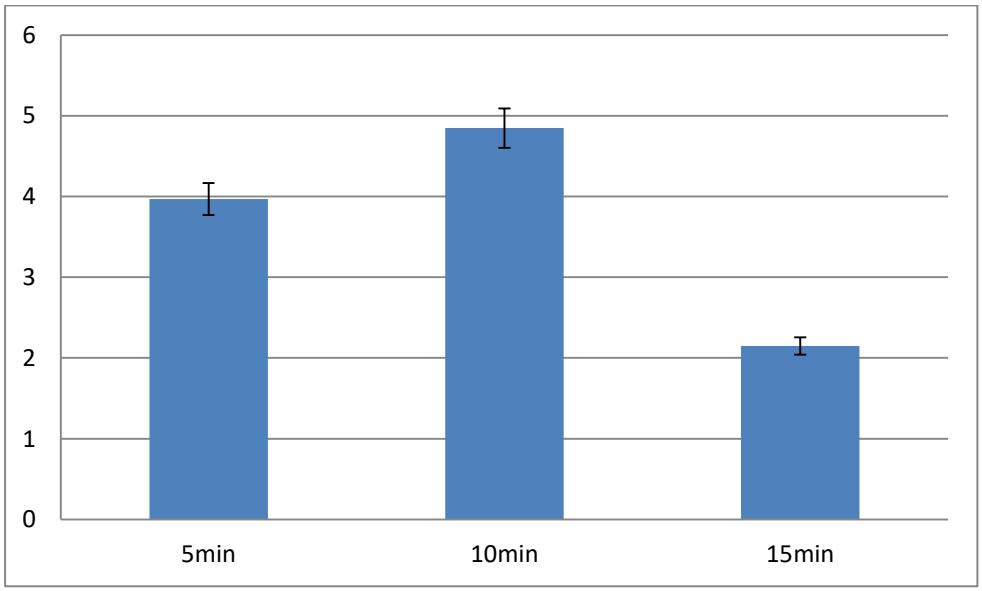

Figure 3-5 Effect of 20g silica gel on reaction yield

3.4.4 Reaction Mechanism:

The reaction mechanism proposed for the modified near-zero temperature ADN synthesis method is shown Figure 3-6. It is estimated that, first, NA splits in to nitronium ions by SA and TFA catalysis and generates nitronium ions and sulfate ions as shown in eq. A and B in Figure 3-6. The nitronium ions react with TFA to produce nitronium-TFA as intermediate product. In the meanwhile, nitronium ions also react with KS to produce potassium and amidosulfate ions. The nitronium ions from nitronium-TFA go toward amidosulfate and potassium ion from KS goes toward TFA to produce K-TFA (potassium trifluoroacetate). It is expected that, in this way, potassium ion does not directly react with nitronium ions to produce byproducts i.e. potassium nitrate and potassium nitrites. This ion exchange between potassium ion and nitronium-TFA is expected to happen because of higher reactivity of potassium ion and high electronegativity of TFA ion. The higher electronegativity of TFA arises from three fluorine atoms present in its small structure, which could provide overall partial yet strong negative charge. It is also estimated that, the presence of TFA, and its strong electronegativity diverts protonation of dinitramide ion from strong acids, especially SA at near-zero temperature which could have caused destruction of dinitramide ion. Dinitramide ion is known to decompose by presence of strong acids such as SA.

In case of addition of conjugate bases alumina or silica gel, they act as proton acceptor. They could accept proton or positively charged ion from potassium ion or hydronium ions from SA or NA. In absence of these conjugate bases, the protons from SA or NA could have reacted with amidosulfate ion causing reduction in total ADN yield.

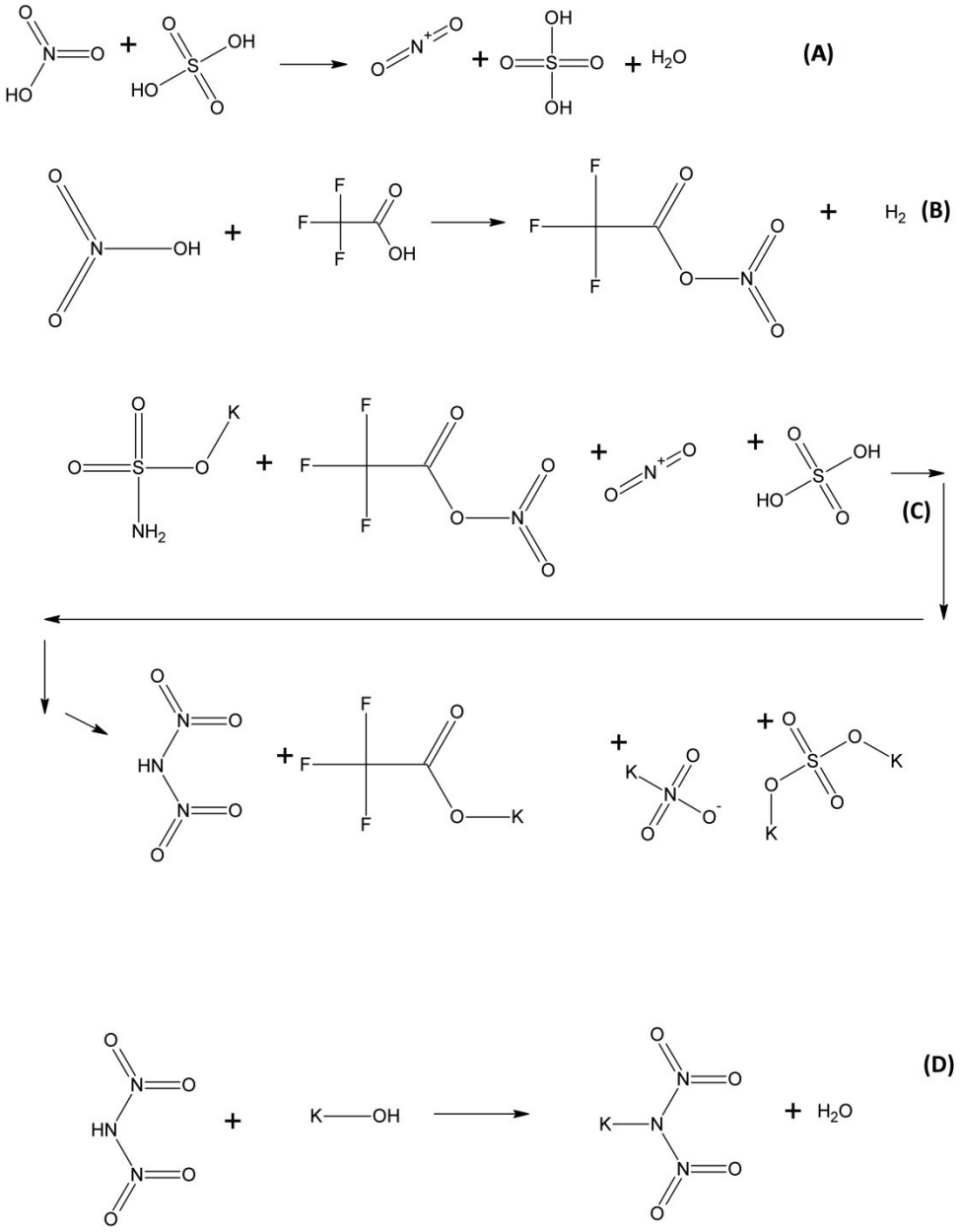

Figure 3-6 Reaction mechanism

3.4.5 Ultraviolet spectroscopy:

In these experiments, sampling using pipette resulted in high volumetric error due to the corrosive acids. Secondly, in case of experiments where solid additives were used, filtration was required to remove insoluble silica gel and alumina, which otherwise would have affected the UV-vis results.

Therefore, in these experiments, UV-Vis was performed after obtaining a mixture consisting primarily of potassium dinitramide and potassium trifluoroacetate by extraction of neutralized mixture with acetone and 2-

propanol as described in experimental details. The removal of potassium salt of trifluoroacetate was not only a lengthy process and unnecessary but could have reduced the yield due to losses during purification. Secondly, in order to preserve expensive chemicals, each experiment was conducted with minimum quantity of the chemicals possible, based on the reaction beaker. Therefore, the dinitramide content in the final product was usually less than 0.5g, and hence its separation into pure form would have been impossible because it would have stuck to filter paper or beakers. Furthermore, the UV-vis testing of pure trifluoroacetic acid did not show any peaks, which could have possibly interfered Dinitramide peak at 284nm. The UV peaks obtained for experiment number: B-21A is shown in Figure 3-7 which shows characteristic Dinitramide peak at 284nm and shoulder at 325nm.

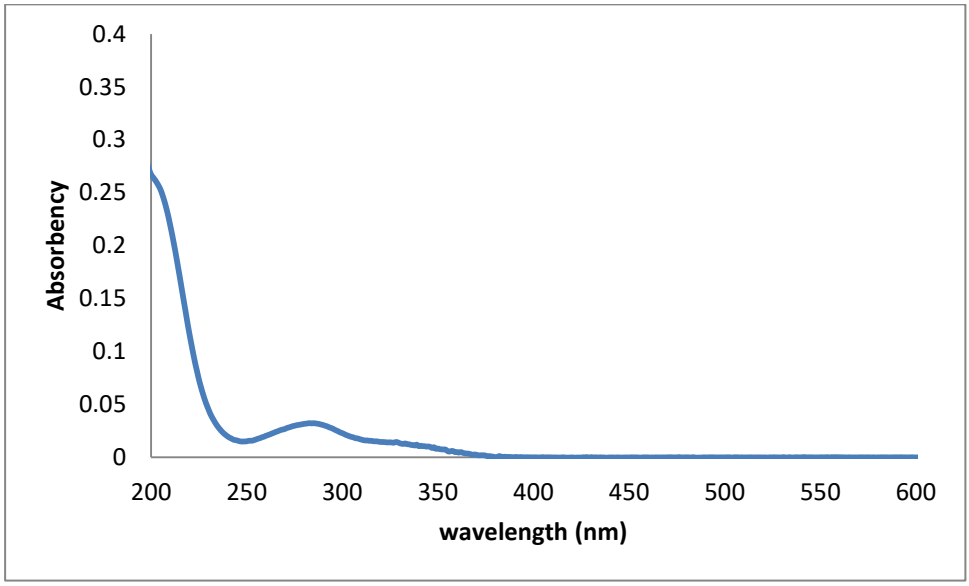

Figure 3-7 UV spectrum of KDN from experiment number B-21A, where 2.8wt.% yield was obtained.

3.5 Conclusions:

In this project, KDN which is an important precursor to ADN, was prepared at near-zero temperature synthesis with investigation of various parameters. It was produced at 0-5^{0}C by nitration of potassium sulfamate with mixed acid nitrating agent consisting of nitric acid, sulfuric acid, trifluoroacetic acid. Previously, synthesis of dinitramide salts at 0-5^{o}C was achievable only by

expensive nitronium salts such as NTFB or N_2O_5. Once KDN was synthesized successfully in trace amounts, optimization studies were performed to identify suitable reaction compositions and additives to increase the yield. It was identified that, nitration of 5g potassium sulfamate with a mixture consisting of 20ml nitric acid, 20ml sulfuric acid, 5ml trifluoroacetic acid and 20g silica-gel at 0-5^{o}C for 10min, produced up to 5wt. % KDN. The spent silica-gel and acids can be recycled and hence further reduces the raw material usage. Although the yield in this project is not up to the mark of industrial feasibility, and requires further investigation with respect to more reaction parameters and temperature ranges to further optimize the reaction yield.

Chapter 4. **Ammonium Dinitramide, Prilling and Sonication**

4.1 Introduction:

In this chapter, effects of prilling and sonication on ADN produced by method 1 (ultralow temperature nitration of potassium sulfamate) were studied because ADN produced by near-zero temperature experiments was less in quantity required for these experiments. The synthesized ADN was purified, dried and then subject to 3 type of experiments as discussed in the sections 4.2.

The process of filling rocket propellants into rockets is called grain casting. The term ”grain” is use to define solid block of propellant that goes into rocket fuel chambers, some examples are shown in Figure 4-1 (Agarwal, 2010, p. 226). The most important requirement of grain casting is to achieve maximum theoritical mean density (TMD), as higher TMD means more fuel mass can be added into fuel chamber. The shape of the solid propellant grain is used to control its burn rate and thrust by virtue of exposed surface area within each shape.

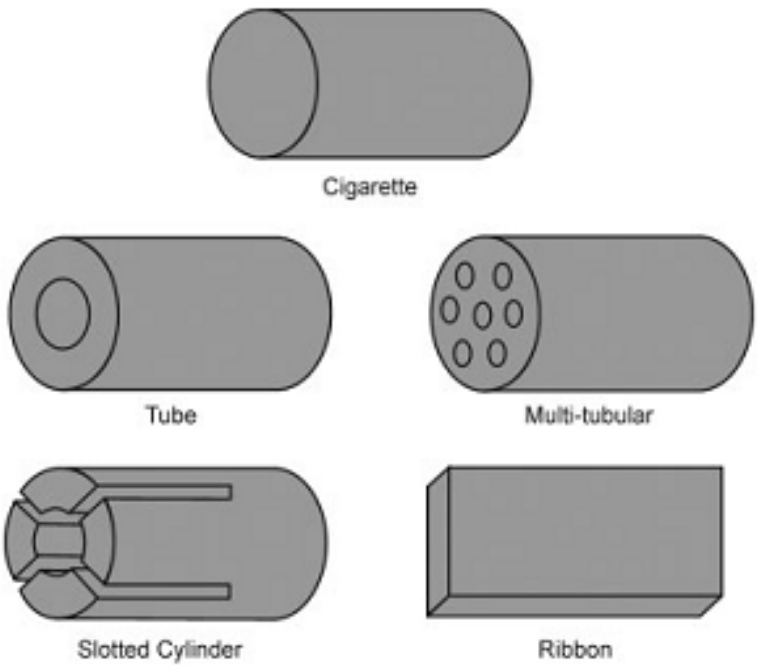

Figure 4-1 Different shapes of Grains (Agarwal, 2010, p. 226)

There are 2 methods of grain casting, i.e. melt grain casting and solid grain casting. In melt grain casting method, the molten propellant is added in to mold and solidified under controlled cooling conditions (Akhavan, 2004). However, there are several drawbacks of this method such as low theatrical mean density of propellant in the grain, volumetric expansion or compression, cracks, bubbles, decomposition of propellant etc (Teipel, 1999). Melt grain casting is not suitable for ADN based propellants because, ADN undergoes volumetric expansion in it molten state (Larson & Wingborg, 2011). Furthermore, ADN generates gases due to decomposition in its molten state. Due to these two major factors, melt casting of ADN based propellants is not suitable, as it would lead to cracks, bubbles and gaps in the final grain.

The basic idea of solid grian casting is to compress propellant into desired shapes and fill in fuel chamber of the rocket. Within solid grain casting method, there are several variations, such as piston compression, ram compression, ram-screw compression, and vacuum compression etc (Akhavan, 2004, p. 145). In piston compression method, single or double pistons are used, depending on the requirements as shown in Figure 4-2, and this method is suitable for propellants which are insensitive to friction.

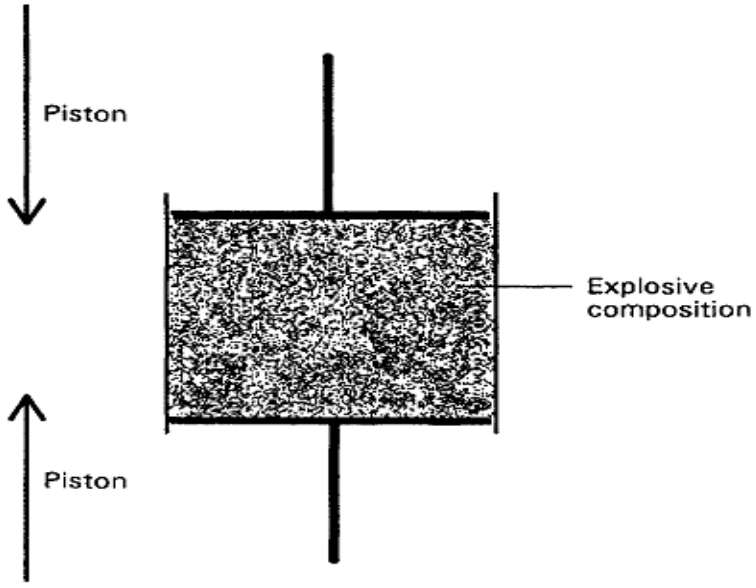

Figure 4-2 Double piston compression (solid grian casting) (Akhavan, 2004, p. 144)

Vacuum casting method is used for propellants, which are sensitive to friction. In this method, propellant is wrapped with rubber diagraph, connected to

vacuum line and placed inside high-pressure oil bath for compression as shown in Figure 4-3 (Akhavan, 2004).

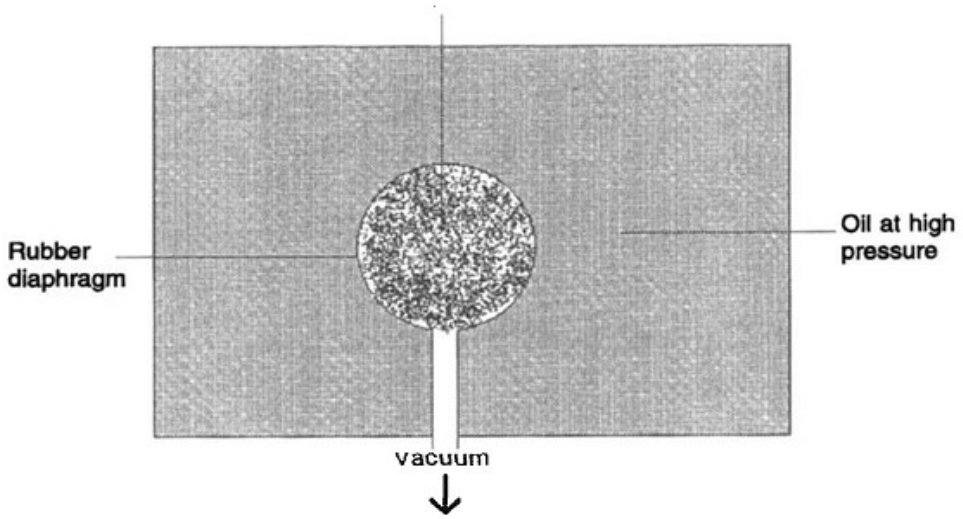

Figure 4-3 vacuum compressiong grain casting (Akhavan, 2004, p. 146)

In ram extrusion-compression and ram-screw compression methods, pre-mixed propellant consisting of polymers, binders and cross linkers and other additives is extruded in to desired shapes as shown in Figure 4-4. This method is suitable for propellant compositions, which can give plentiful processing time before hardening, as it is a time consuming method. In addition, propellant composition must consist of highly viscous polymer, so that the grain can retain its shape. The difference with ram extrusion-compression and ram-screw compression method is that they are batch and continuous process respectively (Akhavan, 2004, p. 147).

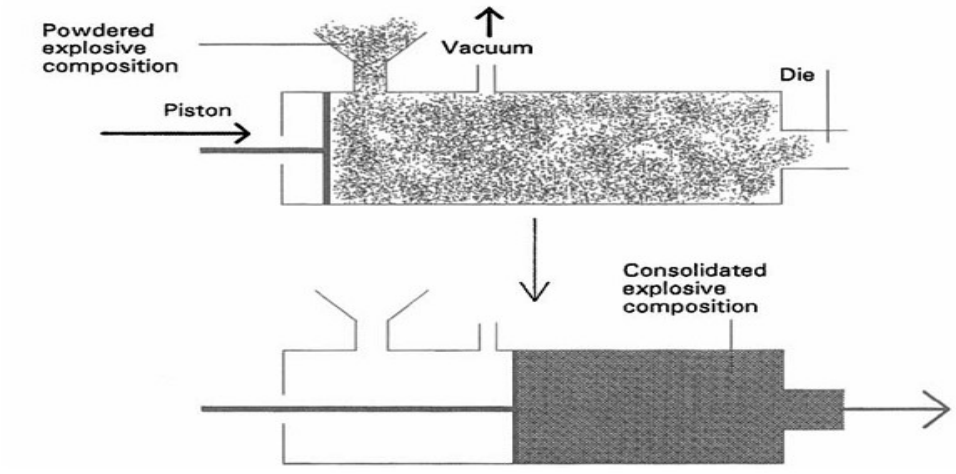

Figure 4-4 Ram compression (Akhavan, 2004, p. 147)

In case of solid grain casting of any propellant, the particle morphology of energetic material plays an important role in achieving high TMD. The particle morphology consisting of spherical or low aspect ratio shapes offer better filling and hence higher TMD. In case of ADN, the crystal morphology of as-synthesized raw ADN is similar to needle like shape. Therefore, it is of utmost significance to change crystal morphology of ADN particles.

There are two methods reported for changing crystal morphology of ADN, i.e. melt prilling and spray prilling as described previously in section 2.6. However, application of ultrasound radiations to modify crystal morphology of ADN has not been reported yet. Ultrasound based crystal morphology alteration has been performed on few other energetic materials with promising results (Kim, et al., 2011; Bayat & Zeynali, 2011), therefore, in this project, the study of ultrasounds was extended to ADN particles.

Ultrasound treatment was utilized to modify crystal structure of ADN followed by coating with polymers to decrease moisture absorption. The ADN used in these experiments was synthesized by conventional ultralow temperature method because; near zero temperature, method's yield now is not enough for producing ADN in several grams quantity. Furthermore, several additives were introduced into the process to decrease particle agglomeration to obtain free flowing particles in micro-nano meter range. As additive, Cab-o-Sil, Cetyltrimethylammonium bromide (CTAB) and graphene were selected due to their unique properties. The ability of Cab-o-Sil is well established as agglomeration inhibitor for ADN prilling (Ramaswamy, 2000) , (Teipel, 1999). The addition of graphene in energetic composites of nitro methane has been demonstrated to increased stability, burn rate and its function as fuel component (Sabourin, et al., 2009). Furthermore, application of graphene in polymer composites are numerous and they have been utilized to impart certain properties on the host material, such as anti-corrosive coating via epoxy/graphene composite (Chang, et al., 2014) where planner structure of graphene acts as a barrier toward water and humidity. In other applications, lotus leaf effect of rough surfaces is created to reduce moisture absorption via reduction in surface energy as demonstrated by (Nguyen, et al., 2012) (Ke, et al., 2011). Another application of polystyrene/graphene as super hydrophobic

fibers was demonstrated by (Asmatulu, et al., 2011). In synthetic replication of the said phenomenon, the roughness is introduced via coating with micro-nano particles on substrate (Sarkar & Saleema, 2010). CTAB was used as cationic dispersing agent for graphene nano particles by (Vadukumpully, et al., 2009) and many others. Therefore, graphene was added into ADN composites to increase its hydrophobicity by reducing surface energy of coated ADN particles.

The prilling and polymer coating of ADN was performed to increase its hydrophobicity which increases it's shelve life. Therefore, only hydrophobic polymers were used for coating purposes. Among hydrophobic polymers, the polymers which are combustible and produces low molecular weight decomposition products, are preferred. These polymers assists in propellant combustion, and act as fuel component for oxidizer i.e. ADN.

Therefore, in these experiments, application of ultrasound on ADN particles was investigated. The core parameters tested in these experiments were sonication medium, feasibility of simultaneous polymer coating, and effect of additives like Graphene and Cab-O-Sil. The results of these experiments were compared with ADN prilled samples produced by literature reported methods. The coating of ADN reduces the moisture absorption, which consequently increases its shelf life and offers ability to work in humid conditions such as in Malaysia.

4.2 Experimental procedure and Analytical methods:

In this project, a new method for alteration of ADN crystal morphology was developed. Therefore, several experiments based on trial and error were performed until a practical and reproducible method was developed. Once a method was identified, then the experiments were performed with that method to determine reproducibility and with different polymers such as PS and HTPB.

4.2.1 ADN Synthesis:

ADN used in this study was synthesized according to method two given in section 3.2.2 (ultralow temperature nitration of KS).

4.2.2 Solvent crystallization:

In these experiments, 0.5g of pristine ADN was dissolved in 10ml acetone. Another solution of 20ml Dichloromethane was prepared with coating polymer, cab-O-Sil and graphene. The two mixtures were mixed followed by evaporation in rotary evaporator at 45^0C and 50 mbar pressure at 200 rpm to obtain the final solid sample. The purpose of these experiments was to identify the effect of Cab-O-Sil and coating polymers in direct application.

4.2.3 Polymers:

The poly acrylate and cellulose acetate, used in some initial coating experiments was obtained by commercial source. Mechanical Engineering department of University of Nottingham generously provided polystyrene, and HTPB (III) was purchased from Dalian Tuowei International Trade Co. Research grade Toulene diisocyanate (TDI), Glycerol was purchased from Merck Chemicals.

4.2.4 Melt Prilling:

Melt prilled samples were prepared according the method given by (Heintz, et al., 2009). 0.5g ADN added in 50ml paraffin oil at 100^0C under agitation, followed by addition of 2wt. % cab-o-sil. Once the ADN was uniformly suspended, temperature was reduced to room temperature. Now, the ADN was filtered and washed with n-hexane to remove traces of paraffin oil. The obtained ADN particles were then added to mixture of polymer (PS or HTPB) in 50ml dichloromethane and evaporated in rotary evaporator to obtain coated samples (Heintz, et al., 2009).

4.2.5 Ultrasound treatment in Toluene, DCM and DCE, and Coating with Polystyrene:

0.5g ADN was added to 50ml solvent along with 1wt. % Cab-o-Sil, 2wt. % CTAB (Cetyltrimethylammonium bromide), 5wt. % polystyrene and 1wt %

Graphene powder (Graphene Supermarket, Graphene Nano powder, 8nm flakes AO-2). The mixture was then sonicated (Elmasonic P, Elma) for 60min at 60^0C at 37 kHz, 100% power in a glass test tube. After sonication, the mixture was poured into another beaker containing 100ml n-hexane. The content was then sonicated for 5min to avoid particle agglomeration. Then solution was evaporated at 45^0C in vacuum to obtain ADN particles.

Due to high number of combinations, the quantities of additives such as CTAB, Cab-O-Sil and Graphene was used as it was reported in literature. Cab-O-Sil quantity as anti-caking agent (agglomeration inhibitor) for ADN was reported to be between 0.25~5wt. % range with preference to lowest amount possible which gives free flowing particles (Highsmith, et al., 2000). Furthermore, the small ADN quantity used in each experiment further limited the minimum quantity to 1wt. % i.e. 50mg due to weight scale limitations. Similarly, the lower limit for graphene was constrained by weight machine and was selected according the literature reported values of graphene in graphene-polymer composites (Galpaya, et al., 2012). Furthermore, coating polymer quantity was selected according to literature reported values for ADN (Heintz, et al., 2009).

In other attempts, toluene was replaced with DCM and(or) DCE while the procedure remained the same.

4.2.6 Ultrasound treatment in Toluene and Coating with HTPB:

In case of coating of ADN particles with HTPB, the HTPB polymer mixture was first prepared and then 5~20wt% with respect to ADN was used for coating purpose. The HTPB coating mixture was consisted of 10wt% of Toulene diisocyanate (TDI), 10wt% Glycerol and 80wt% HTPB monomer as shown in Table 4-1.

Table 4-1 Composition of HTPB polymer

Chemical Name	Type	Weight percentage
TDI	Crosslinker	10
Glycerol	Catalyst	10

HTPB monomer	Monomer	80

The glycerol was used as curing catalyst and TDI was used as cross linker (Kohga, 2009). The prepared HTPB mixture was added to ADN particles after 60minutes of sonication in toluene. Followed by addition in n-hexane and drying for 60min at 70^0C to cure HTPB.

4.2.7 Ultrasound treatment in Paraffin oil:

0.5g ADN was added to 50ml paraffin oil along with 1wt. % Cab-o-Sil, 2wt. % CTAB (Cetyltrimethylammonium bromide) and 1~2wt. % Graphene. The mixture was than sonicated (Elmasonic P, Elma) for 60min at 60^0C at 37 KHz, 100% power in a glass test tube. After sonication, n-Hexane was added to the mixture for dilution, so that it can be easily filtered. After filtration, it was washed with n-Hexane to obtain ADN particles. The obtained Particles consisted of ADN, CTAB, Graphene, and Cab-O-sil were then added to polymer solution in DCM and evaporated to obtain coated particles.

In another procedure, ADN mixture after sonication was centrifuged to remove access oil, instead of filtration and the coating was performed by similar method.

4.2.8 Scanning electron microscopy (SEM):

ADN in its raw form have a long needle shape structure with high aspect ratio ranging from 1:10 to 1:100 (Ramaswamy, 2000). Therefore, in order to visualize the particle shape of ADN in its raw form and after experiments, Scanning electron microscope is used. It is one the most important analytical tool in this series of experiments and was perform using FESEM FEI (Quanta-400 instrument) at low and ultralow vacuum levels. The samples were dried overnight prior to analysis at room temperature in humidity controlled chamber at 20%RH, due to low critical humidity value of the ADN (Cui, et al., 2010); and high relative humidity of atmosphere. The particle size was measured qualitatively with the measuring scale generated by the instrument.

The high energy and zoom levels were avoided, as they cause decomposition in the ADN samples.

4.2.9 Differential Scanning Calorimeter and Thermogravimetry (DSC-TGA):

The thermal characteristics of the samples were analyzed by DSC/TGA (Mettler Toledo 1 STAR) system in the temperature range of 35^0C to 300^0C at 10^0C.min^{-1} heating rate. Few mg of the samples were placed in the 40µl Aluminum pans with lids and 2~3 pinholes were made in the lid to avoid over pressurization of the pan by gases evolved during decomposition. In case of only a hole made in the aluminum pan cover, the gases will generate an upward thrust while leaving the aluminum pan, leading to alteration of the results as a peak of weight increment. Melting point, decomposition initiation point, and the heat of decomposition were calculated using proprietary Mettler star-E software.

4.2.10 Moisture absorption test:

ADN has low critical moisture absorption limit i.e 55.2%RH, (Cui, et al., 2010) and very high water solubility (Wingborg, 2006).

Therefore, it was important to determine the effect of polymeric coatings on the ADN particles. Hence, the moisture absorption test was performed by placing 0.3~0.5g of sample in enclosed environment with uniform airflow rate of 5l/min measured by anemometer (DO2003, Delta Ohm srl, Italy). The humidity of the chamber was maintained by passing the air from saturated solution of ammonium nitrate which gives 65±2%RH (Wexler, 2003). The samples were weight at 60min intervals to determine percentage of moisture absorption for duration of 240min.

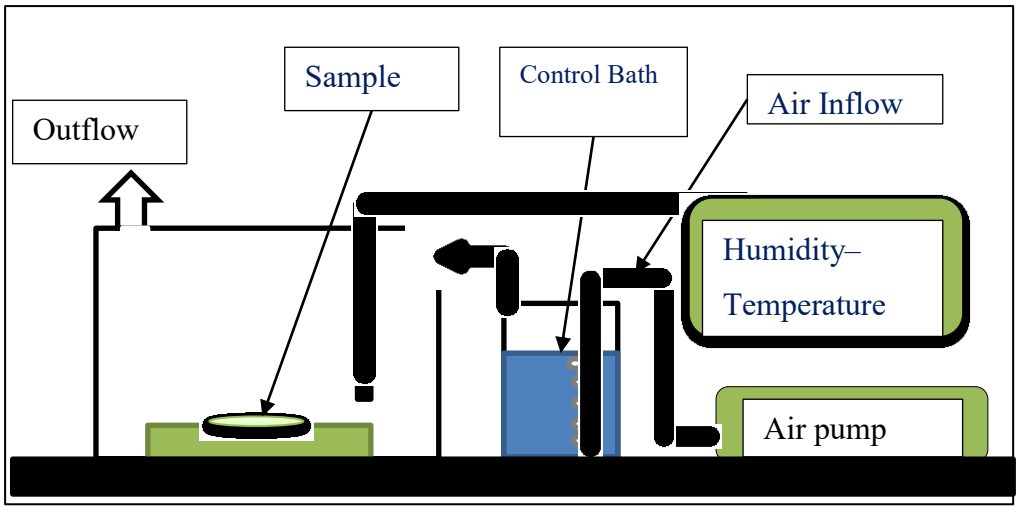

Figure 4-5 Experimental Setup for Moisture absorption test

4.2.11 Bomb calorimeter:

This test was performed in Bomb Calorimeter (PARR 6100EF), but only for selected samples due to its large sample requirement (0.5~1g). It was performed under nitrogen atmosphere.

4.3 Experimental results and Discussion:

In this section, experimental data, results, and discussion based on ADN sonication and prilling is presented.

4.3.1 Experimental data:

In this section details of all the experiments performed for prilling and coating of ADN samples is given. In all these experiments, 0.5g ADN was used, unless stated otherwise. SEM of raw ADN used in these experiments is shown Figure 4-6 and it was used to compare ADN samples obtained from reported experiments. These experiments were titled as S-X, where X was the experiment number.

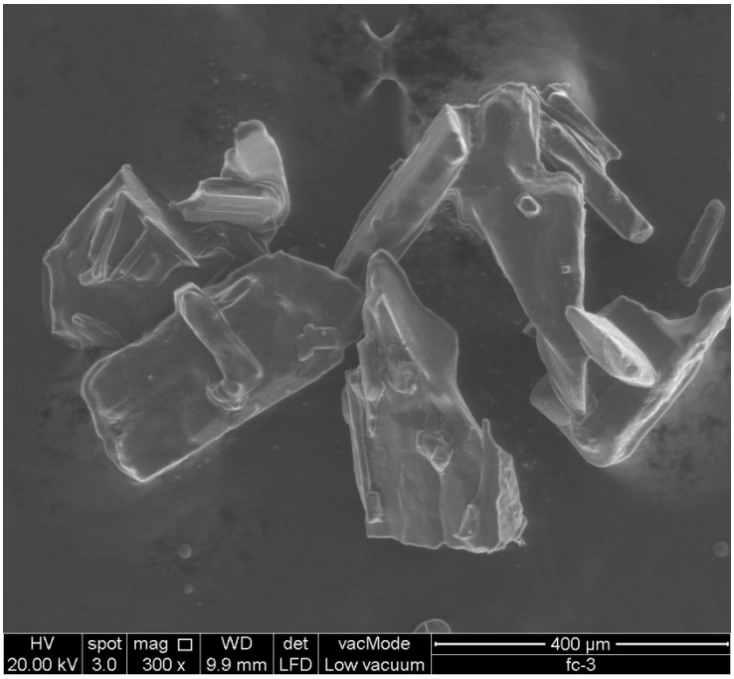

Figure 4-6 SEM of Raw ADN synthesized for these experiments shows long needle like particles.

4.3.1.1 S-1

0.5g ADN dissolved in ethyl acetate, followed by mixing with solution of 2wt. % Poly acrylate. 1wt. % Cab-O-Sil and DCM. Then it was dried at 45^0C in vacuum rotary evaporator to obtain the sample as shown in Figure 4-7.

4.3.1.2 S-2:

0.5g ADN was dissolved in ethyl acetate, and then mixed with 5wt. % Poly acrylate solution in DCM and dried at 45^0C in vacuum rotary evaporator to obtain this sample as shown in Figure 4-7.

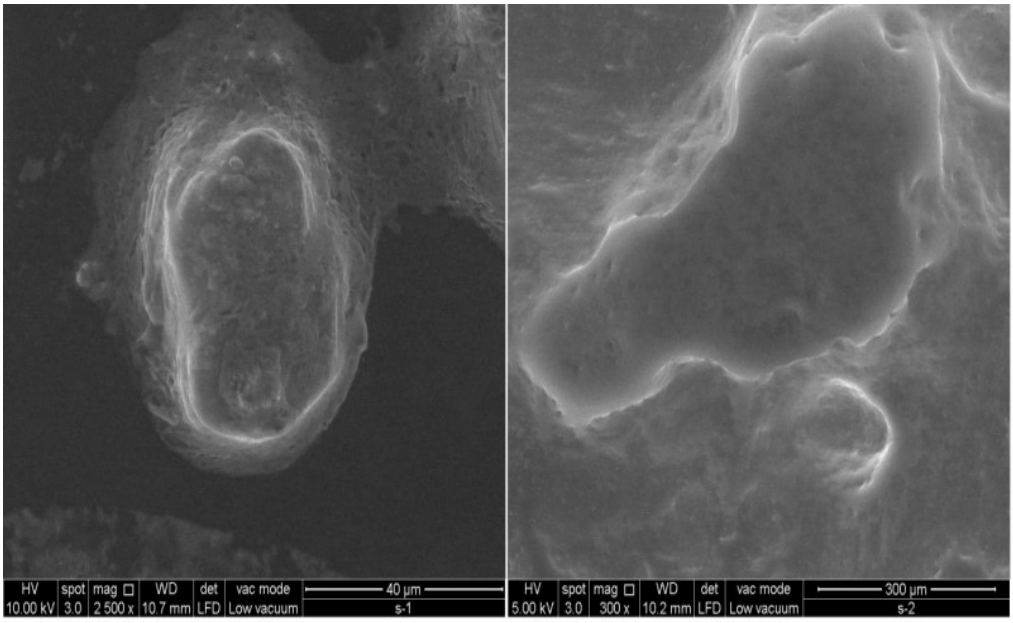

Figure 4-7 Sample S-1 (left) and S-2 (right) in SEM shows that samples were not converted into Prills, and absorbed moisture during the storage and SEM testing as evident from the smudgy edges of sample.

4.3.1.3 S-3 and S-4:

Regular prilling of ADN by melting in paraffin oil for comparison with other samples, however sample failed to crystalize and turned into yellow liquid. The conversion of ADN based samples into yellowish liquid was also reported by (Oliveira, et al., 2012). It happens due to higher moisture content in the sample. Another reason for yellow liquid is due to super cooling and high surface energy (Heintz, et al., 2009).

4.3.1.4 S-5:

Regular prilling of ADN by melting in paraffin oil for comparison with other samples and then coated with 2% Poly acrylate solution in DCM. Sample spilled during processing and hence considered failed.

4.3.1.5 S-6:

ADN dissolved in acetone and then added to dichloromethane containing 2% Poly acrylate and 1% cab-o-sil. Then it was dried to obtain the ADN crystals.

4.3.1.6 S-7:

Repetitions of experiment S-5, to produce melt prilled ADN. However, the SEM analysis of the sample shows virtually no change in crystal morphology as shown in Figure 4-8.

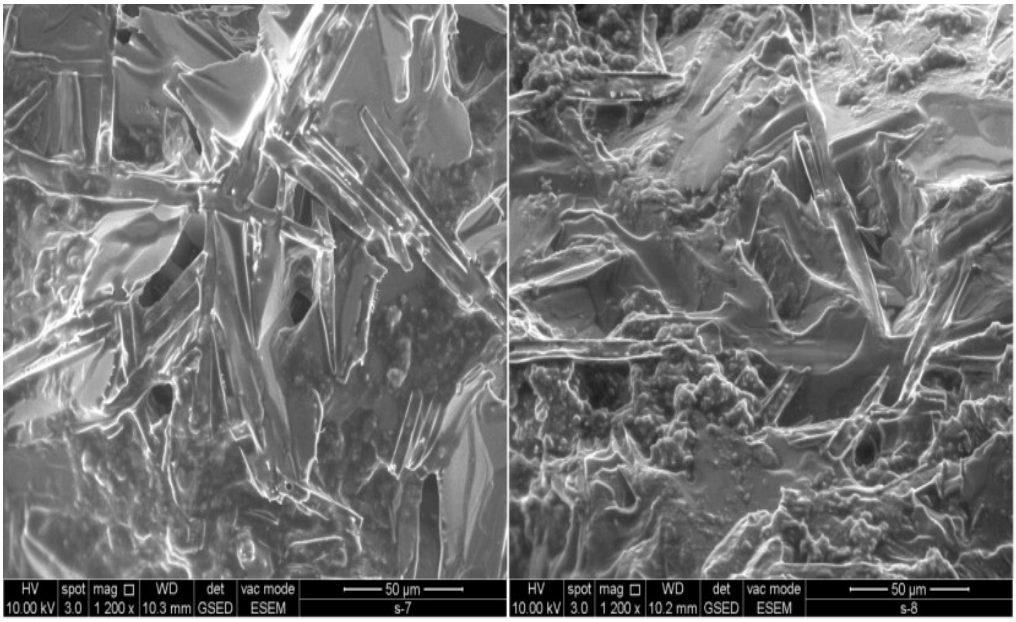

Figure 4-8 S-7(left) and S-8(right), produced by melt prilling of ADN showing no change in crystal morphology as compared to raw ADN as shown in Figure 4-6.

4.3.1.7 S-8:

Half of the prilled sample from experiment S-7 was coated with 2% polycarbonate and marked as S-8 in Figure 4-8.

4.3.1.8 S-9:

ADN was dissolved in acetone and mixed with dichloromethane containing 5wt. % polydimethylsiloxane (PDMS) and then dried to obtain the sample.

4.3.1.9 S-10:

Repetition of experiment S-9, but ADN failed to crystalize and turned into yellow liquid.

4.3.1.10 S-11:

Repetition of experiment S-9 and S-10, but samples obtained same as raw ADN, as shown in Figure 4-9.

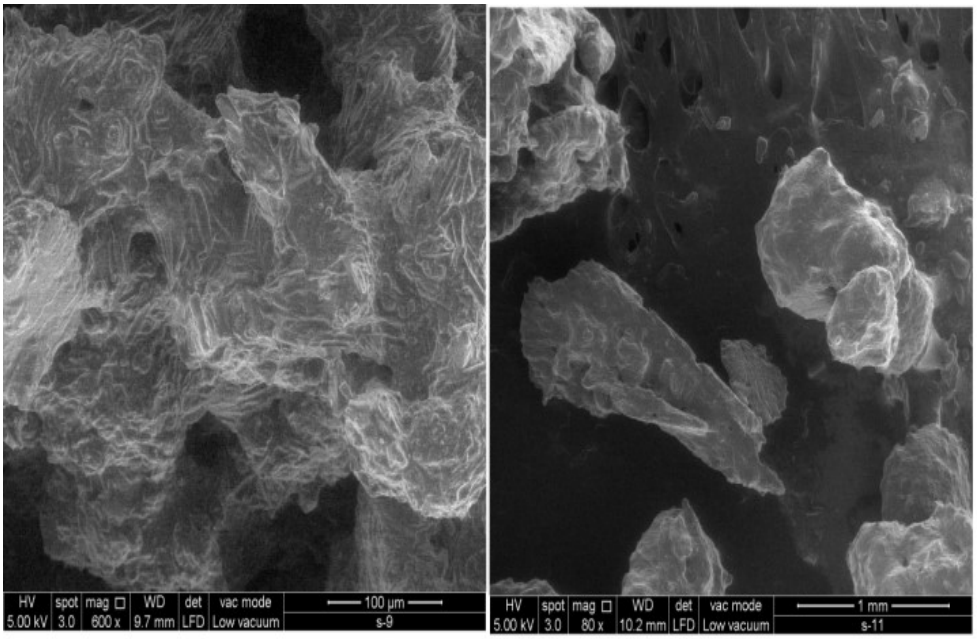

Figure 4-9 sample S-9 and S-11, showing no change in crystal morphology

4.3.1.11 S-12:

0.5 ADN was dissolved in acetone and mixed with 5wt. % epoxy in dichloromethane however sample failed to crystalize and turned into yellow liquid as it happened in experiment S-10.

4.3.1.12 S-13:

Paraffin oil was used as sonication medium for ADN at 80^{0}C, and the sonication was continued until ADN was melt and properly dispersed as the paraffin oil. The paraffin oil shows tendency of overheating and exceeding the sonicator-set temperature limit due to ultrasound vibrations. This overheating of the paraffin oil allows melting of ADN.

The sample was then divided into 2 parts, one part was washed with n-hexane and other part was centrifuged in order to remove paraffin oil. No additives were used in this experiment.

4.3.1.13 S-14:

Same procedure as experiment S-13, however, Cab-O-Sil was added to remove agglomeration in the sample as it was encountered in later dry stages of the sample in experiment S-13.

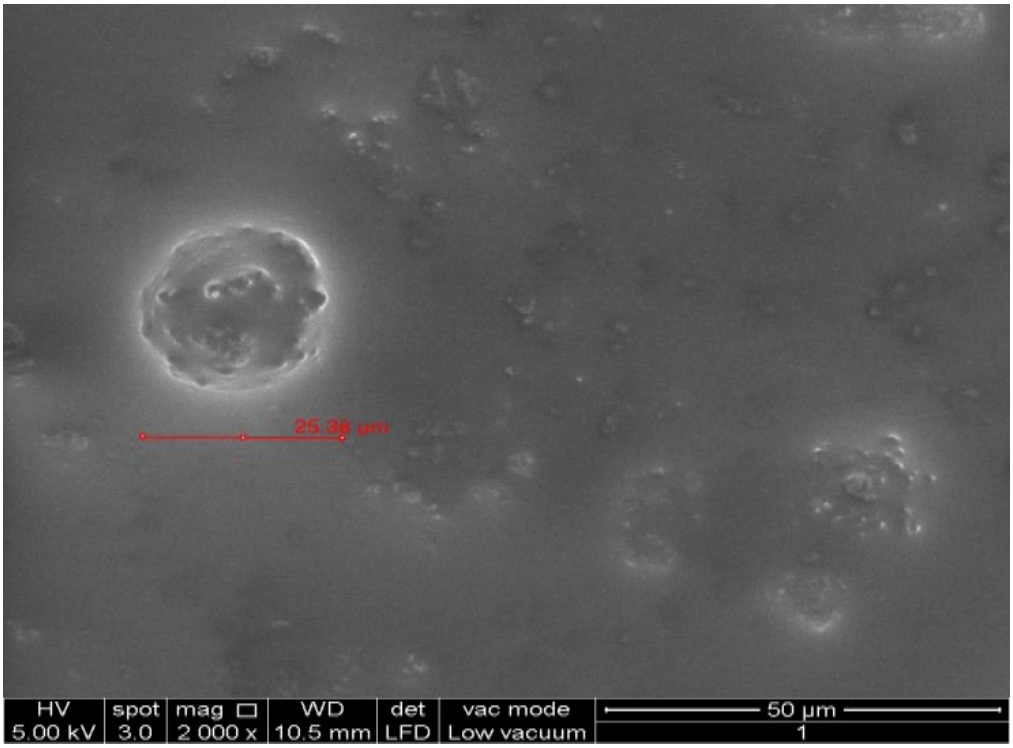

Figure 4-10 S-14, First attempt at sonication showing spherical ADN crystals. Ultrasound induced agitattion in molten ADN created tiny droplets of ADN, just like Melt prilling, which when cooled, converted into spherical particles.

4.3.1.14 S-15:

In this experiment, petroleum ether was used as non-continuous phase instead of paraffin oil, however it was evaporated during sonication and displayed poor dispersion properties with respect to ADN. Therefore, petroleum ether was not used again for sonication.

4.3.1.15 S-16:

ADN was sonicated in paraffin oil and then it was filtered to remove paraffin oil from ADN however, the pour size of filter paper was too big to retain ADN particles. In another attempt, Nano-filter paper was used but it also failed to yield because the process was extremely slow and the humid conditions caused liquefaction of the sample ADN.

4.3.1.16 S-19:

In this experiment, sonication was performed in toluene as non-continuous phase. Then it was coated with poly acrylate. In this sample, UV-spectrum was obtained to confirm that there was no sign of decomposition caused by sonication to ADN Figure 4-11.

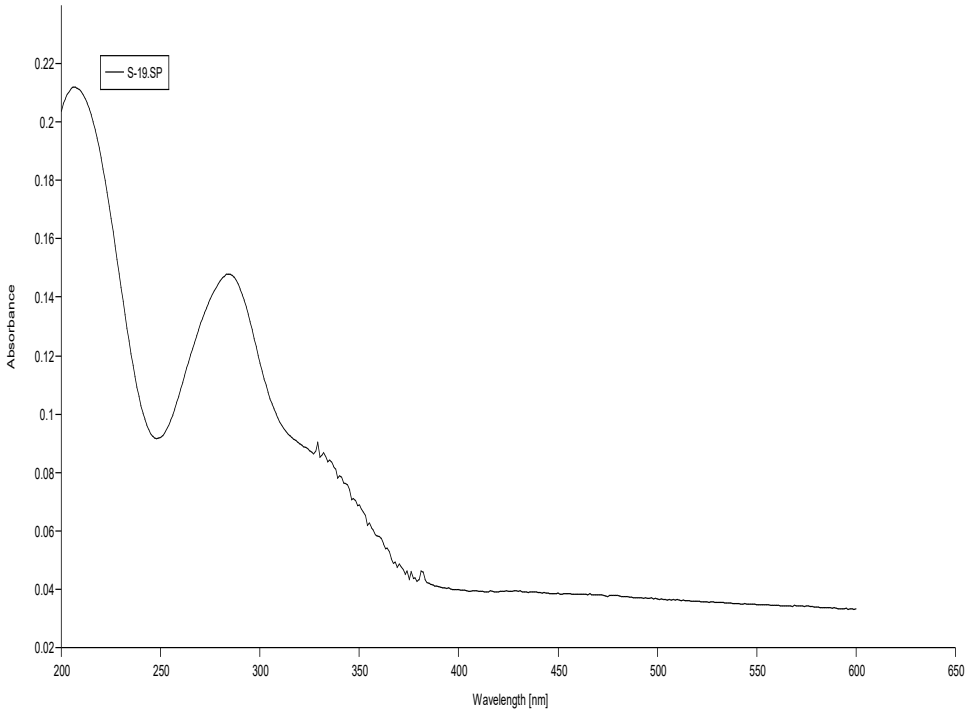

Figure 4-11 UV-spectrum of S-19 showing dinitramide ion peak at 284nm

4.3.1.17 S-20:

In this experiment, sonication of 0.5g ADN in paraffin was repeated. And centrifugal separation and filtration by diluting paraffin oil with n-hexane was

attempted. Followed by coating with poly acrylate was performed. Melting point of the sample was determined by DSC-TGA and was 89.42°C

4.3.1.18 S-21:

ADN was sonicated in paraffin oil, and was removed with partial success by multiple centrifuge operations with mixture of paraffin oil and dichloromethane. The sample was coated with methyl-metha acrylate and poly vinyl alcohol. Melting point of the sample was 92°C.

4.3.1.19 S-22:

In this experiment, ADN was sonicated in toluene along with CTAB and 10% coating polymer, i.e. poly methyl-metha acrylate. However, addition of hydrophilic coating polymer caused problems in proper dispersion of ADN.

4.3.1.20 S-23:

In this experiment, first n-hexane was tried as medium of sonication however due to its evaporation and poor dispersion of ADN, it was replaced with toluene, and the experiment was performed as per routine. It was coated with 3% poly methyl-metha acrylate by using dichloromethane solution which was precooled to -20^0C. The low temperature was used to avoid agglomeration of ADN particles and immediate crystallization, as ADN is prone to super cooling (Teipel & Heintz, 2005) (Heintz, et al., 2009). After mixing, the entire solution was evaporated at $45C^0$ temperature. Sample is shown in Figure 4-12 at different magnifications. Melting point of the sample was 91.48°C.

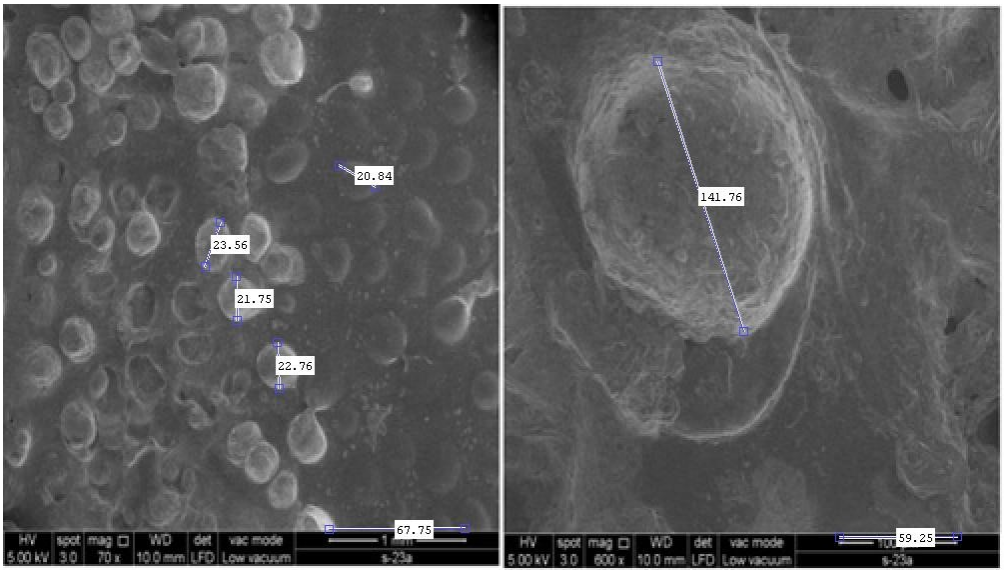

Figure 4-12 Sample S-23, on left side, at 1mm magnification shows spherical ADN particles with diamter in range of 200µm to 350µm range. , (1pixel=14.7um). In right side image, 1 particle was magnified and shows ADN particle with 230µm. (1pixel=1.6µm)

4.3.1.21 S-24:

ADN was sonicated in toluene at 80^{0}C for 1 hour at 37 khz and 100% power. The sonication medium was consisted of CTAB 3wt% and cab-o-sil 1wt%. After sonication, the sample was poured into dichloromethane solution containing 20% poly methyl-metha acrylate solution under strong agitation. It was dried completely to obtain the final sample. The sample turned into a thick agglomerated semi-solid due to higher polymer content. Melting point of the sample was 79°C. The use of poly methyl-metha acrylate as coating polymer was abandoned due to their hydrophilic nature. Melting point of the sample was 93°C.

4.3.1.22 S-25, S-26, S-27, S-28, S-29, S-30 and S-31:

In these experiments, ADN was sonicated in toluene along with additive like Cab-O-sil, graphene and CTAB. However, the coating polymer, i.e. Polystyrene 5-10wt% was also added into the toluene mixture to perform coating at the same time. In experiment S-27, Graphene was added to further decrease the agglomeration of ADN particles. All these experiments were

performed to obtain reproducibility and to find feasible experiment procedure. The images of the samples are shown in Figure 4-13 and Figure 4-14, and melting points of some the samples are shown in Table 4-2 .

Table 4-2 samples and their melting points according to DSC-TGA

Sample name	Melting point
s-27	93°C
s-29	79°C (impure stock ADN caused low MP)
s-30	77°C (impure stock ADN caused low MP)
s-31	92°C

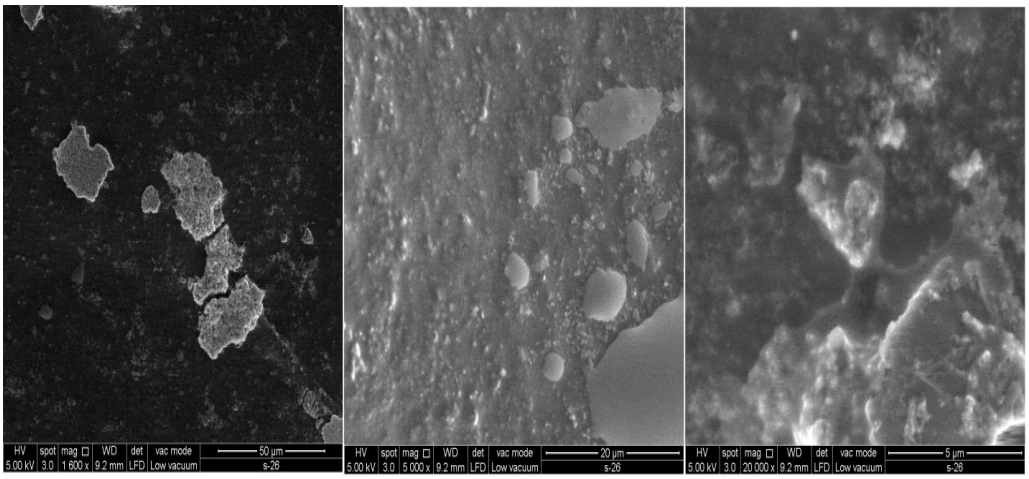

Figure 4-13sample S-26, at different levels of magnification

4.3.1.23 S-32, S-33 and S-34:

In these experiments, ADN was sonicated in similar way as it was it experiments S-25 to S-31, however the coating was performed by cellulose acetate.

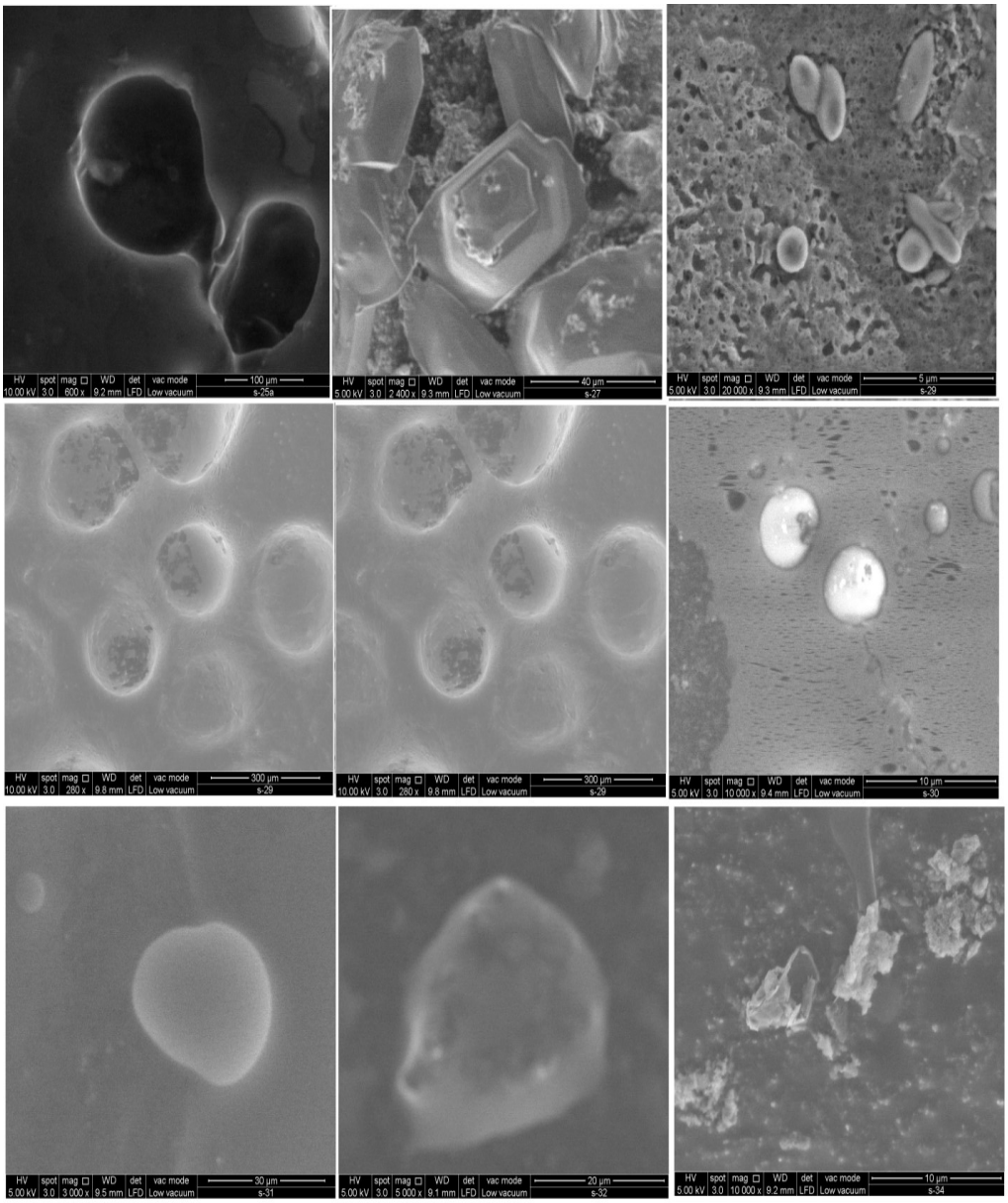

Figure 4-14 samples obtained from experiment S-25 to S-34 showing reproducibility of crystal morphology comprising of spherical and octagonal shapes as compared to raw ADN shown previously in Figure 4-6 .

4.3.1.24 S-35, S-36, S-37, S-38, S-39:

These experiments were performed with absence of Graphene, CTAB or Cab-O-Sil to determine their effect on ADN sonication samples.

4.3.1.25 S-40:

This experiment was repetition of Polystyrene 5wt. % coating

4.3.1.26 S-41and S-42:

In this experiment, ADN was coated with 20wt. % HTPB. The composition of HTPB was 0.17g HTPB, 0.015g Toluene di-isocyanate (TDI), and 0.015g glycerol. Where, TDI was used as curing agent for HTPB and glycerol was used as curing catalyst. Due to very high polymer content, sample obtained by the experiment was in the form of polymeric lumps. The SEM images of the samples showed homogenized matrix of ADN with HTPB as shown in Figure 4-15 and Figure 4-16.

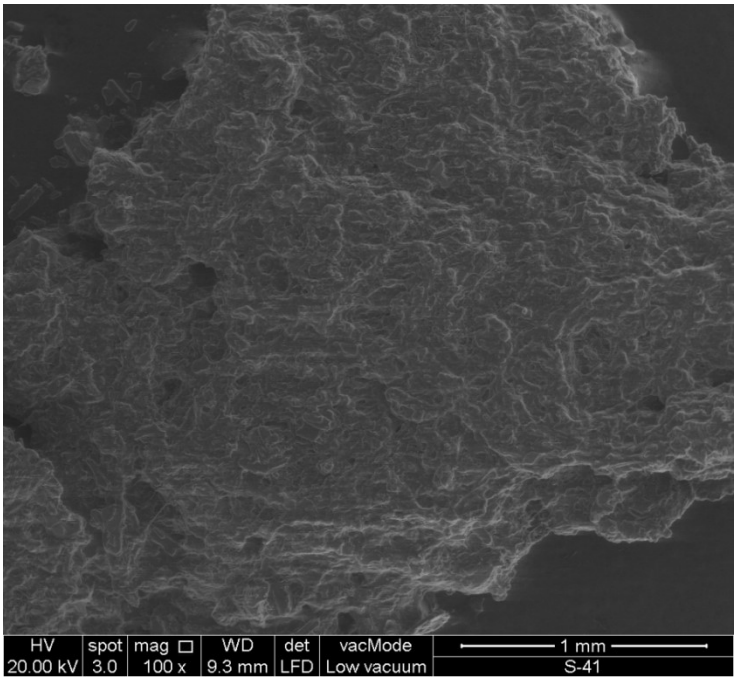

Figure 4-15 Homogenized mixture of ADN and HTPB polymer (S-41). In 20wt. % HTPC coated samples, ADN particle size and shape was not visible due to thick polymer coating.

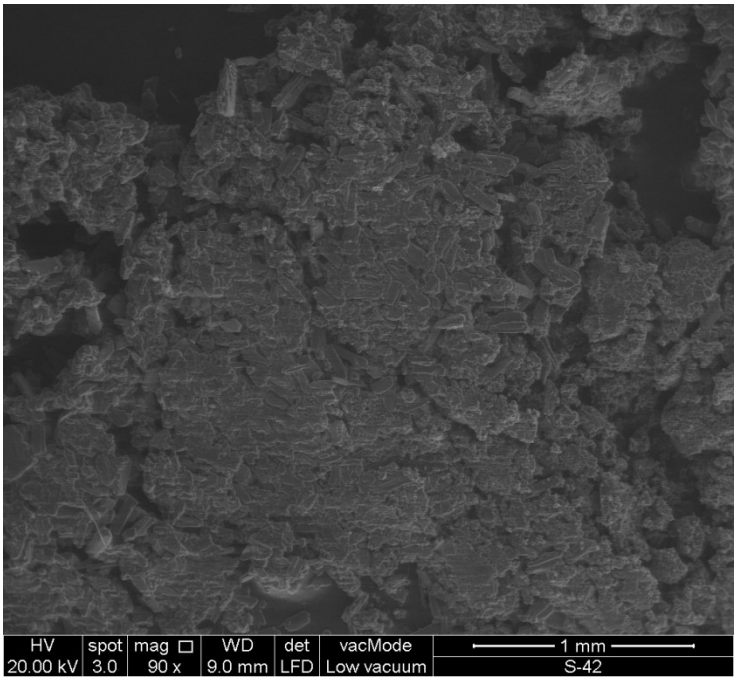

Figure 4-16 ADN and HTPB composite (S-42), a repitation of exp S-41, shows identical texture as that of S-41.

4.3.1.27 S-43

In this experiment, ADN was coated with 5wt. % HTPB

4.3.1.28 S-45

This sample was obtained by conventional melt prilling and coated with 5wt. % PS as shown in Figure 4-17.

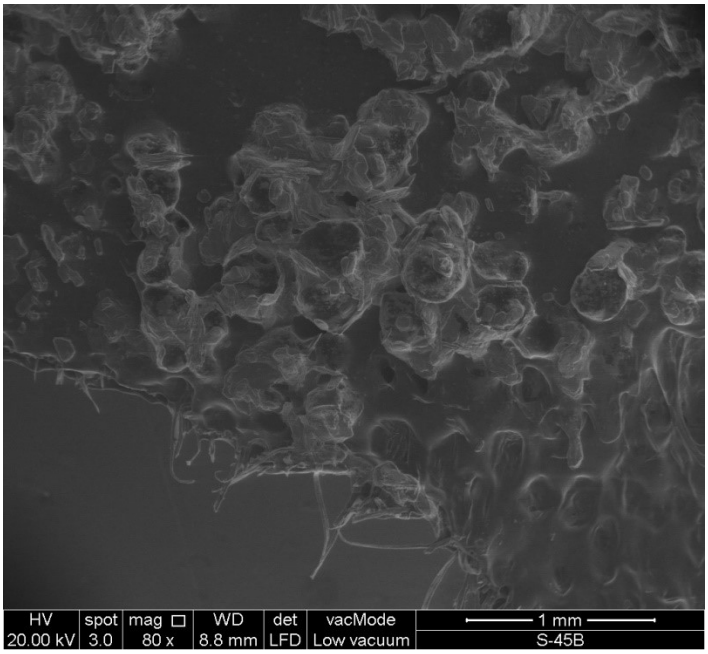

Figure 4-17 S-45, this sample was obtained for comparision of sonicated ADN samples with Melt prilled samples.

4.3.2 Results and discussion:

The main objective of these experiments was to alter crystal morphology of as synthesized, raw ADN particles in to spherical or low aspect ratio particles, which could offer better TMD. Furthermore, due to higher moisture absorption of ADN particles, it was necessary to perform hydrophobic polymer coating. The main issue with existing method was the use of molten ADN during the process, which leads to decomposition of ADN particles, and was inherently dangerous process. Therefore, a new method based on ultrasound treatment was utilized for alteration of ADN crystal morphology, and hydrophobic polymer coating was incorporated in the method as well. The main criterions for ultrasound treatment of ADN were selection of suitable sonication medium. In this case, an organic liquid, which has no solubility towards ADN and solubility toward coating polymer, was highly desirable. Furthermore, the boiling point of the said organic liquid should be high enough to sustain ultrasound treatment without evaporation because, ultrasound increases rate of natural evaporation by means of increasing surface area between air and liquid surface (Spotar, et al., 2015). Another important criterion for sonication medium was ease of removal, which in this case implies vacuum evaporation.

Vacuum evaporation was necessary because it removes the excess solvent (organic liquid) without exposure to atmosphere, which was highly humid.

Apart from sonication medium, other important parameters to determine practicality of this process were the ability to alter crystal morphology of ADN particles, reduction in moisture absorption and identical performance as that of raw ADN. The performance of sonicated ADN particles was determined by means of DSC-TGA testing and compared with each other.

4.3.2.1 Selection of sonication medium and polymer:

The major criteria for sonication of any substance are the selection of suitable liquid medium. ADN sonication requirements include good dissipation of ADN, insolubility towards ADN, solubility of coating polymer, high boiling point to sustain sonication at 60^0C and ease of removal at the end of experiment. Among all the solvents tested, only toluene was able to perform well in all aspects. Other solvents that were tested include petroleum ether, n-hexane, Paraffin oil and dichloromethane. The usage of highly volatile solvents such as n-hexane, dichloromethane, and dichloroethane was abandoned on the account of their poor dissipation of ADN particles and evaporation during sonication. The use of paraffin oil as sonication medium was abandoned on the account of polymer insolubility and difficulty of removal. The reduction in particle size is dependent on surface tension of solids (σ) (Teipel & Heintz, 2005).

The surface tension results from difference of surface energy between fluid and gas or between two immiscible liquids. The interfacial tension (γ) is the measure of interfacial energy between two immiscible fluids, either solid-liquid or liquid-liquid, and is given as (Teipel & Heintz, 2005):

$$\gamma_{12} = \gamma_1 + \gamma_2 - 2.\left(\gamma_1^d.\gamma_2^d\right)^{\frac{1}{2}} (1)$$

Where γ_{12}: interfacial tension, γ_1, surface tension of fluid 1 and γ_2, surface tension of fluid 2. In this case, fluid 1 and 2 would be the combinations of ADN, Toulene, Polystyrene (PS), and graphene with each other.

In addition, expression $\left(\gamma_1^d.\gamma_2^d\right)$ Represents dispersion forces at interface of two different materials and their combinations such as ADN, PS, toluene, etc (Teipel & Heintz, 2005). However, the value of dispersion forces can be assumed to be 1, giving (Agrawal, 2005):

$$\gamma_{12} \approx \left(\gamma_1{}^{\frac{1}{2}} - \gamma_2{}^{\frac{1}{2}}\right)^2 \quad (2)$$

And the relation between surface tension and solubility parameter (δ), is given as (Krevelen & Nijenhuis, 2009, p. 230):

$$\delta = 4.1\left(\gamma/V^{1/3}\right)^{0.43} \quad (3)$$

Furthermore, the interfacial energy is affected by crystal structure of ADN. The wetting is favored if the surface energy of solid is higher than surface tension of liquid and low interfacial energy (Krevelen & Nijenhuis, 2009, p. 232). The surface tension of ADN melt ($\sigma = 89mN/m$) (Teipel & Heintz, 2005) is very high due to hydrogen bonding and polarity, compare to water= $72mN/m$, while toluene has a surface tension of $\sigma = 28.4mN/m$. The difference in surface tension hence favors proper wetting and dispersion of ADN in toluene, which is further enhanced by elevated temperature i.e. 60^0C due to inverse temperature dependence of hydrogen bonding. Addition of cationic surfactant, CTAB, with an estimated (hydrophilic-lipophilic balance) HLB equivalent number 13+ (ICI Americas Inc, 1980, p. 21), fail to disperse ADN in highly volatile solvents (BP<50~60^0C). The application of ultrasound irradiation increases surface area between the solid-liquid interfaces and hence contributes to rapid dispersion.

The surface tension $\gamma_{liquid(ADN\ melt)}$ correlates to surface energy, which is used to describe surface tension of solids, σ_{solid}, by (Aqra & Ayyad, 2011):

$$\sigma_{solid} \cong \frac{\gamma_{liquid}}{0.713} \quad (4)$$

From the correlation above, based on bond breaking rule, surface free energy of ADN estimated to be $\sigma_{ADN} = 124.8mN/m$.

Using value of σ_{ADN}, the interaction force between different components of the system were calculated as shown below (Table 4-3) with data from Krevelen (Krevelen & Nijenhuis, 2009, p. 242).

Table 4-3 Interface energy of different components calculated using eq.2

Interface components	Interface Energy
ADN-Toluene	$\gamma_{ADN-Tl} = 34.7 mN/m$
ADN-PS	$\gamma_{ADN-PS} = 22.01 mN/m$
ADN-graphene	$\gamma_{ADN-gr} = 18.82 mN/m$
Toluene-PS	$\gamma_{Tl-PS} = 1.43 mN/m$
Toluene-Graphene	$\gamma_{Tl-PS} = 2.40 mN/m$
Graphene-PS	$\gamma_{gr-PS} = 0.124 mN/m$

The PS and graphene adhesion to ADN can be described by work of adhesion as given by:

$$W_{adh} = \gamma_{s1} + \gamma_{s2} - \gamma_{s1s2} \qquad (5)$$

$$where, \qquad \gamma_{s1s2} = \left((\gamma_{s1})^{\frac{1}{2}} + (\gamma_{s2})^{\frac{1}{2}}\right)^{\frac{1}{2}}$$

Table 4-4 Work of Adhension calculated for different components of the system

Components	Work of Adhesion
ADN-PS	$W_{adn-ps} = 144.81\ mN/m$
ADN-graphene	$W_{adn-gr} = 169.11\ mN/m$
PS-graphene	$W_{Ps-gr} = 88.57\ mN/m$

Work of Adhesion values as shown in Table 4-4, shows good adhesion of ADN to PS ($W_{adn-ps} = 144.81\ mN/m$), because as general rule, negative value of W_{adh} represents poor adhesion and reversibility of the process. Similarly, adhesion of graphane(gr) (Wang, et al., 2009) $(\gamma_{gr} = 46.7 mN/m)$ toward ADN and PS was calculated to be $W_{adn-gr} = 169.11 mN/m$ *and* $W_{gr-ps} = 88.57\ mN/m$ shows good compatibility among them.

Another reason that favors the use of toluene was its boiling point as compared to paraffin oils, which keeps the temperature within set range and do not causes self-heating induced by high intensity agitation by ultrasound.

4.3.2.2 Crystal morphology and particle size:

The crystal structure and size was analyzed by SEM. Long needle like crystal morphology of raw ADN is again shown here as Figure 4-18 for ease of comparison, and compared with reported SEM image of raw ADN as shown in Figure 4-19 (Heintz, et al., 2009). Raw ADN was converted to spherical ADN particles by sonicated and coated with PS (5wt. %) as shown in Figure 4-20. In comparison, melt prilled ADN coated with PS (5wt. %) is shown in Figure 4-21 and literature reported SEM of prilled ADN is shown in Figure 4-22. The particle diameter or dimensions were calculated by Matlab image processing feature. In this feature, pixels were converted to µm by using SEM's calibration scale.

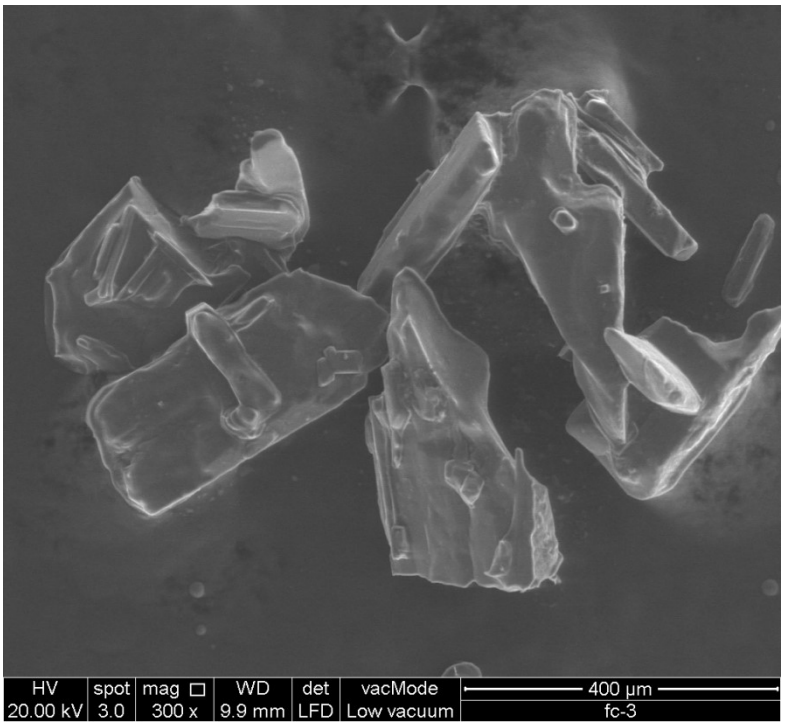

Figure 4-18 SEM image of Raw ADN used in these experiments, shows long needle like shape with high aspect ratio.

Figure 4-19 SEM image of ADN (Heintz, et al., 2009) showing needle like structure.

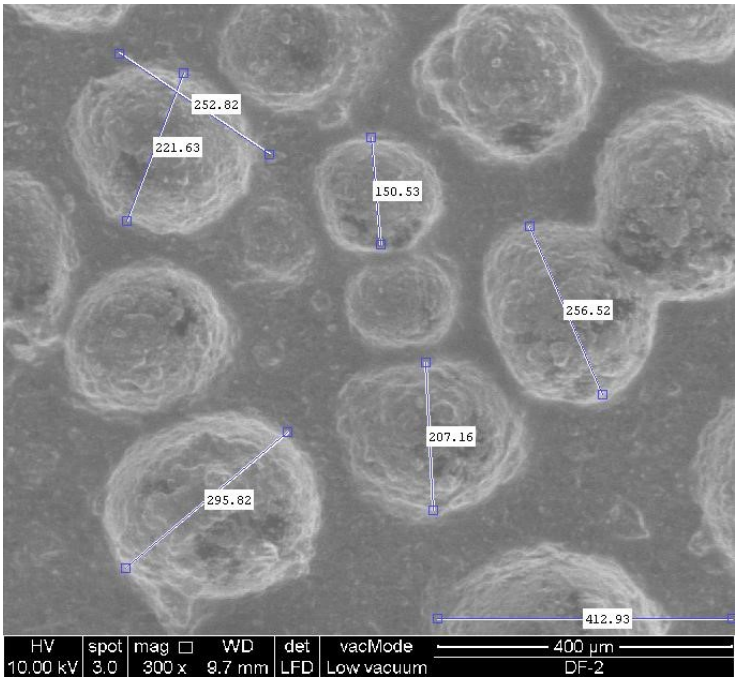

Figure 4-20 SEM image of ADN sonicated and coated with PS (5wt. %)shows spherical particles. The particle diameter ranges from 155µm to 230µm range. (1pixel=1.03µm)

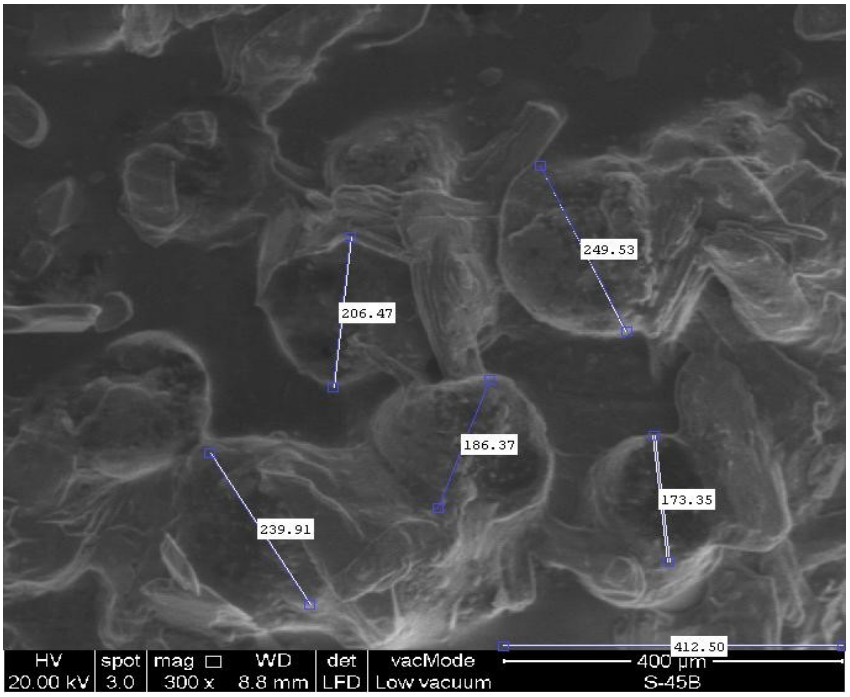

Figure 4-21 SEM image of ADN Melt Prilled, and coated with PS (5wt. %) shows some particles converted to spherical shape and some still in their original shape. The particle dimater ranges from 178µm to 255µm.(1pixel=1.03µm). However, particle agglomeration is visible as different particles are joinned together.

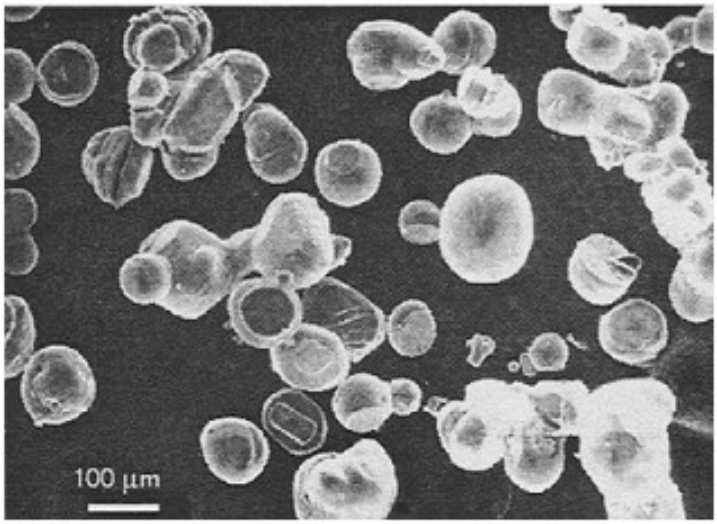

Fig. 1. Micrograph of the ADN prills made by the "prilling tower" technology at Thiokol.

Figure 4-22 Literature reported image of prilled ADN, produced by melting prilling in paraffin oil (Ramaswamy, 2000).

The crystal morphology obtained by sonication is similar to the one obtained by melt prilling process and have spherical shape. The average crystal size determination was not possible by Zeta-sizer due to presence of Cab-o-sil and graphene, which were already in micro and nano meter range respectively. However, from SEM images, Figure 4-20, and Figure 4-21 it can be inferred that particle are in 200µm to 300µm range.

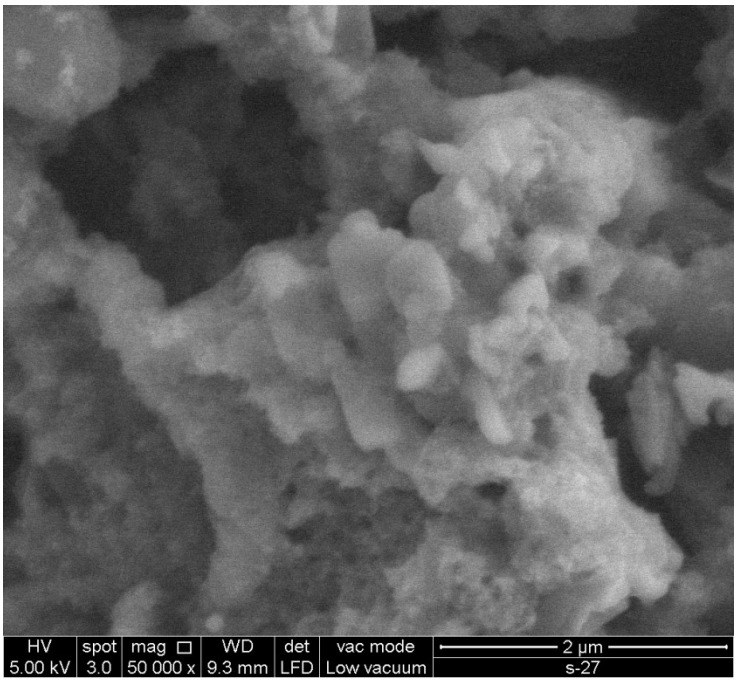

Figure 4-23 Sonicated and PS coated ADN, surface roughness at close-up. The surface roughness increases the distance between particles to reduce agglomration which arises from surface energy. Secondly, the rough surface decreaes the moisture absorption by means of lotuf leaf effect.

Agglomeration was very high in melt prill samples as compared to sonicated sample. The reduction in agglomeration is partly attributed to cab-o-sil as discussed previously, but the major contributing factor for agglomeration inhibition was cationic surfactants and graphene. In experiments without cationic surfactant CTAB and graphene, ADN failed to disperse properly in toluene and some of it remained at the bottom even after up to 3 hours of sonication. The cationic surfactant was believed to reduce the agglomeration because of its low surface energy lipophilic anion. Moreover, the surface roughness is introduced by graphene particle as shown Figure 4-23, which

increases the distance between crystals (Svetovoy & Palasantzas, 2015) and hence reduces attractive forces to further reduce agglomeration.

4.3.2.3 Moisture absorption:

The high moisture absorption in ADN is due to the hydrogen bonding in its crystal structure and can only be overcome by physical means. The moisture absorption testing of ADN coated with hydrophobic polymer i.e. polystyrene embedded with graphene flakes shows reduction in moisture absorption as shown in Figure 4-24. The graphene is hydrophobic material (Wang, et al., 2009) and acts as moisture barrier because of its high aspect ratio (Chang, et al., 2014) (Luechinger, et al., 2008). From the results, it was identified that moisture absorption was lowest for sample coated with, 20wt. % HTPB, however 20wt. % HTPB creates ADN-HTPB matrix or paste rather individual particles (Figure 4-15, Figure 4-16). Therefore, the most suitable coating percentage is 5wt. % with either HTPB or PS. In addition, the moisture absorption of similarly coated samples from sonication and prilling was almost identical in both PS and HTPB based samples, which also suggests the feasibility of sonication as alternate to prilling.

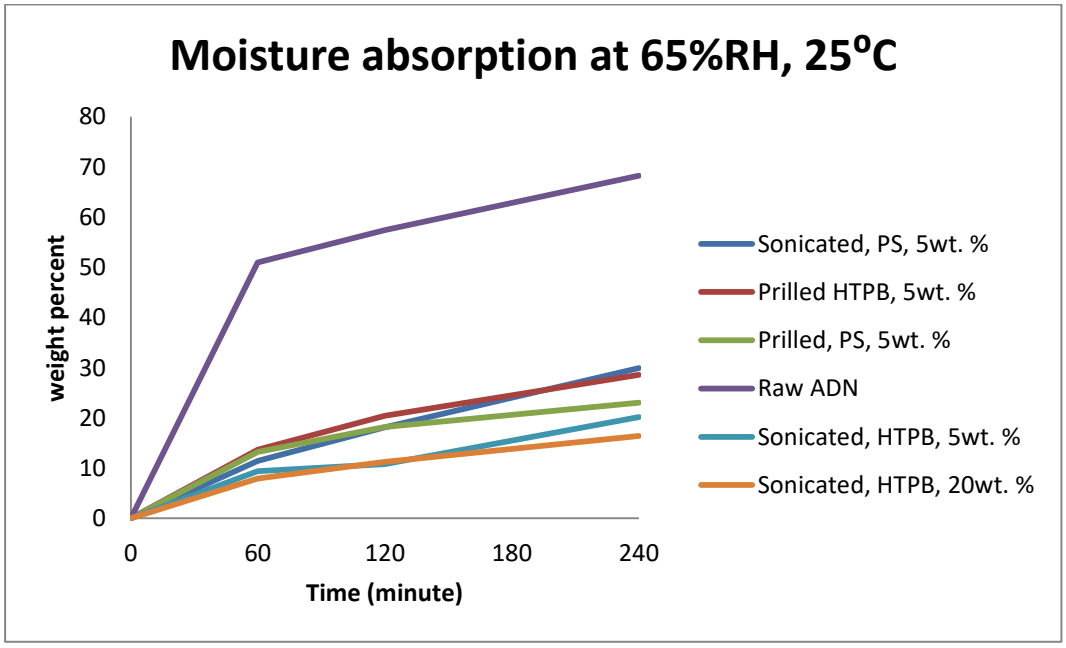

Figure 4-24 :Moisture absorbance of raw ADN and ADN samples prepared bysonication and prilling.

4.3.2.4 Effect of Additives:

Several attempts were made to produce sonicated ADN samples without graphene, CTAB and cab-o-sil. The attempts to sonicate ADN without CTAB resulted in prolonged sonication time and approximately 1/3rd of 0.5g ADN was suspended in the toluene after 180min of sonication. In attempts to produce samples in presence of CTAB but without graphene and cab-o-sil resulted in suspension of the ADN in toluene but became agglomerated during the drying and evaporation step.

The chemical formula of CTAB is shown in Figure 4-25. It is observed that it consists of anionic long carbon chain (19 carbons) and a relatively weak methylammonium bromide cation, which makes it cationic surfactant (Smith & Korgel, 2008).

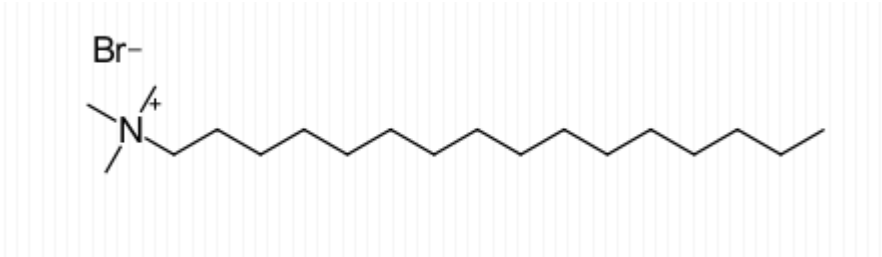

Figure 4-25 Structure of CTAB (Smith & Korgel, 2008)

In case of its usage in ADN sonication, it is estimated that the cationic part i.e. tetramethylammonium bromide attracts ADN because of the overall negative charge of ADN structure. Furthermore, the anionic part of CTAB attracts methyl pendant group of toluene by virtue of partial charges leading to proper suspension of ADN in toluene.

Furthermore, the Cab-Sil is added as protective colloid to promote emulsification and reduction in viscosity (Teipel, et al., 2000). Chemical formula of Cab-O-Sil is silicon dioxide (SiO_2) (Teipel, et al., 2000). The decrease in viscosity and non-Newtonian behavior provides better mechanical energy transfer to surface boundary regions, which in this case is between toluene and ADN. Furthermore, it also decreases the agglomeration of particles by inducing steric hindrance (Teipel, et al., 2000). In this case,

mechanical energy to reduce ADN particle size is provided by ultrasound radiations.

The use of graphene in energetic materials is a novel concept, and so far, it has only been reported for few propellants with improvements in thermal stability (Sabourin, et al., 2009), but it has been used extensively to impart hydrophobic properties into polymers, where it act as physical barrier or produces lotus leaf effect to reduce moisture absorption. Based on these properties, graphene was added into the ADN suspension during sonication to reduce moisture absorption. In addition, graphene usage is estimated to decrease agglomeration in the ADN particles by increasing distance between ADN particles. During moisture absorption testing and thermal analysis it was revealed that the addition of graphene in small quantities does not affect performance of ADN.

4.3.2.5 Thermal analysis:

DSC-TGA results obtained for the samples are shown in Figure 4-26 and Figure 4-27. In Figure 4-28 and Figure 4-29, literature reported DSC curves of raw and prilled ADN are shown for comparison purposes.

In DSC-TGA test of raw ADN, it shows two peaks in the range of 130~220^{o}C range (Yang, et al., 2005) (Matsunnaga, et al., 2012). The first peak indicates decomposition of dinitramide ion and produces ammonium nitrate and N_2O. The second peak, which is minor peak as compared to first peak, indicates decomposition of ammonium nitrate (Matsunnaga, et al., 2012). The exact onset of each peak depends on purity, crystal structure, heating rate and method of testing (Jones, et al., 2005) (Teipel, et al., 2000). The melting point, enthalpy of reaction, and weight loss during the testing was calculated by proprietary Mettler star-E software as discussed previously in section 4.2.9.

The decomposition details from DSC-TGA (Figure 4-26 and Figure 4-27) tests are compiled in Table 4-5 along with reference data. The DSC graph (Figure 4-26) obtained for the samples in these experiments, shows identical results with exception of sonicated HTPB 20wt. %, coated sample where higher quantity of HTPB is considered as reason for delayed burning because it serves as fuel in composite solid fuels.

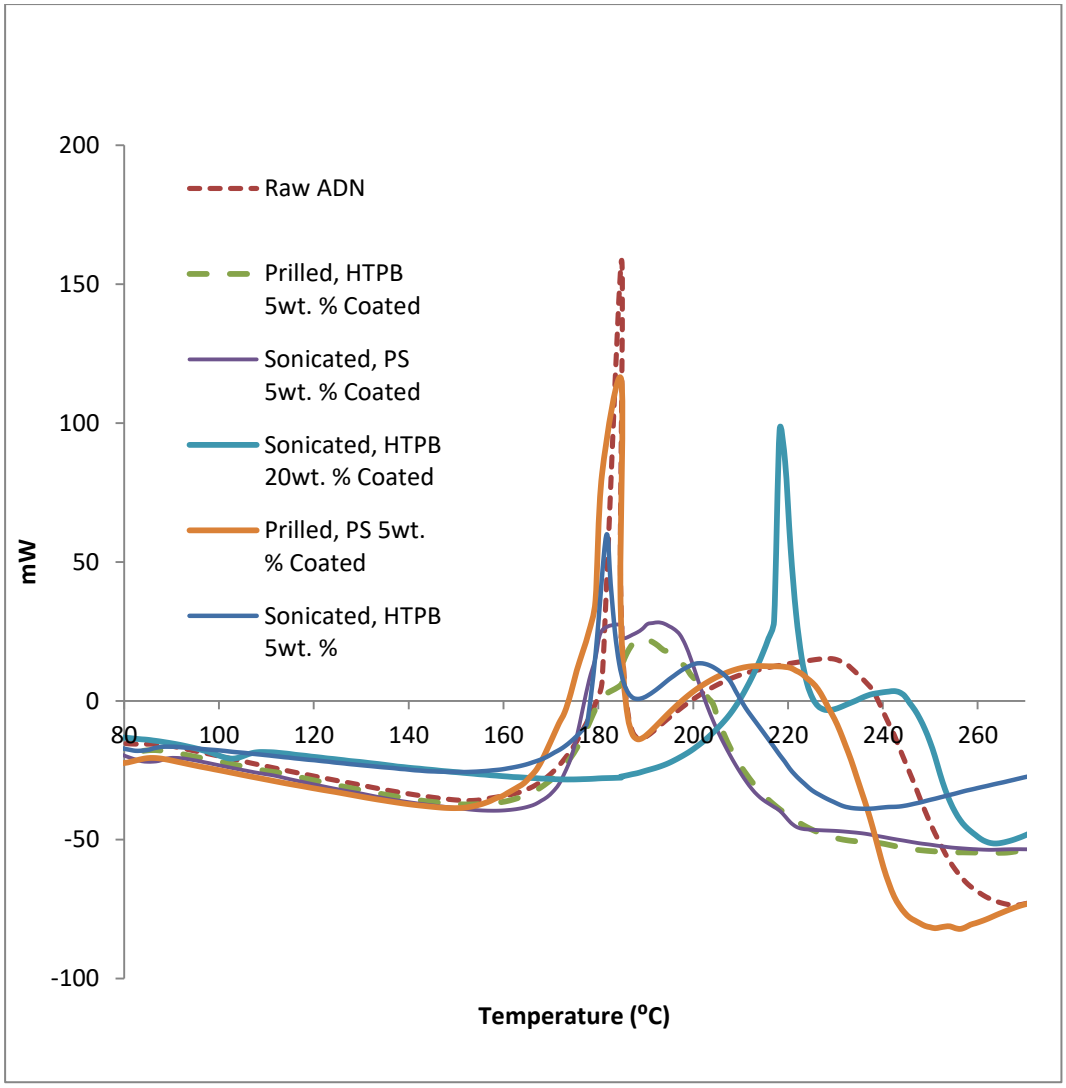

Figure 4-26 Thermal decomposition in DSC obtained for samples at 10^{0}C/min heating rate.

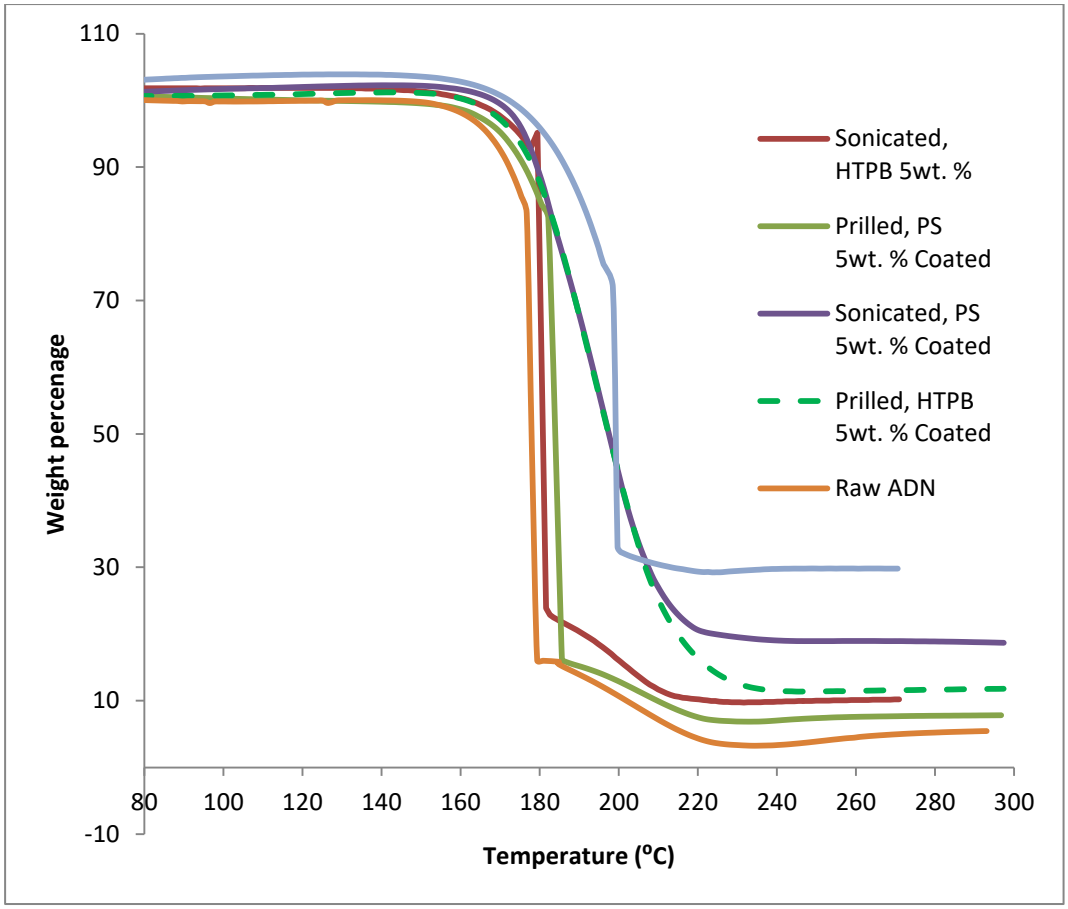

Figure 4-27 TGA obtained for sample at 10^0C/min heating rate

Table 4-5 Details of thermal testing

	Decomposition onset temperature (^{0}C)	Weight loss at decomposition temperature (wt. %)	Enthalpy of decomposition (KJ/g)	Peak (^{0}C)
Raw ADN	177.54	88.96	1.86	193.39
Prilled, PS, 5wt. % coated	181.25	92.2	3.359	186.92
Prilled, HTPB, 5wt. % Coated	170.11	89.72	2.197	190.40
Sonicated, PS,5wt. % coated	171.21	83	1.812	192.74
Sonicated, HTPB 5wt. %	178.53	91.81	1.785	181.34

coated				
Sonicated, HTPB 20wt. % coated	196.91	73.15	2.626	198.94
raw ADN (Figure 4-28,A) (Teipel, et al., 2000)	126.79	--	1.97	159
Prilled ADN (Figure 4-28,B) (Teipel, et al., 2000)	146.92	--	2.157	176
Prilled ADN (Figure 4-29) (Tompa, 2000)	168.08	--	2.019	195.41

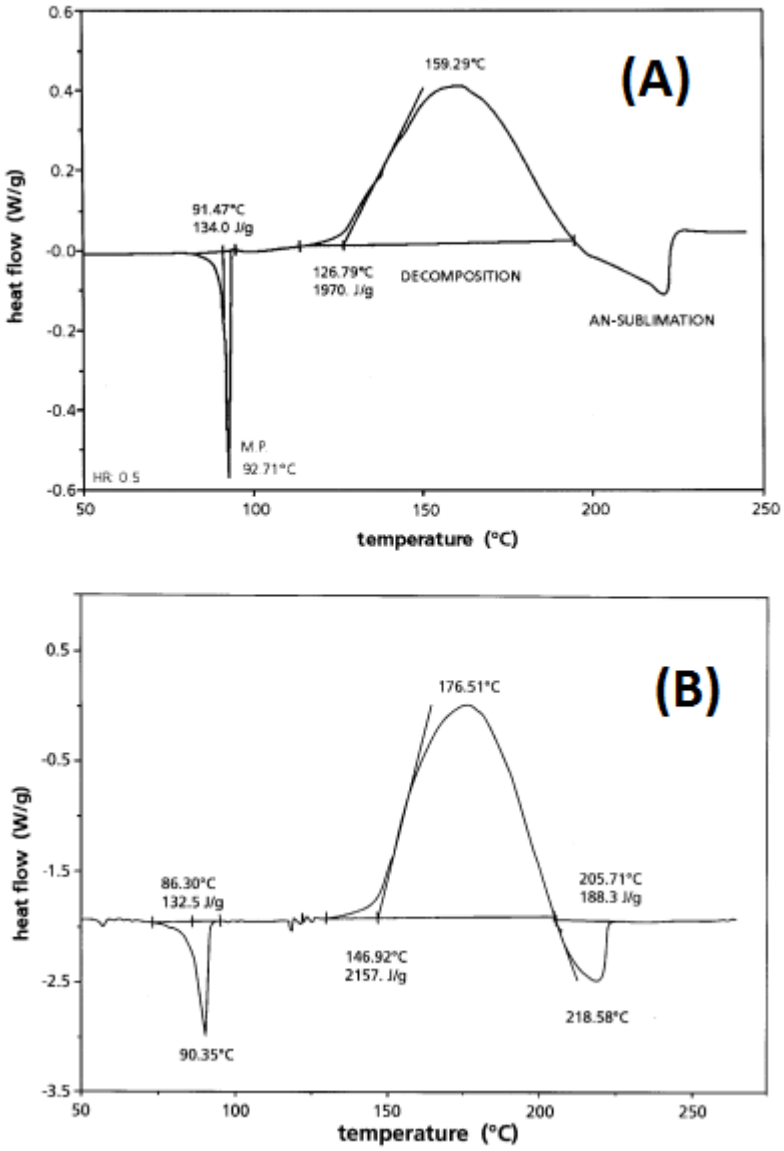

Figure 4-28 Reference prilled ADN DSC curves of raw ADN (A) and prilled ADN (B) (Teipel, et al., 2000)

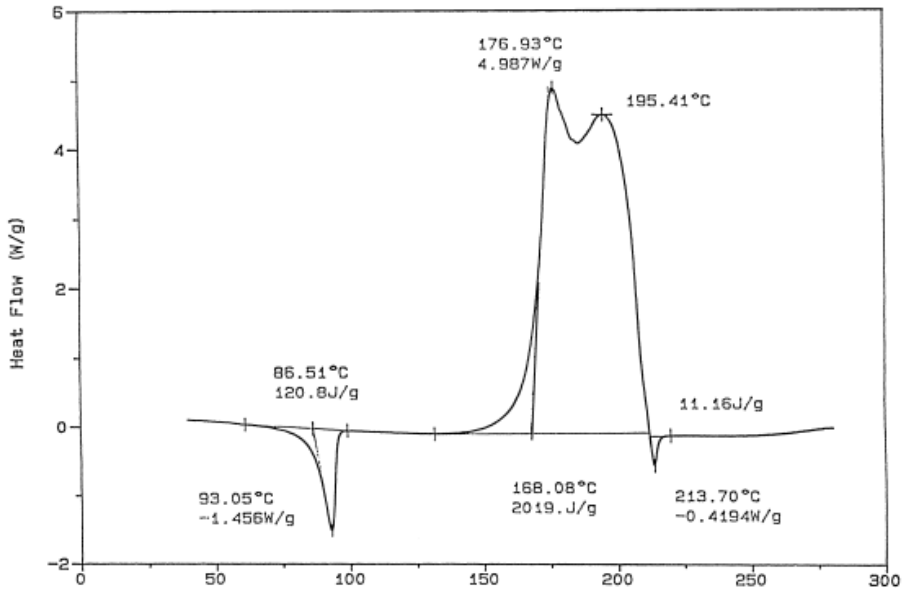

Figure 4-29 Reference prilled ADN DSC (Tompa, 2000)

Similar trends in TGA (Figure 4-27) were also noted, where sonicated, HTPB 20wt% coated sample begun deposition at the highest temperature as compared to all other samples. The overall heat release (enthalpy) during combustion i.e. 1.785-3.359Kj/g (220-416Kj/mol) was in agreement with published values (Vyazovkin & Wight, 1997) (Bottaro, et al., 1997) (Jones, et al., 2005) and as it is shown in Figure 4-28, and Figure 4-29, where it is reported to be 1970~2157j/g (1.97~2.157Kj/g) range (Teipel, et al., 2000).

4.4 Conclusions:

In this method, ADN is suspended in toluene along with cab-o-sil and graphene, which acts as agglomeration inhibitors and CTAB as cationic surfactant to assist in formation of suspension and reduces the sonication time. The optimum results were obtained when 2wt. % Cab-o-sil, 2wt. % CTAB and 1wt. % Graphene was used as additive and 5wt. % polystyrene or HTPB was used for coating of ADN which shows good adhesion as well. The use of these additives and sonication itself did not compromise the thermal stability of ADN as compared to raw and melt-prilled ADN. Furthermore, the crystal morphology and particle size obtained via sonication is comparable to conventional method.

Chapter 5. Electrolytic Decomposition of Ammonium Dinitramide Based Liquid Mono-Propellants in PDMS Micro-Thrusters

5.1 Introduction:

This chapter focuses on electrolytic decomposition of ADN based fuel FLP-103. The ADN used in these experiments was synthesized by conventional ultralow temperature method. The Micro Thrusters and open-beakers used in the electrolysis experiments were fabricated with PDMS via soft lithography technique. Furthermore, video recording and thrust measurement via load cell evaluated the decomposition phenomenon. The detailed background to this project can be found in section 2.10.

5.2 Design considerations, fabrication, and experimental details:

5.2.1 Ammonium Dinitramide based liquid monopropellant Fuel:

The synthesized ADN was converted into monopropellant named as FLP-103 (Appelgren, et al., 2005), having composition ADN 63.4wt. %, water 25.3wt. %, methanol 11.2wt. % and urea 0.1wt. % as shown in Table 5-1. It was prepared by dissolving ADN in deionized water followed by addition of methanol and 0.1wt. % urea as stabilizer. Fuel supply was maintained via syringe pump.

Table 5-1 Propellant composition

	ADN	Methanol	Water	Urea
Formula:	$NH_4N(NO_2)_2$	CH_3OH	H_2O	$CO(NH_2)_2$
Δhf (Kj/mol)	-148	-238.5	-285.8	–333.19 kJ/mol
Weight percentage	63.4%	11.2%	25.4%	0.1%

Density ($gm./cm^3$)	1.84	0.7918	1	1.32

5.2.2 Design considerations:

The design of thruster and its performance is based on performance, characterization, mass flow and ratio of nozzle exit area (Ae) to nozzle throat area nozzle (At), also known as nozzle expansion ratio (Ae/At). These parameters determine the under, over or optimized expansion of the exhaust gases in a given exit pressure (Zhang, et al., 2005). Furthermore, these parameters were determined according to fuel combustion properties, However due to lack of available data for ADN mono-propellant specific optimized thruster specifications in micro scale, especially under electrolytic conditions, A scaled down specifications of a conventional macro thruster was utilized for these experiment with expansion ratio of 4 (Wingborg, et al., 2006). The throat diameter was selected as 250µm due fabrication limit of the cutting plotter.

The thruster was designed as combination of engraving and embossing device, so that both panels can interlock into each other and offer lateral support to inhibit fuel leakage around fuel supply lines and combustion chamber (Figure 5-1). Secondly, to eliminate backpressure and consequently thrust fluctuations, 90° bents were introduced between fuel injection and combustion chamber. These thrust fluctuations could also be attributed to flexibility of PDMS substrate, or inconsistent fuel supply from the syringe pump. However, preliminary tests with straight-fuel-line and with 4-bent-fuel-line showed thrust fluctuations. Therefore, the design used for the experiments reported here (Figure 5-1), consisted of 6-bent-fuel-line did not show fluctuations, hence suggesting the significance of the bends in the fuel line. Furthermore, the dimensions of the combustion chamber are mentioned in Figure 5-2.

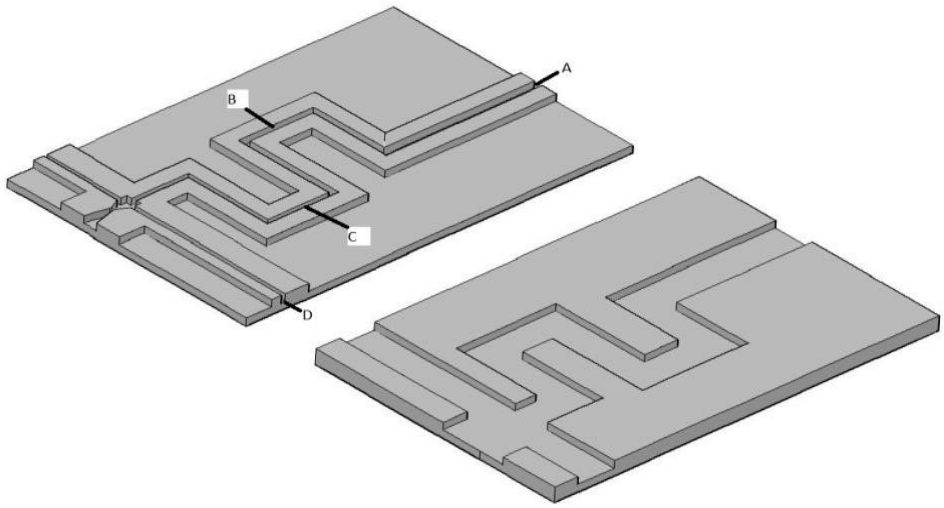

Figure 5-1 AutoCAD rendered image of both sides of the actual thruster, channel width= A: 600µm, B: 400µm, C: 300µm, D: 250µm. The interlocking design offered ease of allignemnt and eliminated leakages.

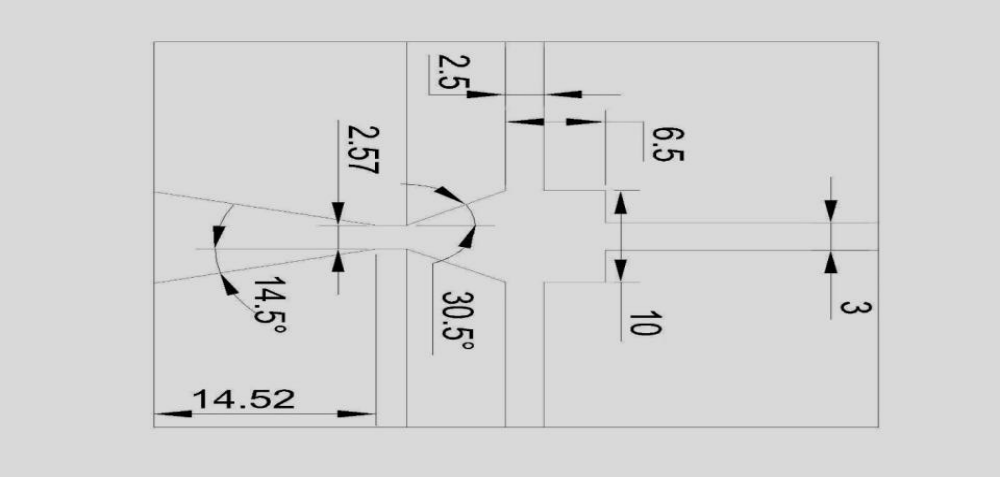

Figure 5-2 Combustion chamber dimensions (scale: 1=100micron).

5.2.3 Fabrication of micro thruster:

The micro thruster fabrication was performed via soft lithography method. First, thruster layout was design in AutoCAD and plotted (Graphtec CE5000 plotter) on 2-layer vinyl sheet laminated on projector transparency sheet. Single vinyl sheet was 100µm thick. The cutting plotter was programed to 23N pressure and slowest cutting speed for accuracy. The 23N pressure was selected by trial and error method until the plotter was able to cut through 2-layer vinyl sheet properly. The final depth of the channels and chamber was 200µm. The vinyl sheet patterns were laminated on the flat plastic surface and

degassed PDMS solution was poured and cured for 2h at 60^0C. Once both sides of the thruster were cured and solidified, they were attached to each other by applying thin layer of tetrabutylammonium fluoride (TBAF) and cured again for 2h at 70^0C under pressure to obtain uniform sealing. The pressure was applied by 2kg dumbbell. After sealing, a syringe needle of 0.6mm diameter and copper wires (Element 14) 0.2mm diameter was inserted at their respected locations, followed by application of TBAF on the insertion point and cured for 2 hours at 70^0C to eliminate leakage around electrode and needle insertion points. The use of copper wires as electrode was demonstrated by (Koh, et al., 2013). Fuel injection line was connected via syringe needle. The graphical representation of the fabrication steps is shown in Figure 5-3.

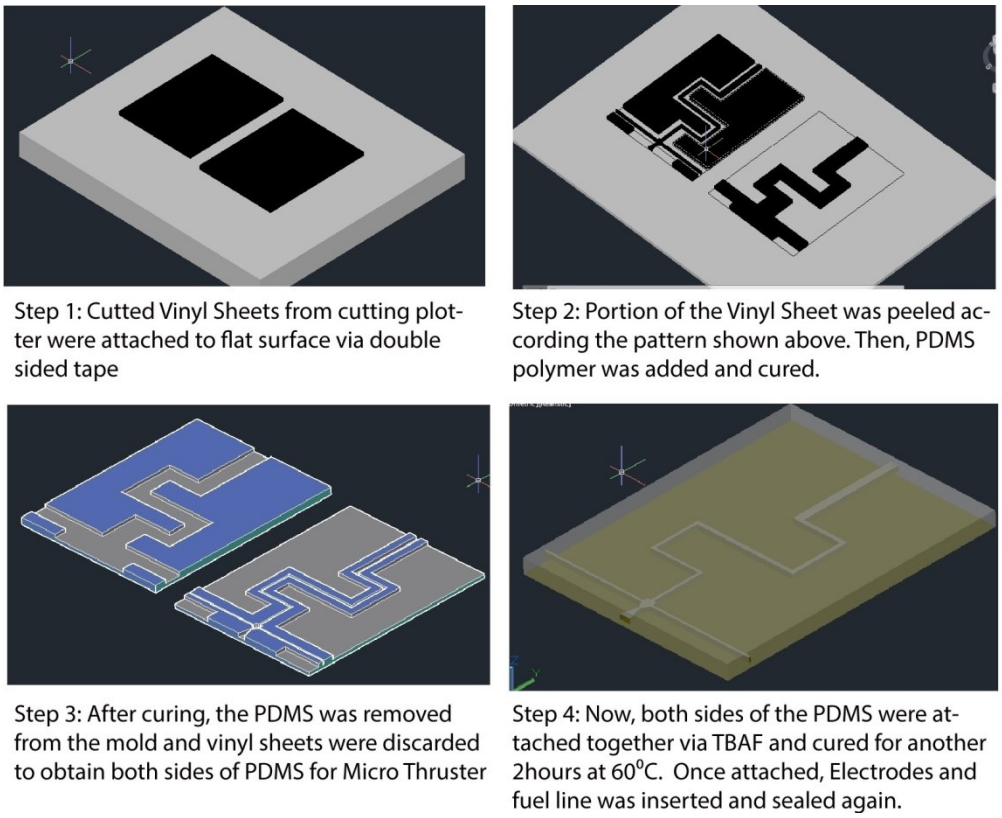

Figure 5-3 Steps of PDMS micro thruster fabrication.

5.2.4 Bubble size measurement:

In order to determine reaction rate with respect to applied voltage and hence, suitable input voltage, size of the bubbles generated during electrolysis was measured. It was performed in the purpose build micro open-chambers. The open-chambers were fabricated with PDMS using appropriately sized molds

as shown in Figure 5-4. In the first step, PDMS polymer was added to flat surfaced paper cup to obtain 1~2mm thick flat surface. Then thin glass microscope slides having dimensions of 100mm length, 1mm thickness, and 25mm width were placed vertically into the now cured PDMS flat surface. Then, more uncured PDMS solution was added until the height of 5~6mm was achieved. The fabrication steps are shown in Figure 5-4. The dimensions of the chamber are shown in Table 5-2

Table 5-2 Dimensions of Rectangular chamber

	Length (mm)	Width (mm)	Height (mm)	Volume (µl)
Dimensions	1	25	5~6	125

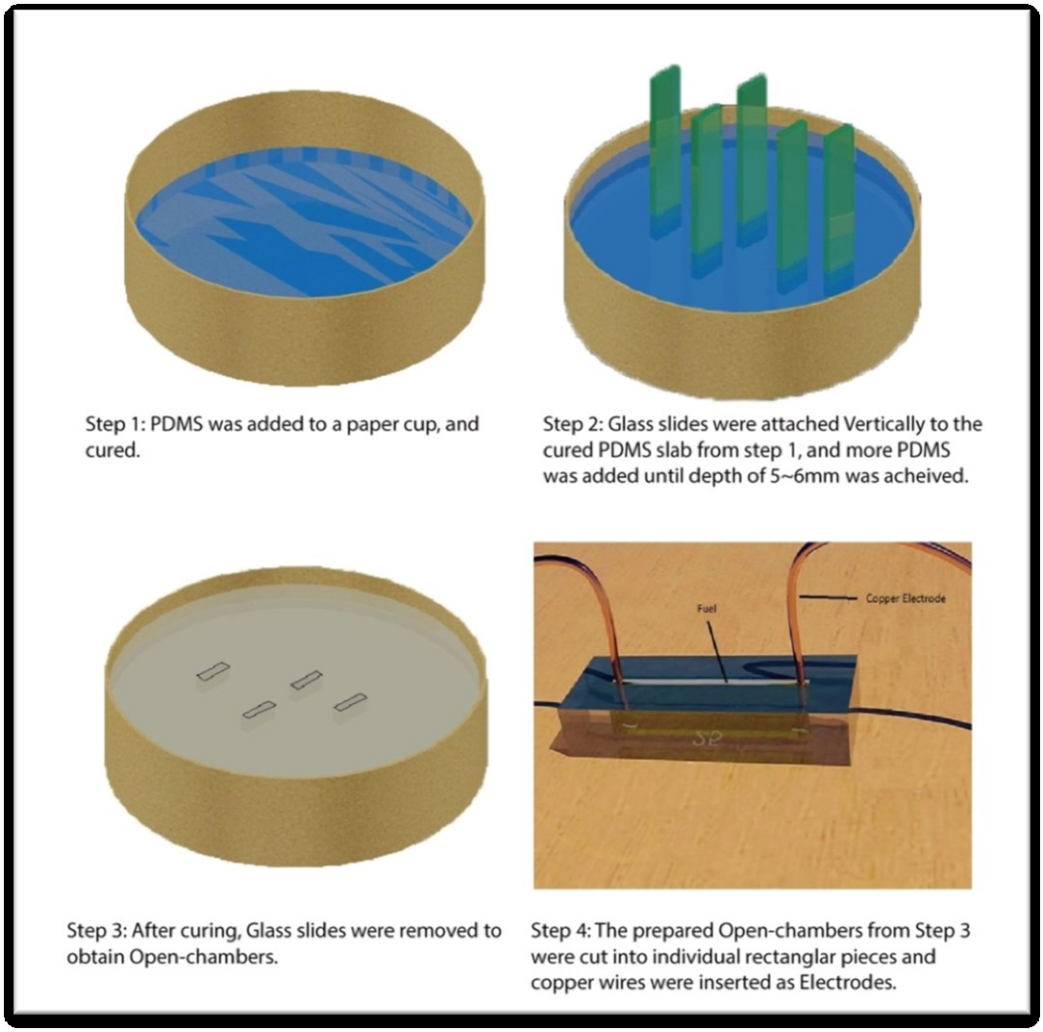

Figure 5-4 Fabrication steps of Open-chamber used for bubble size measurements (Not to Scale).

Once the open-chambers were fabricated, 0.2mm diameter copper wires were installed as electrodes at the edges, 100µl FLP-103 was added and the entire phenomenon was recorded for visual observation with analog scale in the background to determine bubble size. The experimental setup is shown in Figure 5-5.

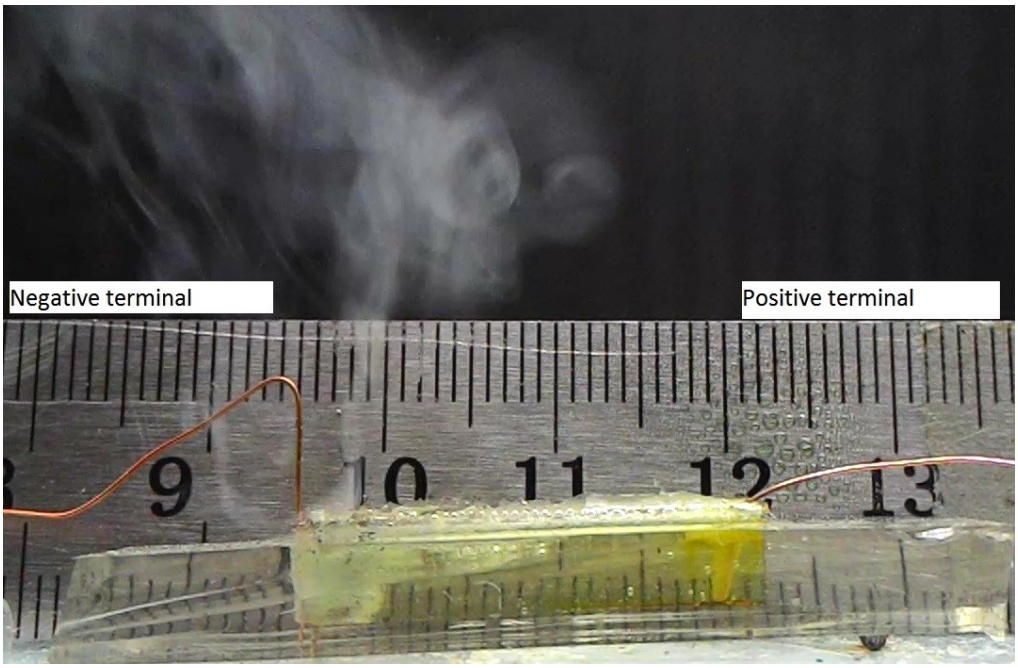

Figure 5-5: Experimental setup used for open-chamber electrolysis. It also shows generation of gas bubbles at negative terminal.

In these experiments, an analog ruler with 1mm least count was placed right behind the open-chamber for estimation and scaling purposes. Then the electrolysis phenomenon was recorded by regular Asus camera at HD resolution (1920*1080, 27 frames per second). After collecting the data, these videos were examined as following.

First, the video was played frame by frame (27 frames per second) to extract frames as picture. Then, distance between two measurements on the analog ruler was measured as pixels, using MATLAB Image Processing Tool, and then converted to mm scale. Pixel to mm conversion was performed by dividing the number of pixels between the known distances on the analog ruler. It was performed 3 times for each video and average was used to

estimate bubble diameter. After start of electrolysis, the bubble diameter was measured at similar intervals for each experiment.

5.2.5 Thrust measruement methods:

Thrust measurement was performed by 2 different methods. Details of these methods are given in next sections.

5.2.5.1 Thrust measurement by Load Cell:

Thrust data was obtained by factory calibrated miniature load cell (LSB200, Futek) placed in front of the exhaust nozzle. Both thruster and Load cell were placed horizontally with respect to ground to avoid accumulation of condensed vapors from exhaust gases on the load cell, which is otherwise avoided by infrared heating of the sensor plate as demonstrated by (Kundu, et al., 2012). Load cell measurements were obtained by placing it in front of the exhaust nozzle at 1mm and 2mm distance to obtain results. The distance of 2mm from thrust exit was considered small enough to represent actual thrust generated by thruster (Wu & Lin, 2010). The distance between thrust exit and the sensor, acts as pressure discontinuation barrier between fuel injection pump and the sensor. The fuel injection pump generates this pressure while pumping fuel into the thruster. Furthermore, the 2mm gap also provides a margin for exhaust gases to escape.

The distance between the thrust exit and sensor is very important parameter, because the gases coming out of the thrust exit can start accumulating on sensor as condensed vapor, and in absence of this gap, the sensor detects the pressure from the fuel pump.

Data was collected directly in computer via propriety Futek software at 100Hz sampling rate and each test was repeated 3 times to obtain consistent data at 1mm and 2mm distance from the nozzle. DC adopter (Elektro Automatik) at fixed 80V and 0.1A setting, supplied electrical power supply to electrodes. The combustion process was recorded by Logitech commercial video camera at 15FPS. The experimental setup is shown in Figure 5-6.

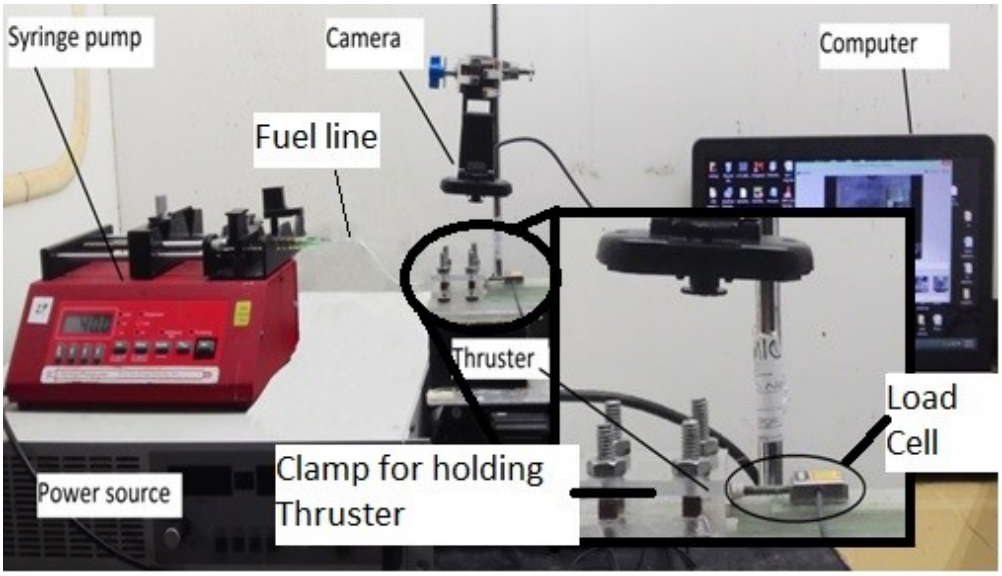

Figure 5-6 Experimental setup used for Thrust data recording

5.2.5.2 Thrust Measurement System:

A dedicated micro newton thrust measurement system (TMS) was designed, fabricated and calibrated as proof of concept for low cost TMS using off the shelve components. TMS was fabricated in-house using acrylic plastic sheets, PDMS, permanent magnets and LDC1000 induction sensor (Figure 5-7) (Texas instrument). The design concept of the TMS is shown in Figure 5-8 and Figure 5-9.

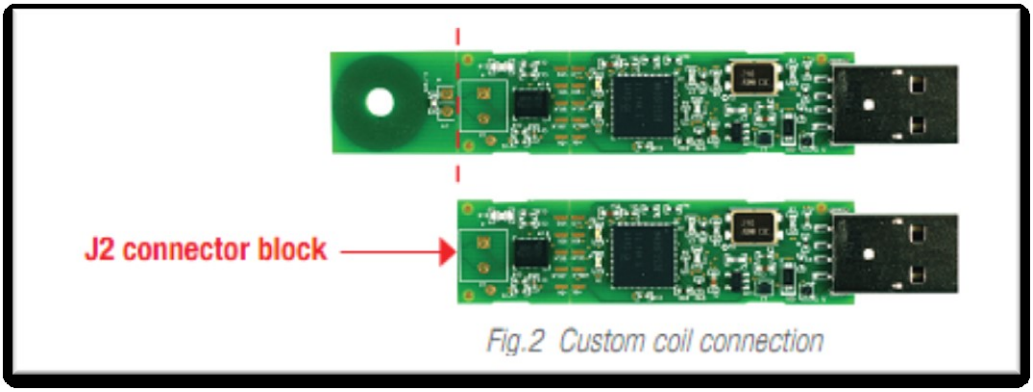

Figure 5-7 Diagram of LDC-1000 sensor (Anon., 2013)

5.2.5.2.1 Fabrication:

The main components of the TMS were LDC-1000 induction sensor and PDMS based torsion rod. The LDC-1000 induction sensor (Figure 5-7)

consists of two parts, one records the data and communicates with the computer, and other is the coil, which works by detecting the presence of metals in front of it coil (Texas Instruments, 2015).

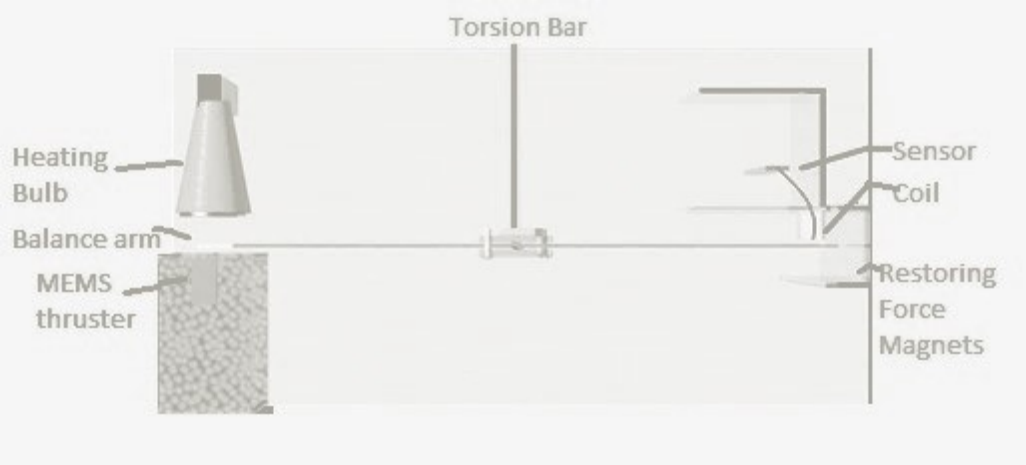

Figure 5-8 AutoCAD generated Top view of the thrust measurement system

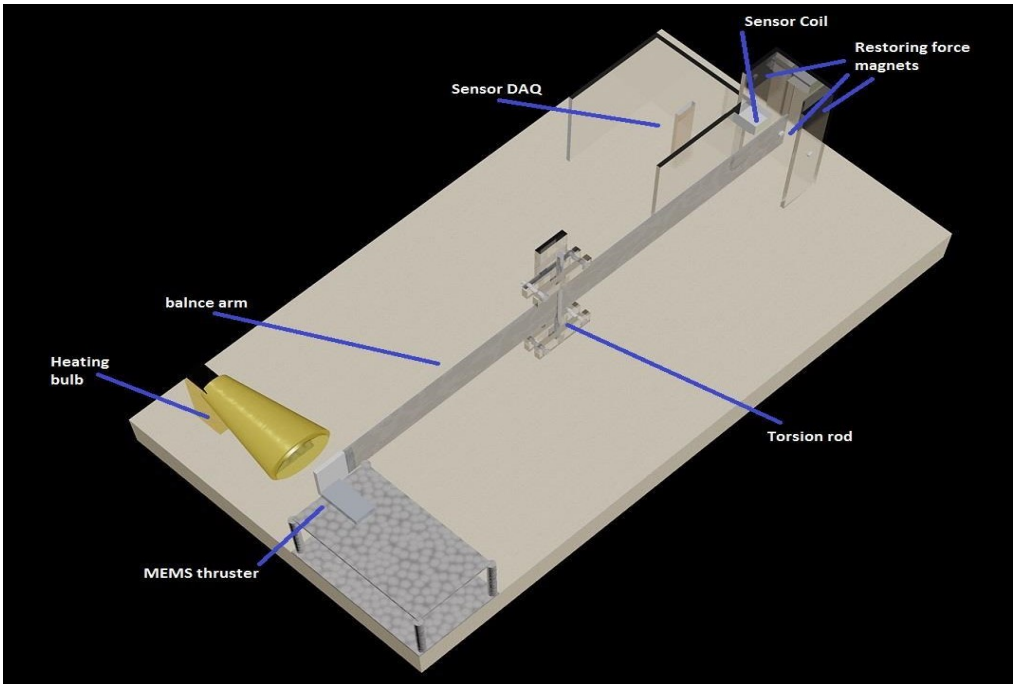

Figure 5-9 AutoCAD generated parameteric veiw of the thrust stand system

The PDMS based torsion rod fabricated with 6mm plastic pipe as mold and 2600*30*1mm aluminum plate, as balance arm, inserted in its center. The plastic pipe was manually cut at the center to make room for balance arm, and then the edges were sealed with epoxy. PDMS was then added into the mold

and cured. After curing, plastic mold and epoxy seals were removed to obtain PDMS torsion rod attached to Aluminum plate (balance arm).

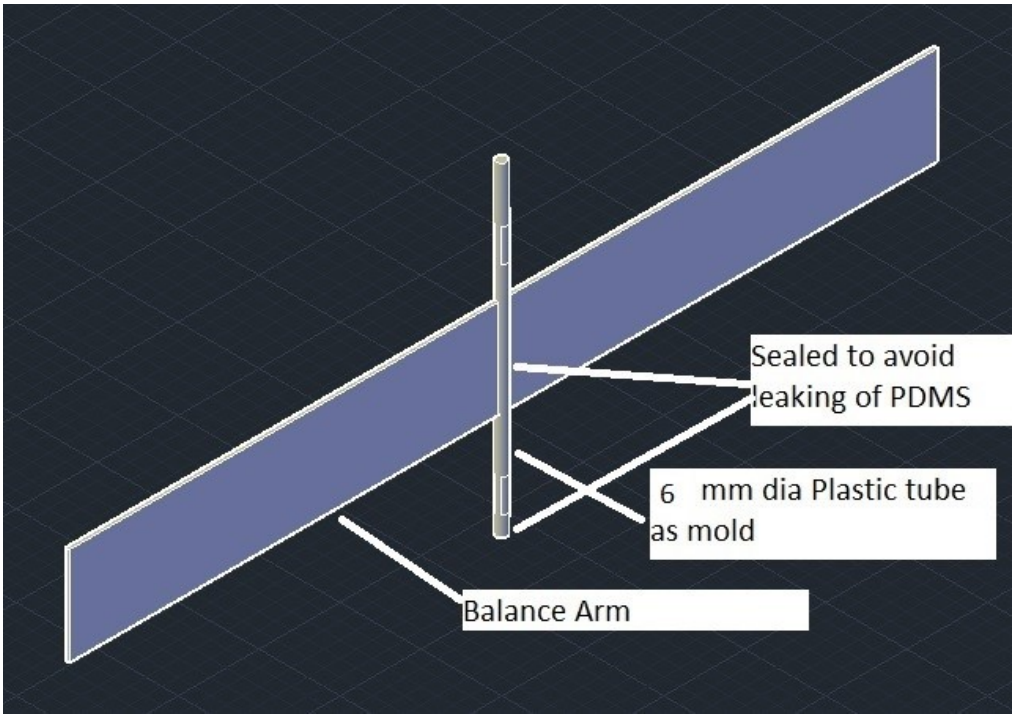

Figure 5-10 Overview of PDMS based torsion rod fabrication.

The fabricated PDMS rod with embedded aluminum plate was then attached to the center of the stand by screw flanges (Figure 5-10). Then, the stand for restoring force magnet was attached to one side of the aluminum plate and sensor's coil was attached on the same side. For the consistency of experiments, a point was marked as impact point on the other side of the aluminum plate for the thrust from the MEMS thrusters.

The magnets on the opposite end of the aluminum plate were installed in such a way that they have similar poles facing eachother, so that the fixed magnets can apply restoring force and maintain the baseline position of the Aluminum plate. The pole orientation of the magnets is shown in the close up of TMS below in Figure 5-11 and Figure 5-12. The complete TMS is shown below in Figure 5-13.

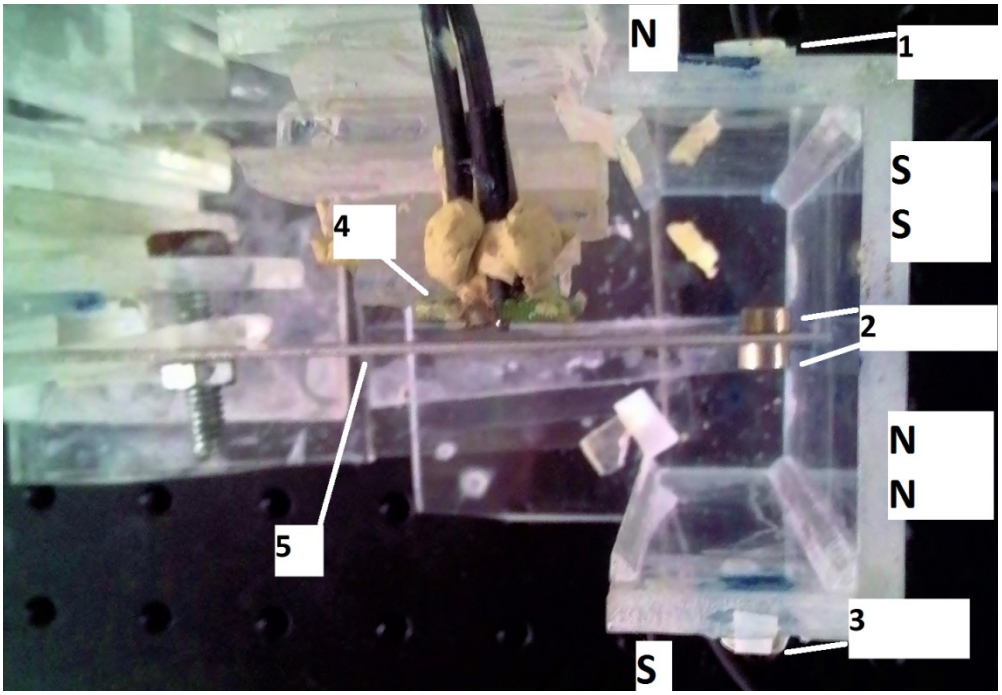

Figure 5-11 : 1,2,3: Magnets, 4:sensor coil, 5: aluminum plate, S: south pole, n:north pole

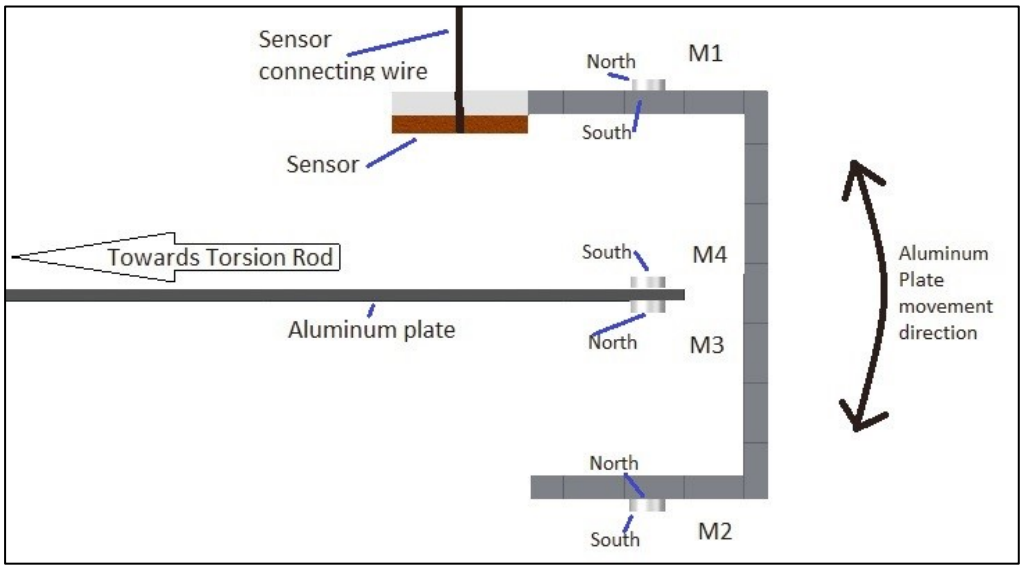

Figure 5-12 Illustrated TOP View of Magnet Positions

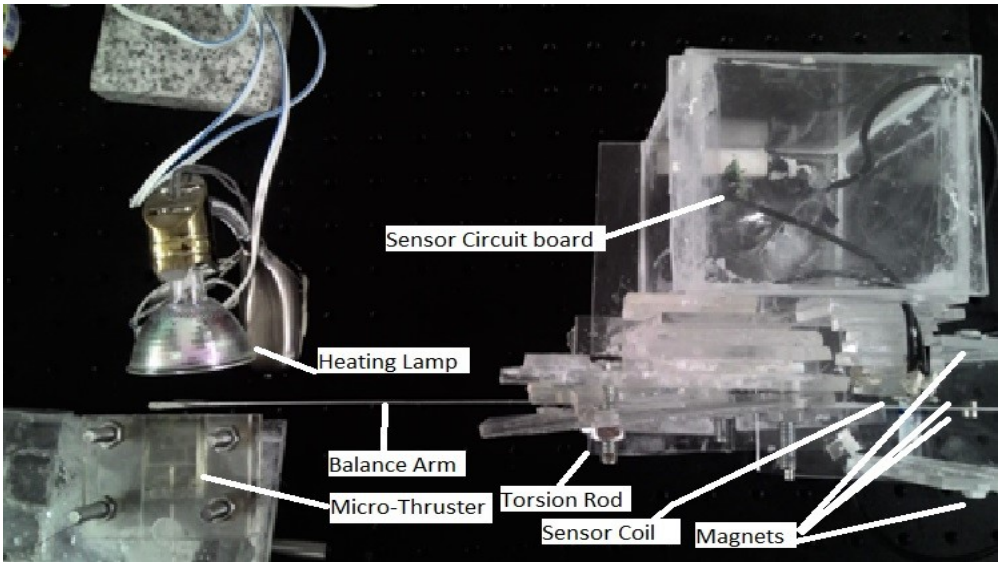

Figure 5-13 Fabricated TMS along with heater bulb and MEMS trhuster

5.2.5.2.2 Calibration:

The calibration of the system was performed by using idle weights, consisting of aluminum chips, via pulley system to redirect the vertical force into horizontal direction.

The calibration method used for the TMS is shown in Figure 5-14, where pre-weighted aluminum chips were added into the weight tray, and the deflection of aluminum plate caused by aluminum chips was recorded and plotted to obtain calibration curves. AutoCAD generated illustration of the calibration process for clarification is shown in Figure 5-15. The calibration was performed three times to obtain consistent values, and the average slope of the curves was used to convert raw data into mg. These calibration curves are shown in Figure 5-16 and values in Table 5-3.

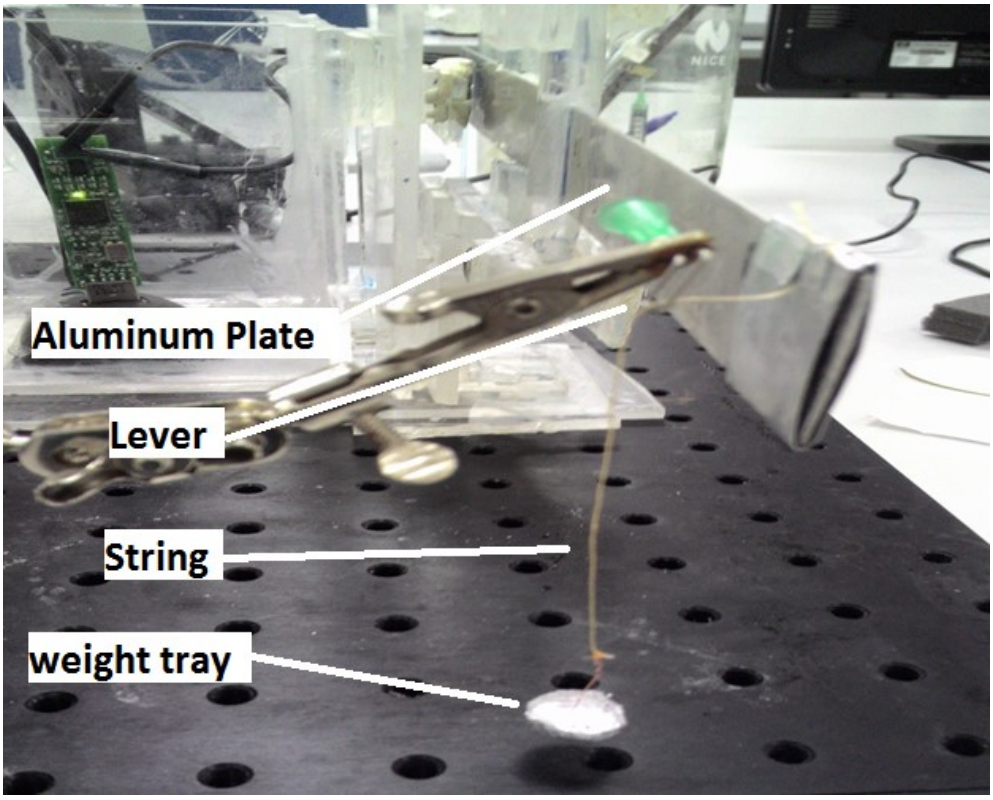

Figure 5-14 TMS during calibration, callibration weights were added in weight tray to record the movement generated by their pull on the aluminum plate.

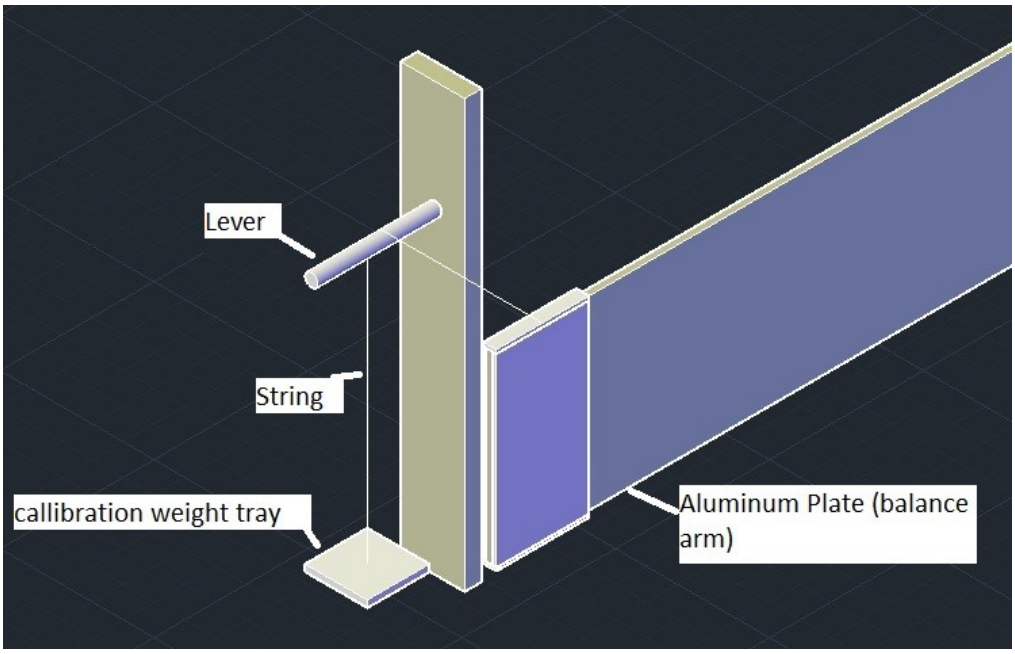

Figure 5-15 AutoCAD generated view of Callibration process

The default value of micro henry (μh) (SI derived unit of Electrical Inductance) from the sensor does not reach zero, increases with increasing distance between sensor and aluminum, and was dependent on the gap

between aluminum plate and sensor. Therefore, first default value of µh with aluminum plate in its idle position, was noted (Table 5-3, Cell: A2). Then change in µh with each addition of idle weight was noted as "Δµh". Now, Δµh was divided by weight (column A) to obtain value of Δµh/mg. These per milligram values (Δµh/mg) were then averaged to obtain the slop constant. The calculations are shown in Table 5-3.

Table 5-3 Sample calculation:

s.#	A	B	C	D	E
1	Idle weights (mg)	Total weight	Sensor value (µh)	Change in sensor value per idle weight (Δµh)	Change in µh per mg (Δµh/mg)
2	0	0	176.876	0	0
3	16.8	16.8	177.318	0.442	0.02631
4	15.6	32.4	177.756	0.438	0.028077
5	16.5	48.9	179.01	1.254	0.076
6	16.4	65.3	179.382	0.372	0.022683
7	17.3	82.6	180.11	0.728	0.042081
8	15.6	98.2	180.492	0.382	0.024487
9	16.5	114.7	181.02	0.528	0.032
10	17.3	132	181.892	0.872	0.050405
11	18	150	182	0.108	0.006
	Algebraic slop:				0.034
	Graphical slop				0.0337

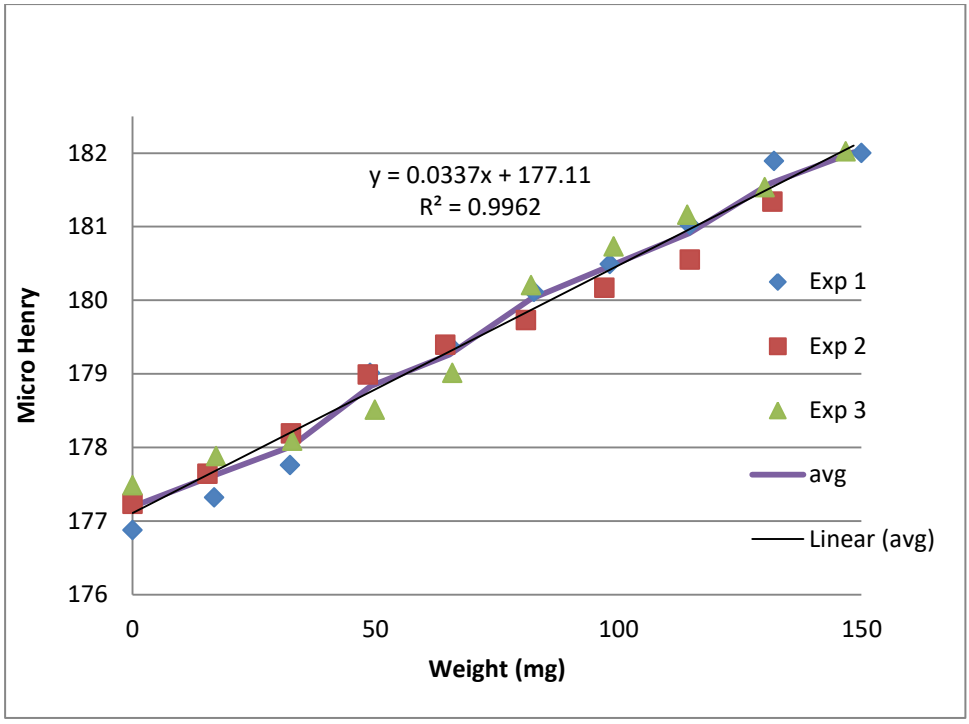

Figure 5-16 Callibration data from 3 experiments is ploted as Exp1,2,3, and average of the experimental data was plotted to obtain linear trend line and graphical slop.

After calibration, the PDMS based Micro thrusters used for generation of thrust via electrolytic decomposition of FLP-103, and for evaluation of the TMS under experimental conditions. The distance between the nozzle of Micro thruster and aluminum plate was maintained at approximately 2mm distance, and fuel flow rate of 40 and 60µl/min was used. On the opposite side of the aluminum plate, a 50W halogen bulb was used as point heating source to immediately evaporate condensed vapors and unburnt fuel from the sensor plate. Moreover, on the other side of the aluminum plate, sensor and permanent magnets were installed.

5.2.5.2.3 Data collection and processing during experiments:

The thrust data collected by USB cable connecting the sensor to computer via LDC-1000 proprietary software in as text file. The raw was then exported to MS Excel where it was processed as following.

1. Before the start of each experiment i.e. electrical power and fuel supply, Data recording was performed in idle conditions, so that

baseline value can be obtained. Then, the obtained baseline value was subtracted from the y-axis data.

2. Then the data was divided by calibration constant i.e. 0.0337 to convert it from micro henry to mg values.
3. The mg-converted data was smoothed by 500-moving-point-average method. In this method, each data point is average of next 500 data points. This method offers smooth and easy to understand graph line while maintaining the accuracy. The accuracy was confirmed by calculating area under the curve for before and after smooth graph as shown below in Figure 5-17. Detailed example calculations are shown in the appendix.

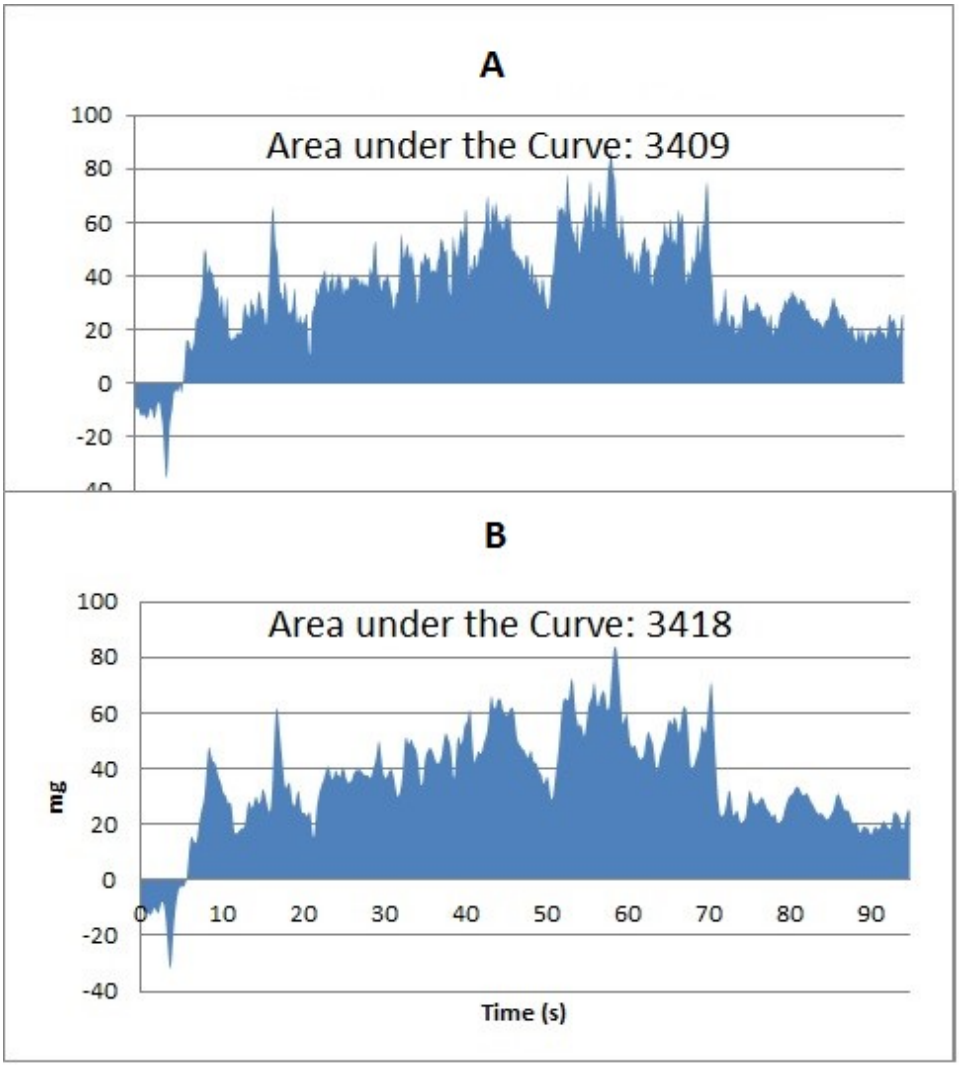

Figure 5-17 (A) Comparision of baseline corrected data with (B) 500 moving point average data

4. Then the data was converted to milli-newton values so that specific impulse could be calculated.

5.3 Results and discussion:

5.3.1 Theoretical calculation of electrolysis:

Electrolysis schematics for FLP-103 are derived on the assumptions according to Springall Robert rules (Akhavan, 2004, p. 81), and existing literature for methanol, water, ammonia and nitric acid electrolysis.

5.3.1.1 Electrolysis of Ammonia

According to (Viste, et al., 2005), electrolysis of aqueous ammonia produces hydrogen gas at cathode and nitrogen gas at anode along with water.

$$6H_2O + 6e^- \xrightarrow{At\ Cathode} 3H_2(g) + 6OH^-$$

$$2NH_3(aq) + 6OH^- \xrightarrow{at\ Anode} N_2(g) + 6H_2O + 6e^-$$

$$2NH_3(aq) \xrightarrow{overl\ all\ electrolysis} N_2(g) + H_2(g)$$

5.3.1.2 Electrolysis of Methanol:

According to (Take, et al., 2007), methanol electrolyzes as following:

$$CH_3OH\ +\ H_2O \xrightarrow{at\ Anode} CO_2\ +\ 6H^+ + 6e^-$$

$$6H^+ + 6e^- \xrightarrow{At\ Cathode} 3H_2$$

However, presence of nitrous acids can significantly change the reaction outcome, as demonstrated by (Xiao, et al., 2006); some of the possible outcomes of the reaction are shown below.

$$CH_3OH + O_2 \xrightarrow{electrolysis} CH_2OH + HO_2$$

$$CH_3OH + NO \xrightarrow{electrolysis} CH_2OH + HNO$$

$$CH_3OH + NO \xrightarrow{electrolysis} CH_3O + HNO$$

$$CH_3OH + NO_2 \xrightarrow{electrolysis} CH_2OH + HONO$$

$$CH_3OH + NO_2 \xrightarrow{electrolysis} CH_3O + HONO$$

5.3.1.3 Electrolysis of Nitric Acid:

According to (Kim, et al., 1999), nitric acid electrolyzes as following:

$$NO_3^- + 3H^+ + 2e^- \xrightarrow{at\ Cathode} HNO_2 + H_2O$$

$$HNO_2 + H^+ + e^- \xrightarrow{at\ cathode} NO + H_2O$$

5.3.1.4 Overall electrolysis:

According to (Thakre, et al., 2014; Vyazovkin & Wight, 1997; Oxley, et al., 1997), decomposition of ADN produces several chemical species, including nitric oxides, nitrogen, hydrogen etc. and according to equation given by (Gronland, et al., 2006) for reaction during thermal decomposition of FLP-103 is shown below.

$$33NH_4N(NO_2)_2 + 22CH_3OH + 94H_2O \xrightarrow[Combustion]{Conventional} 22CO_2 + 204H_2O + 66N_2$$

Based on these above-mentioned equations, the following equation was derived for FLP-103 electrolysis.

$$NH_4N(NO_2)_2 \xrightarrow{Electrolysis} NH_4^+ + N^{-3} + 2NO_2^+$$

These species generated by ADN splitting then reacts with Hydrogen produced at cathode by electrolysis of water and methanol. Leading to formation of ammonium hydroxide, hydroxyl ammonia, nitrogen, carbon dioxide, and, possibly nitric acid. Further decomposition proceeds by electrolysis of species produces during the ADN splitting. In all these equations, it can be observed that, majority of gaseous products were produced

at cathode with exception of carbon dioxide. And, it is most likely that majority of the carbon dioxide further reacted with nascent hydrogen, and further took part in the reaction, because, in Figure 5-19, it can be observed that, there was almost no gas production at anode during electrolytic decomposition.

Furthermore, it is also extremely likely that the ammonium hydroxides and hydroxyl ammonium ions produced at cathode may have reacted with acidic nitrous oxides at cathode to further increase the temperature due to heat of neutralization and could have initiated thermal decomposition as well.

5.3.2 Electrolytic decomposition and preliminary Electrolysis testing:

In order to identify experimental parameters such as voltage, starting location of the electrolysis, fuel line path and avoidance of leakage, several tests were performed in micro thrusters, and in open-chambers.

Input voltage setting was determined by performing electrolysis in micro thrusters at increments of 20V at constant current 0.1A as shown in Table 5-4. In case of micro thruster that was considered as a continuous flow reaction with limited residence time, Fuel flow rate was maintained at 40µl/min. The fuel flow rate was selected by trial and error method as 40µl/min, because, it was a decent compromise between lower and higher flow rate. At lower flow rate, residence time of the fuel would have been higher which could have allowed combustion, however, the thrust during thrust measurement turns out to be very low to be detected confidently. On the other hand, higher flow rate could have spent less time in the combustion chamber of the micro-thruster and might not have had proper ignition, as it is evident from lower specific impulse obtained for 80µl/min experiments (Figure 5-22). During experiment, fuel decomposition was identified as generation of bubbles and gas as it was proposed for another ionic liquid monopropellant HAN by (Yetter, et al., 2007) during electrolytic ignition. Furthermore, bubble generation as a sign of decomposition in pure molten ADN was also reported by (Teipel & Heintz, 2005) and theoretical calculations of electrolysis also suggests generation of

gases during electrolysis. Since both HAN and ADN are ionic propellants, therefore, bubbling was considered as the identifier for occurrence of reaction.

Bubbling was very low during tests performed at below or at 60V. Furthermore, in case of micro thrusters, majority of the fuel came out of nozzle of the micro thruster in liquid form. Therefore, as evident from Table 5-4, the 80V setting was determined as optimum.

Table 5-4 Voltage used for ignition in Micro thrusters under electrolytic conditions

Voltage	Propellant flow rate (µl/min)	Observation
20	40	Negative
40	40	Negative
60	40	Partial, bubbling
80	40	Visible plume of exhaust gases

In case of open-chamber Figure 5-5, which was considered as a batch reaction, 100 µl was used each time. In these open-chambers, gradual decomposition of the fuel continued until end of the exhaustion of fuel in the chamber. Therefore, the fuel decomposition speed was observed by determining the bubble size at similar time intervals for each applied voltage. It was measured from the moment first bubbles appeared on the cathode, until bubbles became immeasurable to due to big size. A comparison of electrolysis at different voltages is shown in Figure 5-18. During the same time, bubble generation at anode was extremely slow, as it is evident from Figure 5-19. During the bubble size measurement, it was observed that 80V,0.1A produced bubbles more rapidly than all other settings. At 20, 40 and 60V, the bubble generation reached a certain point and continued slowly in that range. Furthermore, at 5V, 2.5A setting, reaction proceeded gradually at steady pace as evident form the

nearly straight line ($R^2 = 0.9982$) which could be attributed to electro-resistive heating by large amount of passing current.

It was observed that, highest bubble generation occurred when input setting was 80V, 0.1A, and lowest was achieved at 5V, 2A input setting despite the fact that overall power wattage (10W) was higher as compared to 80V, 0.1A (8W).

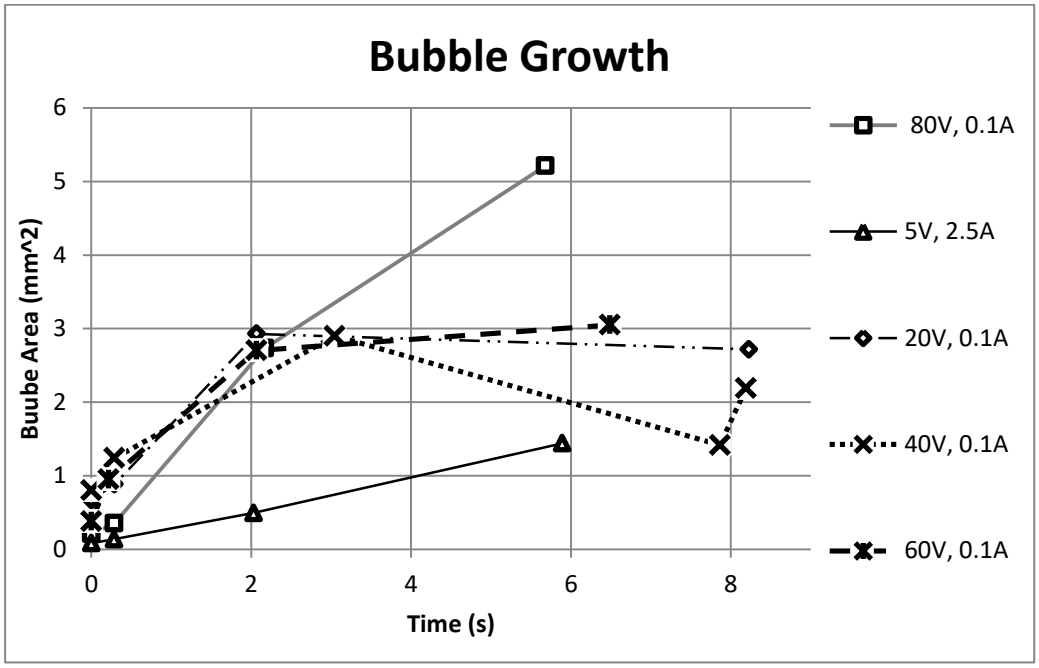

Figure 5-18: Comparison of Bubble growth in different voltage and current input.

In ideal resistive or thermal heating and ignition, the propellant is assumed to gain heat uniformly up to ignition temperature, and ignition starts at the geometric center of propellant mass (Appelgren, et al., 2005). Furthermore, the release of large amount of mass dependent chemical energy at initial ignition heats up the combustion chamber as well as loses energy to the surrounding. If the energy losses to the surrounding were low then propellant would maintain self-sustaining and steady combustion. Such behavior of uniform heating was observed in DSC-TGA results of FLP-103 as shown in Figure 5-20. In Figure 5-20, evaporation of water and methanol can be observed as weight loss in 40 to 140ºC region, followed by decomposition of

ADN at its literature reported decomposition temperature of 140~170ºC (Kappenstein, et al., 2004; Vyazovkin & Wight, 1997) .

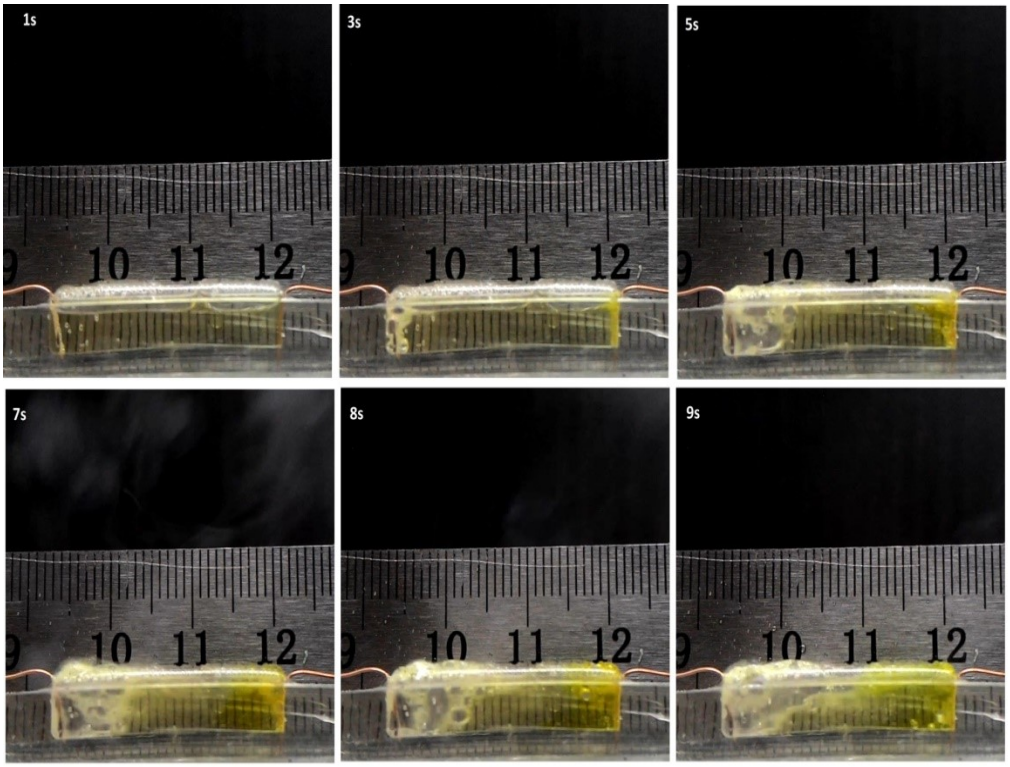

Figure 5-19: Snapshots from Open-chamber electrolysis taken at different intervals. The smoke and effervescence generation at cathode (left) is observable.

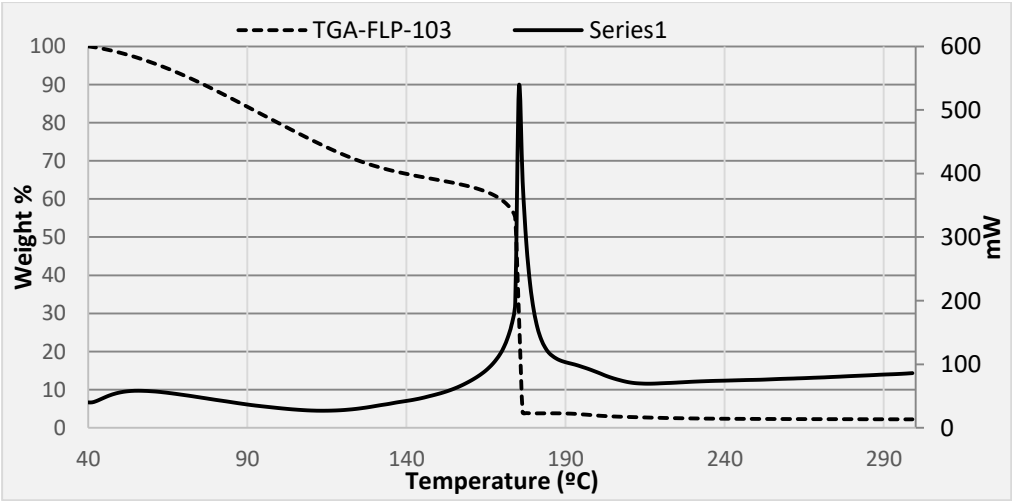

Figure 5-20 : DSC-TGA of FLP-103 obtained at heating rate of 10ºc/min. Weight loss of nearly 40% before start of thermal decomposition at approximately 170°C is in accordance with composition of FLP-103, i.e 63.4wt% ADN.

However, in electrolytic ignition of ionic propellants such as FLP-103, results from (Larsson, et al., 2005) also suggested the non-ideal behavior of ignition

occurrence near electrodes (Figure 5-5, Figure 5-19) at temperature lower than decomposition temperature, while utilizing fraction of energy as compared to what it would have been required for ideal thermal heating conditions. During this process, the fuel undergoes decomposition in liquid phase in contrast to thermal or resistive heating where solvent part of the fuel evaporates (Figure 5-20) before the decomposition of oxidizer part. The said phenomenon was recorded and analyzed by electrolysis in open-chamber, where it was observed that the smoke generation was immediately started at cathode (negative terminal) rather than in between the center of two electrodes as shown in Figure 5-19 with dependence on supplied voltage. It is assumed that ignition initiated by splitting of ADN into Ammonium ion and dinitramide acid followed by dinitramide acid further protonates into nitric acid and nitrous oxide to proceed with combustion of the propellant (Yang, et al., 2005).

From these experiments, it can be deduced that, electrolysis offers ignition of ADN based fuels at much lower energy consumption and especially in the beginning, the ignition proceeds via electrolysis rather thermal resistive heating. Furthermore, the decomposition proceeds via electrolysis predominately occurring at cathode.

5.3.3 Thrust measurement by Load Cell:

The thrust profiles obtained in Micro thrusters are shown in Figure 5-21. It can be observed that maximum thrust was achieved by 80µl/min flow rate (Figure 5-21C), but maximum specific impulse (Isp) was achieved by 40µl/min as shown in Figure 5-22. The specific impulse was calculated according to the equation 1.

$$Isp = \sum F * dT/\dot{m} \qquad (1)$$

Where, F, dT and $\dot{m}$ Represents total force, time change and weight of total fuel respectively.

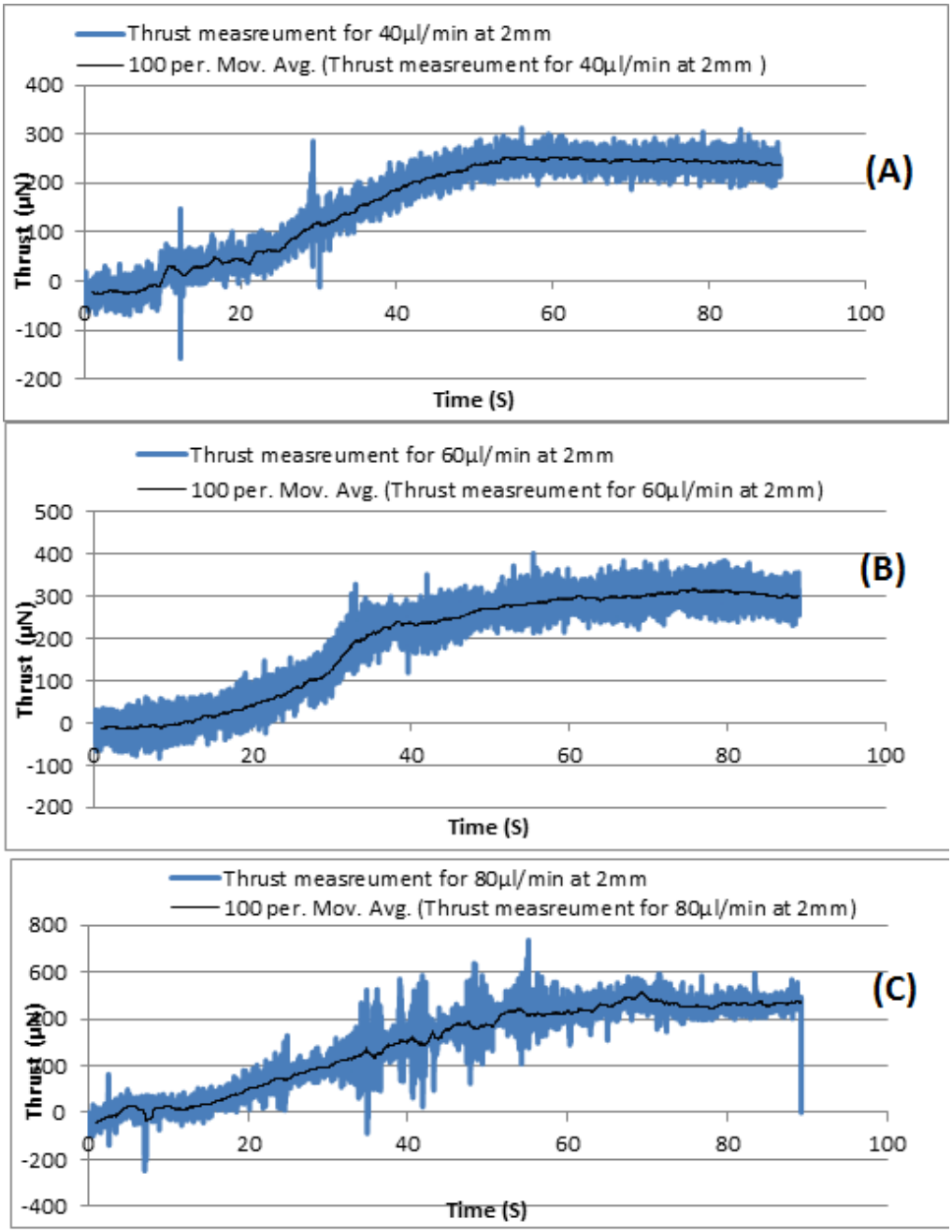

Figure 5-21 Thrust measurement for 40ul/min (A), 60ul/min (B) and 80ul/min(C) propellant flowrate measured at 2mm distance.

The low Isp obtained by 60 and 80µl/min flow rates was due to improper combustion in undersized combustion chamber. This assumption was also supplemented by the failure to record thrust data for 80µl/min at 1mm distance, because of the interference of unburnt liquid fuel with sensor. (Kundu, et al., 2012) Also reported the similar phenomenon where, under constant heating power, vaporizing liquid thruster reached thrust saturation after crossing certain flow rate limit. In Figure 5-23, average maximum thrust obtained for FLP-103 is compared with literature values. Although, literature reported propellants belongs to different category but it suggests the competitive performance of ADN in micro thrusters.

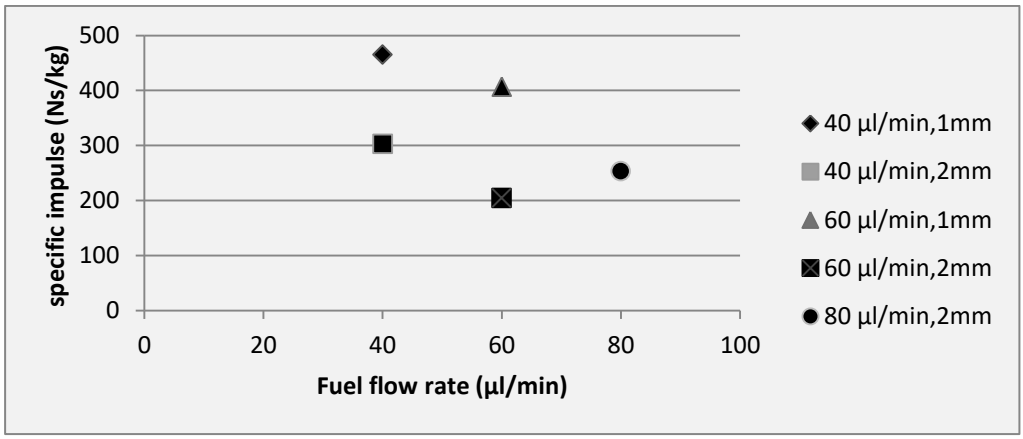

Figure 5-22 Average Specific impulse recorded for FLP-103

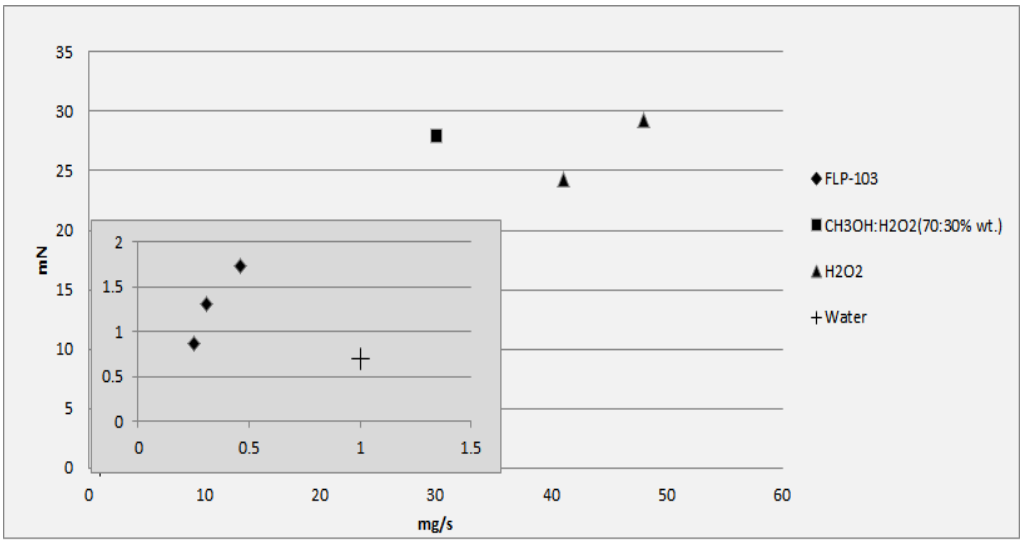

Figure 5-23 Average maximum thrust obtained for FLP-103 is compared thrust obtained in microthrusters based on Hydrogen peroxide, Methanol-Hydrogenperoxide mixture (Huh & Sejin, 2014) and Water (Cheah & Low, 2015).

The maximum experimental Isp obtained in this study is approximately 5 times less than literature reported value 2492Ns/kg for ADN based propellants (Appelgren, et al., 2005). However, several factors contribute to low Isp of Micro thrusters such as higher thermal losses (Cheah & Low, 2015), and low feed pressure (Neff, et al., 2009) and most significantly, the reduced Reynold's number at micro scale nozzles reduces the specific impulse up to 10 times (Yetter, et al., 2007). The thermal losses are directly proportional to surface area, which explains the higher thermal losses at micro level.

Table 5-5: Performance comparison of Electrolytic decomposition with VLM type Micro thrusters.

Micro thruster Material	Electrical power input (W)	Thrust (µn)	Thrust to Power ratio (µn/W)	Reference
PDMS	8	250	31.25	Current study
PDMS	8	310	38.75	
PDMS	8	460	57.5	
Si	30	2.9	0.1	Ye et al
Si	2.4	5	2.08	Maurya et al
Si	7.2	1014	140	Kundu et al
Alumina	9.2	67	7.28	Karthikeyan et al
Zirconia	4.01	582.7	145.31	(Cheah & Low, 2015)

Furthermore, the power consumption was not measured due to "0.1" least count of the ampere meter of the power supply, i.e. 0.1A, and hence amperage reading was displayed as zero during the experiments. Therefore, even if the power consumption is assumed at maximum possible limit, 8W (80V, 0.1A) during the testing, it performs competitively against Micro thrusters based on vaporizing liquid (VLM) as shown in Table 5-5 with compiled data from (Cheah & Low, 2015).

5.3.4 Thrust measurement by Thrust Measurement System:

The thrust curves obtained by TMS are shown in Figure 5-24 for 40 µl/min (A) and 60µl/min(B) propellant flow rate respectively.

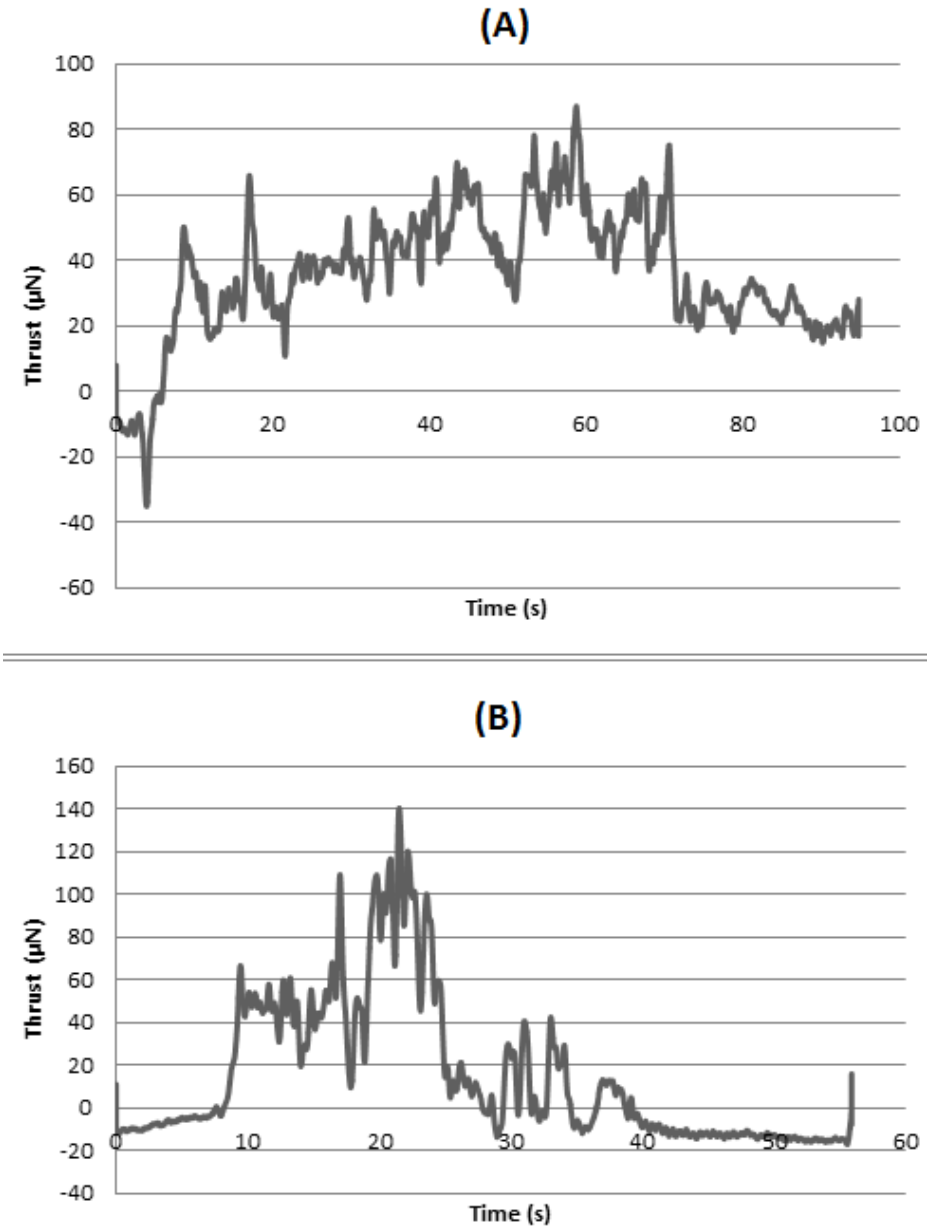

Figure 5-24 Thrust measurement results for 40µl/min(A) and 60µl/min(B) flowrate

The specific impulse calculated for these experiments was compiled in Figure 5-25. The specific impulse was calculated according to following equation:

$$Isp = \sum F * dT/\dot{m}$$

Total force was calculated in the steady region of the graph by integration according to trapezoid rule using Microsoft Excel, then it was divided by the total mass of the fuel used in the specific time period.

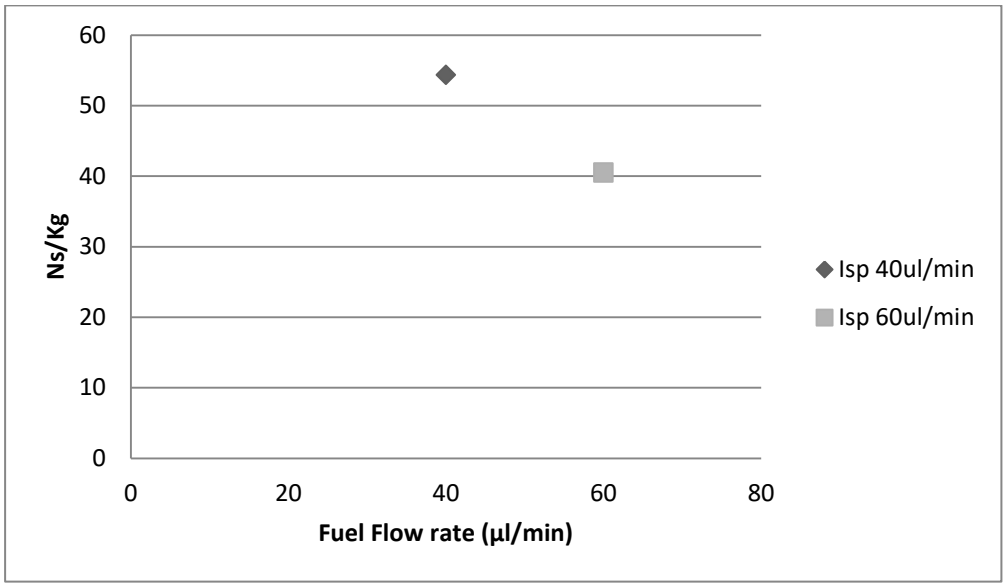

Figure 5-25 Calculated Specific impulse

This type of thrust measurement systems often use Flexural Pivots and overall costs several thousands to fabricate. Furthermore, many systems have used induction sensors to detect deflection of the pivot arm as a way to measure thrust. However, in this method, off shelve; low cost induction sensor by Texas Instrument Inc. LDC-1000 was used without any modifications. Furthermore, the flexural pivot works on the concept of bending of thin metal or plastic plates to provide movement without friction (Jensen & Howell, 2002). Therefore, this idea was exploited by elastic nature of PDMS along with Induction sensor to develop low cost micro newton thrust.

The thrust measurement results obtained by the TMS are promising but suggest further improvements in the TMS. The specific impulse obtained by TMS and load cell (From Section: 5.3.3) are compared in the table below.

Table 5-6 Comparision of Specific impulse obtained from Load cell and TMS

	ISP 40µl/min (Ns/Kg)	ISP 60µl/min (Ns/Kg)

Load cell (a)	300	200
TMS (b)	54.3	40.48
Difference % $\left[\frac{(a-b)*100}{a}\right]$	81.9%	79.76%

From the results (Figure 5-24), it can be observed that TMS detected lower thrust and hence lower ISP (Figure 5-25) as compared to load cell (Table 5-6). The difference between the two systems was attributed to several factors. First, the calibration method used for TMS was not frictionless. The friction coefficient induced between nylon thread and steel pulley i.e. $0.36\mu_K$ (Blau, 2008, p. 195), used during the calibration may have caused less deflection in the aluminum plate as it would have had happened. Secondly, the idle weights used during the calibration had error up to 6wt. %. The error was calculated by weighting the aluminum strip before cutting into chips and comparing it with sum of all the aluminum chips as shown in Table 5-7.

Table 5-7 Percentage Error calculation in Callibration weights (idle weights)

Total weight before cut:	107.8mg
Summed up weight of all Chips (after cutting)	101.5mg
Difference:	6.3mg
% error	5.8%

Another reason for lower thrust detection was air resistance from ambient air. The air resistance on Aluminum plate could have resulted in lower deflection. Furthermore, due to configuration of the TMS and Micro thruster placement, the aluminum plate was pushed away from the thruster during testing, leading to increase in distance between thruster nozzle and aluminum plate. From the experimental results shown in Figure 5-22, it was evident that increasing distance between thruster nozzle and sensor, which in this case is aluminum plate, decreases the recorded thrust.

Therefore, in order to improve the calibration of TMS and hence results, a contactless and friction less calibration system is required. However, despite calibration issues, TMS proves the concept of thrust detection via PDMS based torsion rod in combination with induction sensor by detecting thrust during experiments.

5.4 Conclusions:

In these experiments, Ammonium Dinitramide based green liquid mono-propellant named FLP-103 was synthesized according to publish methods and its potential application as electrolytically decomposing ionic liquid in Micro thrusters was investigated. The Micro thrusters used in this study were fabricated by PDMS via soft lithography. The thrusters used in these experiments were designs by simple yet effective technique to overcome the sealing and backpressure issue in PDMS based micro thruster. The thrust generated by micro thrusters was recorded by Load cell and by In-house fabricated TMS consisting of LDC-1000 induction sensor and torsion rod.

The use of LDC-1000 induction sensor as displacement measurement sensor, coupled with PDMS based torsion rod offers a unique low cost method for evaluation of thrust in micro newton range. Its sensitivity can be further enhanced by using smaller diameter torsion rod, and by increasing the length of aluminum plate. The use of magnets offers reliable restoration of the aluminum plate to its original place and reduces the vibrations. However, further investigation is required to increase the accuracy of the calibration method. There are several methods reported in the literature, such as Electrostatic fins, which can be employed for this purpose but could not be employed in this project due to lack to technical facilities required. Furthermore, the theory of these electronic calibration systems is out of the scope of chemical engineering. The biggest advantage of this system is its low cost, which in this case was less than 200rm for the entire system, including fabrication plastics, sensor, magnets, and aluminum plate.

Under experimental conditions, successful ignition and combustion was achieved by passage of electrical current across the combustion chamber with

continuous flow of propellant FLP-103 using standard copper wires as electrodes. The entire phenomena were analyzed visually and quantitatively. Characterization experiment shows that optimum electrical input used was 80V and 0.1A. The flow rate was increased by 20µl/min step-size beginning from 40µl/min. It was observed that beyond 40µl/min flow rate, thrust efficiency decreased due to volumetric capacity limitations. In the current experimental conditions, 40µl/min was determined as optimum propellant flow rate at 80V and 0.1amp power, which gave up to 465Ns/Kg Isp.

The decomposition of FLP-103 initiated in liquid phase at cathode as soon as the voltage reached the target level and continued successfully as long as the electrical power was provided.

Chapter 6. **Conclusions and future recommendations:**

6.1 Conclusions:

The work presented in this project focuses on development of alternate synthesis route for ADN with higher reaction yield and/or economical reaction conditions such as near zero temperature and shorter reaction time. During this work, existing ADN synthesis methods were examined to identify key areas for further investigation. It was noticed that the presence of strong ions propagates the reaction toward desired product. Among all the studied synthesis methods, synthesis of ADN via nitration of potassium sulfamate with mixture of sulfuric and nitric acid was the most suitable for investigation. In this method, reaction yield is relatively higher than other methods, and most importantly, it uses readily available chemicals in a straightforward method.

Based on the hypothesis, that ADN can be synthesized near zero temperature by addition of strong ions, Trifluroacetic acid (TFA) was selected as suitable addition to the reaction mixture. The results from TFA based experiments successfully produced ADN at near zero temperature, albeit in trace quantities. From this initial success, parametric studies were performed to increase the reaction yield of this modified method. The reaction was performed with different acid compositions, different reaction times, reaction mediums, and with additives known to assist nitration reactions. Among additives, powdered Alumina and Silica gel were tested. The maximum yield i.e. 4.8wt. % was obtained with 20g Silica gel for 10min reaction time.

In the second phase of this project, an alternate method for alteration of particle morphology of ADN was developed. Melting of ADN was common among all the existing methods described for particle size alteration of ADN. However, ADN starts to decompose in molten phase; therefore, another method based on ultrasound was developed to avoid melting of ADN. In this method, ADN particles along with additives like CTAB, Cab-O-Sil and Graphene were suspended in toluene by sonication at 60^{o}C to obtained modified ADN particles. Furthermore, Polymeric coating of ADN particles can be performed simultaneously by addition of desired polymer, preferably

5wt.% polystyrene or HTPB in the ADN mixture. The results obtained were comparative to ADN samples obtained by conventional melt prilled sample with added benefit of low operating temperature, simultaneous coating and no melting.

ADN offers unique ability to be used as both solid and liquid propellant. Moreover, it is ionic in nature, therefore, in third phase of the project, ADN based liquid monopropellant was electrolytically decomposed in micro-thrusters. In micro thrusters, several fuels with exception of ADN, such as ammonium perchlorate, ethanol-hydrogen peroxide, HAN, and volatile gases have been used as propellant. Therefore, an ADN based monopropellant named FLP-103 was employed in micro-thrusters and its combustion behavior and performance was evaluated. The results showed that FLP-103 works comparatively in micro-thruster under electrolytic decomposition. Furthermore, in the tested dimensions of micro-thruster, 40µl/min fuel flow rate gave maximum specific impulse.

In the last phase, as a proof of concept a low cost TMS was fabricated and analyzed. It was fabricated with PDMS based torsion rod and induction sensor. The results from the TMS show that it was able to detect thrust generated by micro-thrusters. However, due to accumulating errors in the calibration process, the recorded thrust was less than it was recorded with load cell during third phase of the project.

6.2 Future recommendations:

The findings of this project offer a sound foundation for future research to be based upon. In ADN synthesis, this study has suggested a modified method where near zero temperature is employed along with addition of TFA and other additives. Therefore, future work can focus on investigation of:

- More combinations of nitrating acid mixture to substrate and reaction time.
- Quantity of additive used.
- Utilization of solid acid such as sulfuric acid activated silica gel.

- Extended temperature range, however, it must be below 25^{o}C to avoid rapid decomposition of reaction mixture.
- Alternate chemicals instead of TFA can be tested.

In ultrasound prilling of ADN particles, further research can be carried out to determine:

- Minimum polymer coating quantity required to achieve maximum hydrophobicity.
- Relationship between particle size and duration of sonication.
- Optimization studies are required to determine quantities of additives required for obtaining ADN particles.

In electrolytic decomposition of ADN as liquid monopropellant, the investigation of evolved gases would help in identifying the complex decomposition route. It can be performed by use of gas detectors, and/or passage of evolved gases from gas phase mass spectrometers. In TMS, future research will include calibration with contactless, frictionless method such as electrostatic fins. It can also include construction of TMS with other materials beside PDMS to evaluate the most suitable option. In Micro thrusters, electrodes made out of other metals or conductive graphene or polymer pastes can be tested to identify the most robust electrodes.

Chapter 7. **Bibliography**

Agarwal, J. P., 2010. *High Energy Materials.* Padstow, Cornwall: Propellants, Explosives and Pyrotechnics.

Agrawal, A., 2005. *Surface Tension of Polymers.* [Online] Available at: http://web.mit.edu/nnf/education/wettability/summerreading-2005short.pdf [Accessed 21 2 2015].

Akhavan, J., 2004. *The Chemistry of Explosives.* Second Edition ed. Cornwall, UK: The Royal Society of Chemistry.

Andreev, A. B. et al., 2000. Stabilization of ammonium dinitramide in the liquid phase. *Russian Chemical Bulletin,* 49(12), pp. 1974-1976.

Anon., 2013 . *LDC1000.* [Online] Available at: http://www.ti.com/lit/ml/slyw022/slyw022.pdf [Accessed 26 11 2015].

Appelgren, P., Larsson, A., Wingborg, N. & Elfsberg, M., 2005. *Characterization and electrical ignition of ADN-based liquid monopropellants.* s.l.:Weapons and Protection, Swedish Defence Research Agency.

Aqra, F. & Ayyad, A., 2011. Surface energies of metals in both liquid and solid states. *Applied Surface Science,* 257(15), pp. 6372-6379.

Asmatulu, R., Ceylan, M. & Nuraje, N., 2011. Study of Superhydrophobic Electrospun Nanocomposite Fibers for Energy Systems. *Langmuir Letter,* 27(2), pp. 504-507.

Atkins, P. & Paula, J. D., 2010. *Physical Chemistry.* Ninth Edition ed. New York, NY 10010: Oxford University Press.

Bayat, Y. & Zeynali, V., 2011. Preparation and Characterization of Nano-CL-20 Explosive. *Journal of Energetic Materials,* 4(29), pp. 281-291.

Blau, P. J., 2008. *Friction Science and Technology: From Concepts to Applications.* Second Edition ed. s.l.:CRC Press.

Bose, A. K. et al., 2006. Cold microwave chemistry: synthesis using pre-cooled reagents. *Tetrahedron Letters,* Volume 47, pp. 3213-3215.

Bottaro, J. C., Penwell, E. P. & Schmitt, R. J., 1997. 1,1,3,4-Tetraoxo-1,2,3-triazapropene Anion, a New Oxy Anion of Nitrogen: The Dinitramide Anion and Its Salts. *American Chemical Society,* 119(40), pp. 9405-9410.

Bottaro, J. C., Schmitt, R. J., Penwell, P. E. & Ross, D. S., 1993. *Method of forming Dinitramide salts.* United States of America, Patent No. 5198204.

Brown, H. C. & Wirkkala, R. A., 1966. Trifluoroacetic Acid as a Medium for Electrophilic Substitution Reactions. Rates and Isomer Distribution for the Bromination, Nitration, and Mercuration of Benzene and Toulene in Trifluoroacetic Acid. *Journal of the American Chemical Society,* 5 april, 88(7), pp. 1447-1451.

Cannizzo, L. et al., 1998. Utilization of ammonium dinitramide (ADN) in Propellant formulations. *Thiokol Corporation.*

Chang, K.-C.et al., 2014. Room-temperature cured hydrophobic epoxy/graphene composites as corrosion inhibitorfor cold-rolled steel. *Carbon,* Volume 66, pp. 144-153.

Cheah, K. H. & Jit Kai, C., 2013. Fabrication of Embedded Microstructures Via Lamination of Thick Gel-Casted Ceramic Layers. *International Journal of Applied Ceramic Technology,* pp. 2-11.

Cheah, K. H. & Low, K.-S., 2015. Fabrication and performance evaluation of a high temperature co-fired ceramic vaporizing liquid microthruster. *Journal of Micromechanics and Microengineering,* 25(1).

Chen, S.-J. & Pan, S.-S., 2011. A force measurement system based on an electrostatic sensing and actuating technique for calibrating force in a micronewton range with a resolution of nanonewton scale. *Measurement Science and Technology,* 22(4).

Choudary, B. M. et al., 2004. *Process for the preration of dinitramidic acid and salts thereof.* USA, Patent No. US 6,787,119 B2.

Ciaramitaro, D. A. & Reed, R., 2000. *ADN Stabilizers.* s.l. Patent No. US 6113712.

Cui, J. et al., 2010. Study on the crystal structure and Hygroscopicity of Ammonium Dinitramide. *Journal of Chemical and Engineering Data,* 55(9), pp. 3229-3234.

Dean, J. A., 1998. *Lange's Handbook of Chemistry.* Fifteenth Edition ed. s.l.:McGRAW-HILL, INC.

Easly, C. J. et al., 2009. Rapid and inexpensive fabrication of polymeric microfluidic devices via toner transfer masking. *Lab on a Chip,* 9(8), pp. 1119-1127.

Fuhr, F. D.-I. I., 2008. *Crystallization of the energetic oxidizer salt ammonium dinitramide: Theoretical and experimental considerations.,* Halle-Wittenberg, Germany: s.n.

Galpaya, D. et al., 2012. Recent Advances in Fabrication and Characterization of Graphene-Polymer Nanocomposites. *Graphene,* 1(2), pp. 30-49.

Gettwert, V., Bohn, M. A., Fischer, S. & Weiser, V., 2015. *Performance of ADN/GAP Propellants Compared to Al/AP/HTPB.* Rome, Italy, s.n., pp. 1-10.

Golofit, T., Maksimowski, P. & Biernacki, A., 2010. Optimization of Potassium Dinitramide Preparation. *Propellants, Explosives, Pyrotechnics,* Volume 35, p. 261–265.

Golofit, T., Maksimowski, P. & Biernacki, A., 2010. Optimization of Potassium Dinitramide Preparation. *Propellants, Explosives, Pyrotechnics,* Volume 35, pp. 1-5.

Gronland, T.-A.et al., 2006. *Reactor for ammonium dinitramide-based liquid monopropellants and process for the decomposition.* USA, Patent No. 7137244.

Hahma, A., Edvinsson, H. & Ostmark, H., 2010. The Properties of Ammonium Dinitramide(ADN): part 2: Melt Casting. *Journal of Energetic Materials,* Volume 28, pp. 114-138.

Heintz, T. et al., 2009. Ammonium Dinitramide (ADN)- Prilling, Coating, and Characterization. *Propellants Explosives and Pyrotech,* march, Issue 34, pp. 231-238.

Highsmith, T. K., Mcleod, C. S., Wardle, R. S. & Hendrickson, R., 2000. *Thermally-stabilized priiled ammonium dinitramide particles, and process for making the same.* s.l. Patent No. us 6136115.

Hughes, E. B. & Oldfield, S., 2004. *Traceable calibration of the 2-axis thrust vector in the millinewton range.* Cagliari, Sardinia, Italy, European Space Agency.

Huh, J. & Sejin, K., 2014. Desing, fabrication and thrust measurement of a micro liquid monopropellant thruster. *Journal of Micromechanics and Microengineering,* 24(10).

ICI Americas Inc, 1980. *The HLB System: A time-saving guide to emulsifier selection,* Wilmington, Delaware: ICI Americas Inc.

Janson, S. W., Helvajian, H., Hansen, W. W. & Lodmell, J., 1999. *Microthrusters for nanosatellites.* Pasadena, CA, Aerospace Corporation,.

Jensen, B. D. & Howell, L. L., 2002. The modeling of cross-axis flexural pivots. *Mechanism and Machine Theory,* 37(5), pp. 461-476.

Jensen, T. L. et al., 2010. Isocyanate-Free and Dual Curing of Smokeless Composite Rocket Propellants. *Propellants, Explosives, Pyrotechnics,* Issue 35, pp. 1-12.

Jones, D. E. et al., 2005. Characterization of ADN and ADN-Based Propellants. *Propellants, Explosives, Pyrotechnics,* 30(2), pp. 140-147.

Jones, E. D. et al., 2005. Characterization of ADN and ADN-Based Propellants. *Propellants, Explosives, Pyrotechnics,* 2(30).

Kappenstein, C., Batonneau, Y. & Wingborg, N., 2004. *Non Toxic Ionic Liquids as Hydrazine Substitutes. Comparison of Physico-Chemical Properties and Evaluation of ADN and HAN.* Cagliari, Sardinia, Italy, NASA Astrophysics Data System.

Ke, Q. et al., 2011. Fabrication of mechanically robust superhydrophobic surface based on silica micro-nanoparticles and polydimethylsiloxane. *Surface & Coatings Technology,* Volume 205, pp. 4910-4914.

Kim, J.-W.et al., 2011. Evaporation Crystallization of RDX by Ultrasonic Spray. *Industrial & Engineering Chemistry Research,* 50(21), pp. 12186-12193.

Kim, K.-W.et al., 1999. Electrolysis of nitric acid by using a glassy carbon fiber column electrode system. *Journal of Radioanalytical and Nuclear Chemistry,* 245(2), pp. 301-308.

Kohga, M., 2009. From Cross-linking to Plasticization – Characterization of Glycerin/HTPB Blends. *Propellants Explosives Pyrotech,* Volume 34, p. 436– 443.

Koh, K. S., Chin, J. & Chik, F. W. K., 2013. Role of electrodes in ambient electrolytic decomposition of hydroxlammonium nitrate (HAN) solutions. *Propulsion and Power Research,* 3(2), pp. 194-200.

Koizumi, H., Komurasaki, K. & Arakawa, Y., 2004. Development of thrust stand for low impulse measurement from microthrusters. *Review of scientific instruments,* 75(10), pp. 3185-3190.

Krevelen, D. V. & Nijenhuis, K. T., 2009. *Properties of polymers.* 4 ed. Amsterdam: Elsevier.

Kundu, P., Bhattacharyya, T. K. & Das, S., 2012. Design, fabrication and performance evaluation of a vaporizing liquid microthruster. *Journal of micromechanics and microengineering,* Volume 22.

Kuppa, R. & Moholkar, V. S., 2010. Physical features of ultrasound-enhanced heterogeneous permanganate oxidation. *Ultrasonics Sonochemistry,* Volume 17, pp. 123-131.

Landsem, E. et al., 2010. Mecahnical Properties of Smokeless Composite Rocket Propellants Based in Prilled Ammonium Dinitramide. *Propellants, Explosives, Pyrotechnics,* Issue 35.

Landsem, E. et al., 2012. Mechanical Properties of Smokeless Composite Rocket Propellants Based on Prilled Ammonium Dinitramide. *Propellants Explos. Pyrotech,* 37(6), p. 691–698.

Langlet, A., Ostmark, H. & Wingborg, N., 1999. *Method of preparing dinitramidic aicd and salts thereof.* United States of America, Patent No. 5976483.

Larson, A. & Wingborg, n., 2011. Green Propellants Based on Ammonium Dinitramide (ADN). In: J. Hall, ed. *Advances in Spacecraft Technologies.* Slavka Krautzeka: FOI-Swedish defence research Agency, pp. 139-156.

Larson, A., Wingborg, N., Elfsberg, M. & Appelgren, P., 2005. *Electrical ignition of new environmental-friednly proprellants for rockets and spacecrafts.* Monterey, CA, IEEE, pp. 497 - 500.

Larsson, A., Appelgren, P., Wingborg, N. & Elfsberg, M., 2005. *Characterization and electrical ignition of ADN-based liquid monopropellants.* s.l.:Weapons and Protection, Swedish Defence Research Agency.

Lidstrom, P., Tierney, J., Wathey, B. & Westman, J., 2001. Microwave assisted organic synthesis-a review. *Tetrahedron,* 57(589), pp. 9225-9283.

Liu, J., 2014. *Liquid Explosives.* 1st ed. Beijing, China: Springer-Verlag GmbH Berlin Heidelberg.

Lobanova, A. A., II'yasov, S. G., Popov, N. I. & Sataev, R. R., 2002. Chemistry of Urea Nitro Derivatives: II. Synthesis of Nitramide from N,N'-Dinitreurea. New Reactions of Nitramide. *Russian Journal of Organic Chemistry,* 38(1), pp. 1-6.

Lobanova, A. A., Il'yasov, G. S. & Sakovich, V. G., 2010. Nitramide. *Russian chemical Reviews,* 79(9), pp. 819-833.

Luechinger, N. A., Athanassiou, E. K. & Strak, W. J., 2008. Graphene-stabilized copper nanoparticles as an air-stable substitute for silver andgold in low-cost ink-jet printable electronics. *Nanotechnology,* 19(44), p. 445201.

Luk'yanov, O. A., Gorelik, V. P. & Tartakovskii, V. A., 1994. Dinitramide and its salts*, 1. Synthesis of dinitramide salts by decyanoethylation of N,N-dinitro-β-aminopropionitrile. *Russian Chemical Bulletin,* 43(1), pp. 89-92.

Luk'yanov, O. A. et al., 1996. Dinitramide and its salts 10.*Synthesis of dinitramide salts from N,N,-dinitro derevatives of organic amides. *Russian Chemical Bulletin,* april, 45(4), pp. 863-868.

Luk'yanov, O. A. & Tartakovsky, V. A., 2000. Synthesis and Characterization of Dinitramidic Acid and Its Salts. In: T. B. B. W. R. P. Z. Vigor Yang, ed. *Solid Propellant Chemistry, Combustion, and Motor Interior Ballistics.* s.l.:American Institute of Aeronautics and Astronautics, pp. 207-219.

Malani, R. S., Moholkar, V. S. & Choudhury, H. A., 2013. Acid catalyzed biodiesel synthesis from Jatropha oil: Mechanistic aspectsof ultrasonic intensification. *Chemical Engineering Journal,* Volume 231, pp. 262-272.

Malesa, M., Skupinski, W. & Jamroz, M., 1999. Separation of Ammonium Dinitramide from Reaction Mixture. *Propellants, Explosives, Pyrotechnics,* Issue 24, pp. 83-89.

Matsunnaga, H., Habu, H. & Atsumi, M., 2012. Thermal behavior of new oxidizer ammonium dinitramide. *Journal of Thermal Analysis and Calorimetry,* 111(2), pp. 1183-1188.

Mireles, B., 2016. *Delocalization of Electrons.* [Online] Available at: http://chemwiki.ucdavis.edu/Core/Theoretical_Chemistry/Chemical_Bonding/Valence_Bond_Theory/Resonance/Delocalization_of_Electrons
[Accessed 9 7 2016].

Nazeri, G. H., Mastour, R., Fayaznia, M. & Keyghobadi, P., 2008. Synthesis of Ammonium Dinitramide by Nitration of Potassium and Ammonium Sulfamate. The Effect of Sulfamate Conterion on ADN Purity. *Iran. J. Chem. Chem. Eng,* 27(1), pp. 85-89.

Neff, K., King, P., Anflo, K. & Mollerberg, R., 2009. *High performance green propellant for satellite applications..* Denver, Colorado, AIAA, pp. 2-5.

Nguyen, D. D., Tai, N.-H., Lee, S.-B. & Kuo, W.-S., 2012. Superhydrophobic and superoleophilic properties of graphene-based sponges fabricated using a facile dip coating method. *Energy & Environmental Science,* Issue 7, pp. 7908-7912.

Olah, G. A., Malhotra, R. & Narang, S. C., 1988. Reagents and Methods of Aromatic Nitration. In: *Nitration Methods and Mechanisms.* s.l.:Wiley-Interscience, pp. 9-102.

Olah, G. A., Malhotra, R. & Narang, S. C., 1989. *Nitration Methods and Mechanisms.* s.l.:WILEY-VCH.

Olah, G. A., Narang, S. C., Olah, A. J. & Lammertsma, K., 1982. Recent aspects of nitration: New Preparative methods and mechanistic studies (A Review). Volume 79, pp. 4487-4494.

Olah, G. A. & Squire, D. R. eds., 1991. Methods for preparing Energetic Nitrocompounds: Nitration with Superacids systems, Nitronium Salts, and Related Complexes. In: *Chemistry of Energetic Materials.* s.l.:s.n.

Oliveira, J. I. S. d. et al., 2012. Assessment of the synthesis routes conditions for obtaining ammonium dinitramide by the FT-IR. *The Journal of Aerospace Technology and Management,* 04(1), pp. 269-278.

Orieux, S., Rossi, C. & Esteve, D., 2002. Thrust stand for ground tests of solid propellant microthrusters. *Review of Scientifc Instruments,* 73(7), pp. 2694-2698.

Ostmark, H. et al., 2000. The properties of ammonium dinitramide (ADN): Part 1, basic properties and spectroscopic data. *Journal of Energetic Materials,* 18(2-3), pp. 123-138.

Ostmark, H. et al., 2002. *Detonation Properties and Reaction Rate Modeling of Melt Cast Ammonium Dinitramide (ADN).* s.l., s.n., pp. 775-780.

Oxley, J. C. et al., 1997. Thermal Decomposition Studies on Ammonium Dinitramide (ADN) and 15N and 2H Isotopomers. *The Journal of Physical Chemistry A,* Volume 101, pp. 5646-5652.

Packan, D., Bonnet, J. & Rocca, S., 2007. *Thrust Measurements with the ONERA Micronewton Balance.* Florence, Italy , s.n.

Pang, W.-q.et al., 2013. Effect of Ammonium Dinitramide (ADN) on the Characteristics of Hydroxyl Terminated Polybutadiene (HTPB) Based Composite Solid Propellant. *Journal of Chemical Science and Technology,* 2(2), pp. 53-60.

Qadir, L. R. et al., 2003. Sonochemically induced decomposition of energetic materials in aqueous media. *Chemosphere,* March, 50(8), pp. 1107-1114.

Ramaswamy, A., 2000. Energetic-material combustion experiments on propellant formulations containing prilled ammonium dinitramide. *Combustion, Explosion, and Shock Waves,* 36(1), pp. 119-124.

Riego, J. m. et al., 1996. Sulfuric Acid on Silica-gel: an Inexpensive Catalyst for Aromatic Nitration. *Tetrahedron Letters,* 37(4), pp. 513-516.

Roberts, E., 1951. *Process of the Production of Guandine and Derivatives Thereof.* s.l. Patent No. 2884437.

Ross, D. S., Kuhlmann, K. F. & Malhotra, R., 1983. Studies in Aromatic Nitration. 2. N-NMR study of the Nitric ACid/Nitronium Ion Equilbrium in Aqueous Sulfuric Acd. *Journal of the American Chemical Society,* 105(13), pp. 4299-4302.

Rossi, C., Larangot, B., Lagrange, D. & Chaalane, A., 2005. Final characterization of MEMS-based pyrotechnical microthruster. *Sensors and Actuators A: Physical,* 121(2), pp. 508-514.

Rossi, C. et al., 2006. Solid Propellant Microthrusters on Silicon: Design, Modeling, Fabrication, and Testing. *Journal of Microelectromechanical Systems,* DECEMBER, 15(6), pp. 1805-1815.

Ru, C. et al., 2014. Design and Fabrication of MEMS-Based Solid Propellant Microthrusters Array. *Applied Mechanics and Materials,* Volume 490-491, pp. 1042-1046.

Russel, T. P., Block, S., Piermarini, G. J. & Miller, P. J., 1996. Pressure, Temperature Reaction Phase Diagram for Ammonium Dinitramide. *Journal of Physical Chemistry,* 100(8), pp. 3248-3251.

Sabourin, J. L. et al., 2009. Functionalized Graphene Sheet Colloids for Enhanced Fuel/Propellant Combustion. *ACS Nano,* 3(12), p. 3945–3954.

Saikia, A., Sivabalan, R., Gore, G. M. & Sikder, A. K., 2012. Microwave-Assisted Quick Synthesis of Some Potential high Explosives. *Propellants,Explosives, Pyrotechnics,* Issue 37, pp. 540-543.

Santacesaria, E., Gelosa, D. & Carra, S., 1977. Basic Behavior of Alumina in the Presence of Strong Acids. *Industrial & Engineering Chemistry Product Research and Development,* 16(1), pp. 45-47.

Santhosh, G., Venkatachalam, S., Kanakavel, M. & Ninan, K. N., 2002. Study on the formation of dinitramide using mixed acid nitrating agents. *Indian Journal of Chemical Technology,* Volume 9, pp. 223-226.

Santhosh, G., Venkatachalam, S. & Ninan, K. N., 2010. *Synthesis and evaluation of energetic materials,* Cochin, Kottayam: Beehive Digital Concepts.

Santhosh, G., Venkatachalam, S. & Ninan, K. N., 2010. *Synthesis and evaluation of energetic materials,* cochin, Kottayam: beehive digital concepts.

Santosh, G. et al., 2003. Adsorption of ammonium dinitramide (ADN) from aqueous solutions 1.Adsorption on powdered activated charcoal. *Journal of Hazardous Materials,* Volume B98, pp. 117-126.

Sarkar, D. K. & Saleema, N., 2010. One-step fabrication process of superhydrophobic green coatings. *Surface & Coating Technology,* Volume 204, pp. 2483-2486.

Sarvari, M. H., Tavakolian, M. & Ashenagar, S., 2010. Nitration of aromatic compounds using alumina sulfuric acid (asa) as a novel heterogeneous system and mg(no2)2.6h2o as nitrating agent in water. *Iranian Journal of Science & Technology, Tansaction A,* 34(A3), pp. 215-225.

Schmitt, R. J., Bottaro, J. C., Penwell, P. E. & Bomberger, C., 1994. *Process for forming ammonium dinitramide salt by reaction between ammonia and a nitronium containing compound.* s.l. Patent No. 5316749.

Schmitt, R. J., Bottaro, J. C., Penwell, P. E. & Bomberger, C., 1995. *Process for forming a dinitramide salt or acid by reaction of a salt or free acid of an n(alkoxycarbonyl)n-nitroamide with a nitronium-containing compound followed by reaction of the intermediate product respectively with a base or alcohol.* s.l. Patent No. 5415852.

Shlyapochnikov, V. A. et al., 1994. Dinitramide and its salts 4.* Molecular structure of dinitramide. *Russian Chemical bulletin,* september, 43(9), pp. 1522-1525.

Shlyapochnikov, V. A. et al., 1994. Dinitramide and its salts, 4. Molecular structure of dinitramide. *Russian Chemical Bulletin,* 43(9), pp. 1522-1525.

Smith, D. K. & Korgel, B. A., 2008. The importance of the CTAB surfactant on the colloidal seed-mediated synthesis of gold nanorods.. *Langmuir,* 24(3), p. 644–649.

Spotar, S. et al., 2015. A revisit to the separation of a binary mixture of ethanol–water using ultrasonic distillation as a separation process. *Chemical Engineering and Processing: Process Intensification,* Volume 87, pp. 45-50.

Stern, A. G. et al., 1998. *Process for preparing Ammonium Dinitratmide.* s.l. Patent No. US005714714A.

Suzuki, S. et al., 1997. *Synthetic method for forming Ammonium Diniramide (ADN).* United States of America, Patent No. 5659080.

Svetovoy, V. B. & Palasantzas, G., 2015. Influence of surface roughness on dispersion forces. *Advances in Colloid and Interface Science,* Volume 216, pp. 1-19.

Szilagyi, I., Konigsberger, E. & May, P. M., 2009. Spectroscopic characterisation of weak interactions in acidic titanyl sulfate-iron (ii) sulfate solutions. *Dalton Trasactions,* Issue 39, pp. 7717-7724.

Takahashi, K., 2006. *Contemporary technology and application of MEMS rocket.* Toulouse, France, American Society of Mechanical Engineers.

Take, T., Tsurutani, K. & Umeda, M., 2007. Hydrogen production by methanol–water solution electrolysis. Volume 164, pp. 9-16.

Tedder, J. M., 1955. The use of tricluoroacetic anhydride and related compounds in organic synthesis. *Chemical Reviews,* 55(5), pp. 787-827.

Teipel, U., 1999. Production of Particles of Explosives. *Propellants, Explosives, Pyrotechnics,* Volume 24, pp. 134-139.

Teipel, U., 1999. Production Particles of Explosives. *Propellants, Explosives Pyrotechnics,* Issue 24, pp. 134-139.

Teipel, U. & Heintz, T., 2005. Surface Energy and Crystallization Phenomena of Ammonium Dinitramide. *Propellants,Explosives,Pyrotechnics,* 30(6), pp. 404-411.

Teipel, U., Heintz, T. & Krause, H. H., 2000. Crystallization of Spherical Ammonium Dinitramide (ADN) particles. *Propellants, Explosives, Pyrotechnics,* Volume 25, pp. 81-85.

Texas Instruments, 2015. *LDC1000 Inductance-to-Digital Converter.* [Online] Available at: http://www.ti.com/lit/ml/slyb212/slyb212.pdf [Accessed 25 11 2015].

Thakre, P., Duan, Y. & Vigor, Y., 2014. Modeling of ammonium dinitramide (ADN) monopropellant combustion with coupled condensed and gas phase kinetics. *Combustion and Flame,* 161(1), pp. 347-362.

Tompa, A. S., 2000. Thermal analysis of ammonium dinitramide (ADN). *Thermochimica Acta,* Volume 357, pp. 177-193.

Urbanski, T., 1964. *Chemistry and Technology of Explosives.* Warszawa: PWN-POLISH SCIENTIFIC PUBLISHERS.

Vadukumpully, S., Paul, J. & Valiaveettil, S., 2009. Cationic surfactant mediated exfoliation of graphite into graphene flakes. *Carbon,* 47(14), pp. 3288-3294.

Venkatachalam, S., santosh, G. & Ninan Ninan, K., 2004. An overview on the synthetic routes and properties of Ammonium Dinitramide (ADN) and other dinitramide salts. *Propellents, Explosives, Pyrotechnics,* 3(29), pp. 178-187.

Viste, F., Cooper, M. & Botte, G. G., 2005. On the use of ammonia electrolysis for hydrogen production. *Journal of Power Sources,* 142(1), pp. 18-26.

Vorder, C. & Skifs, H., 2011. *Method of producing salts of Dinitramic Acid.* s.l. Patent No. US7981393 B2.

Vyazovkin, S. & Wight, C. A., 1997. Ammonium Dinitramide: Kinetics and Mechanism of Thermal Decomposition. *J. Phys. Chem. A,* 101(31), pp. 7217-7221.

Vyazovkin, S. & Wight, C. A., 1997. Ammonium Dinitramide: Kinetics and Mechanism of Thermal Decomposition. *J. Phys. Chem.,* Volume 101, pp. 5653-5658.

Wang, S., Zhang, Y., Abidi, N. & Cabrales, L., 2009. Wettabiity and Surface Free Energy of Graphene Films. *Langmuir,* 25(18), p. 11078–11081.

Wexler, A., 2003. Practical Laboratory Data. In: D. R. Lide, ed. *CRC Handbook of Chemistry and Physics.* New York: CRC press, p. 25.

Wingborg, N., 2006. Ammonium Dinitramide-Water: Interaction and Properties. *Journal of Chemical and Engineering Data,* 51(5), pp. 1582-1586.

Wingborg, N., 2011. *ADN Propellant Development.* Saint Petersburg, EUCASS association.

Wingborg, N., Eldsater, C. & Skifs, H., 2004. *Formulation and characterization of ADN-based liquid monopropellants.* Cagliari, Sardinia, Italy, European Space AGency.

Wingborg, N., Johansson, M. & Bodin, L., 2006. *Initial development of a laboratory rocket thruster for ADN-based liquid monopropellants,* Tumba: FOI-Swedish Defence Research Agency.

Wu, M.-H. & Lin, P.-S., 2010. Design, fabrication and characterization of a low-temperature co-fired ceramic gaseous bi-propellant microthruster. *Journal of Micromechanics and Microengineering,* 20(8).

Wu, M.-H. & Yetter, R. A., 2009. A novel electrolytic ignition monopropellant microthruster based on low temperature co-fired ceramic tape technology. *Lab Chip,* 9(7), pp. 910-916.

Xiao, C.-X.et al., 2006. NO2-catalyzed deep oxidation of methanol: Experimental and theoretical studies. *Journal of Molecular Catalysis A:Chemical,* 252(1-2), pp. 202-211.

Yan, A. H., Appel, B. C. & Gedrimas, J. G., 2009. *MilliNewton Thrust Stand Calibration Using Electrostatic Fins.* Orlando, Florida, USA, American Institute of Aeronautics and Astronautics.

Yang, R., Thakre, P. & Yang, V., 2005. Thermal Decomposition and Combustion of Ammonium Dinitramide (review). *Combusiton, Explosion, and Shock Waves,* 41(6), pp. 657-679.

Yetter, R. A. et al., 2007. Combustion issues and approaches for chemical microthrusters. *International Journal of Energetic Materials and Chemical Propulsion,* 6(4), pp. 393-424.

Zhang, K. L., Chou, S. K., Ang, S. S. & Tang, X. S., 2005. A MEMS-based solid propellant microthruster with Au/Ti igniter. *Sensors and Actuators,* A(122), pp. 113-123.

APPENDIX:

8.1 Appendix for Chapter 3:

An example calculation is shown in Table 0-1 below.

Table 0-1 Example calculation of yield calculation for near-zero temperature(method 2) experiments.

Sample name:	D-11A	Remarks
ε	35.91	$\boldsymbol{\varepsilon} = 5640\frac{\mathrm{L}}{\mathrm{mole.\,cm}} * \frac{1\mathrm{mole}}{145\mathrm{g}}$ $\boldsymbol{\varepsilon} = \frac{35.91\mathrm{L}}{\mathrm{g}*\mathrm{cm}}$
Mol wt.	145	Molecular weight of KDN
Sample conc. (g/l)	0.0448	Solution prepared using final product of experiment in water
A	0.0277	Absorbency % obtained by UV spectroscopy
Conc. Obtained by UV (g/l)	0.000771	$\mathrm{c} = \frac{\mathrm{A}}{\varepsilon \mathrm{l}} = \frac{0.0277}{35.91*1} = 7.7\mathrm{e}-4$
Purity	1.72 wt. %	$\mathrm{Purity} = \frac{\mathrm{Conc.\,Obtained\ by\ UV}}{\mathrm{Sample\ conc}}$ $\mathrm{Purity} = \left(\frac{0.000771}{0.0448}\right) * 100 = 1.72\%$
Sample weight	7.72g	From final product of experiment
Substrate weight	5g	Weight of KS used in experiment
KDN quantity	0.1328g	$KDN\ quantity = \frac{Purity * sample\ weight}{100}$

		$KDN\ quantity = \frac{1.72 * 7.72}{100}$ $= 0.1328g$
Reaction yield%	2.65%	$yield = \frac{KDN\ quantity}{substrate\ weight} * 100$ $yield = \frac{0.1328}{5} * 100$ =2.65%

Table 0-2 Sample Calculation of yield for ultra low temeprature experiment (method 1)

Sample name:	CA	Remarks
ε	35.91	$\boldsymbol{\varepsilon} = 5640 \frac{\mathrm{L}}{\mathrm{mole.cm}} * \frac{1\mathrm{mole}}{145\mathrm{g}}$ $\boldsymbol{\varepsilon} = \frac{35.91\mathrm{L}}{\mathrm{g*cm}}$
Mol wt.	145	Molecular weight of KDN
Sample conc. (g/l)	0.010495	Solution prepared using final product of experiment in water
A	0.2859	Absorbency % obtained by UV spectroscopy
Conc. Obtained by UV (g/l)	0.007961	$\mathrm{c} = \frac{\mathrm{A}}{\varepsilon \mathrm{l}} = \frac{0.2859}{35.91*1} = 0.007961$
Purity	75.85 wt. %	$\mathrm{Purity} = \frac{\mathrm{Conc.\ Obtained\ by\ UV}}{\mathrm{Sample\ conc}}$ $\mathrm{Purity} = \left(\frac{0.007961}{0.010495}\right) * 100$ $= 75.85\%$
Sample weight	9g	From final product of experiment
Substrate weight	20g	Weight of KS used in experiment
KDN quantity	6.827g	$KDN\ quantity = \frac{Purity * sample\ weight}{100}$

		$KDN\ quantity = \frac{75.85 * 9}{100}$ $= 6.827g$
Reaction yield%	34.13%	$yield = \frac{KDN\ quantity}{substrate\ weight} * 100$ $yield = \frac{6.827}{20} * 100$ =34.13%

Table 0-3 Purity and reaction yield calculation by UV spectroscopy of ADN obtained by Ultralow temperature experiment (method 1). KDN obtained by the experiment was converted to ADN.

Sample name:	Dt-1	Remarks
ε	41.99	$\boldsymbol{\varepsilon} = 5640 \frac{\mathrm{L}}{\mathrm{mole.\,cm}} * \frac{1\mathrm{mole}}{124\mathrm{g}}$ $\boldsymbol{\varepsilon} = \frac{41.99\mathrm{L}}{\mathrm{g*cm}}$
Mol wt.	124	Molecular weight of ADN
Sample conc. (g/l)	0.01	Solution prepared using final product of experiment in water
A	0.4053	Absorbency % obtained by UV spectroscopy
Conc. Obtained by UV (g/l)	0.00965	$\mathrm{c} = \frac{\mathrm{A}}{\varepsilon \mathrm{l}} = \frac{0.4053}{35.91*1} = 0.00965$
Purity	96.51 wt. %	$\mathrm{Purity} = \frac{\mathrm{Conc.\,Obtained\ by\ UV}}{\mathrm{Sample\ conc}}$ $\mathrm{Purity} = \left(\frac{0.00965}{0.01}\right) * 100$ $= 96.51\%$
Sample weight	13.53g	From final product of experiment
Substrate weight	53.3g	Weight of KS used in experiment

KDN quantity	13.05g	$KDN\ quantity = \frac{Purity * sample\ weight}{100}$ $KDN\ quantity = \frac{96.5 * 13.53}{100}$ $= 13.05g$
Reaction yield%	24.5%	$yield = \frac{KDN\ quantity}{substrate\ weight} * 100$ $yield = \frac{13.05}{53.3} * 100$ =24.5%

8.2 Appendix for Chapter 5:

The example calculations and data processing perform on experimental data is given below.

8.2.1 Step 1:

The raw experimental data (Figure 0-1) from the LDC software was exported to Microsoft excel.

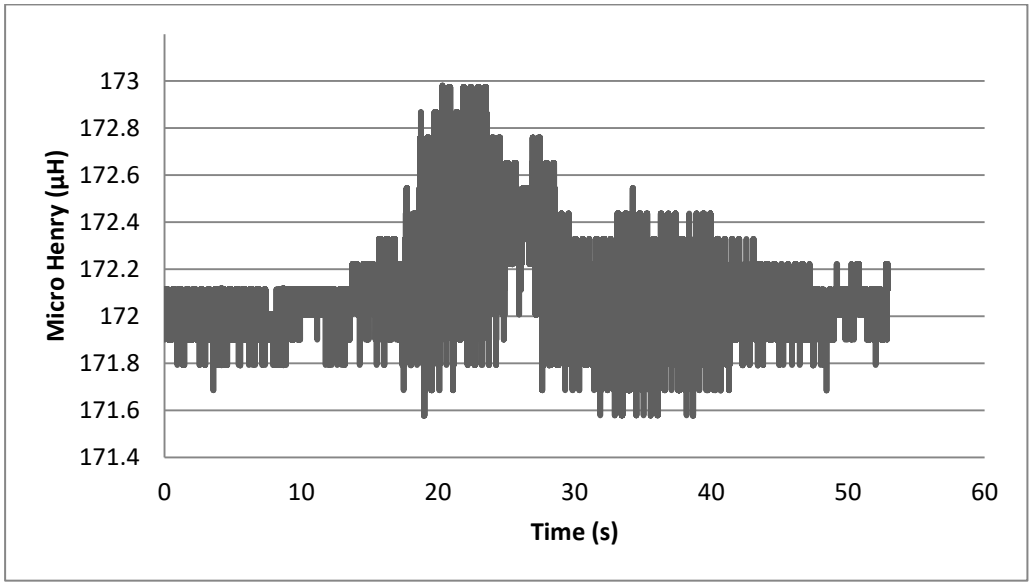

Figure 0-1 Raw experimental data at 6000Hz sampling rate for 60µl/min flowrate experiment

8.2.2 Step 2:

Now baseline correction was performed on this data shown in Figure 0-1 by subtracting 172.007µh, because it, 172.007µh, was the starting baseline value for the sensor. The graph obtain after this step is shown in Figure 0-2.

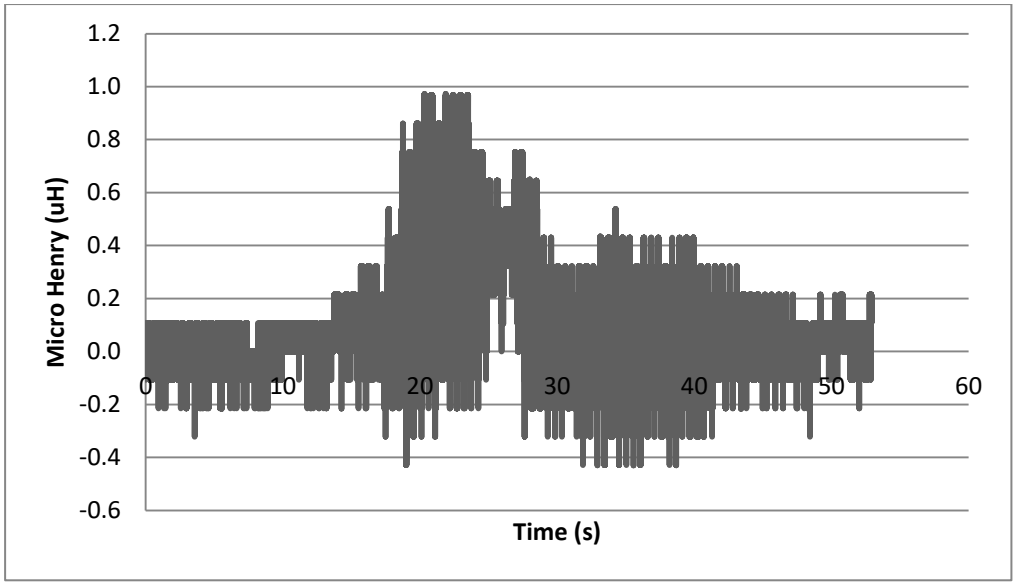

Figure 0-2 Baseline corrected data rate for 60µl/min flowrate experiment

8.2.3 Step 3:

Now, the graph values, as shown in Figure 0-2, were divided by 0.0321µh/mg to convert micro henry into milligram values. This 0337 µh/mg value was obtained from calibration. The graph obtained after this step is shown in below Figure 0-3. After converting to milligram values, the data was converted into micro newton by using conversion factor, 9.8, as shown in Figure 0-4.

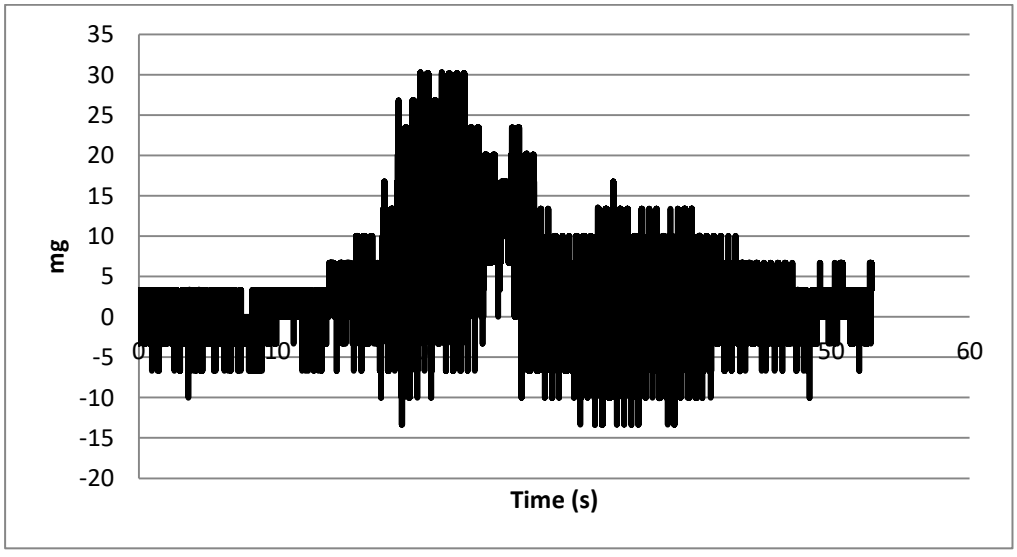

Figure 0-3 Milligram converted data rate for 60µl/min flowrate experiment

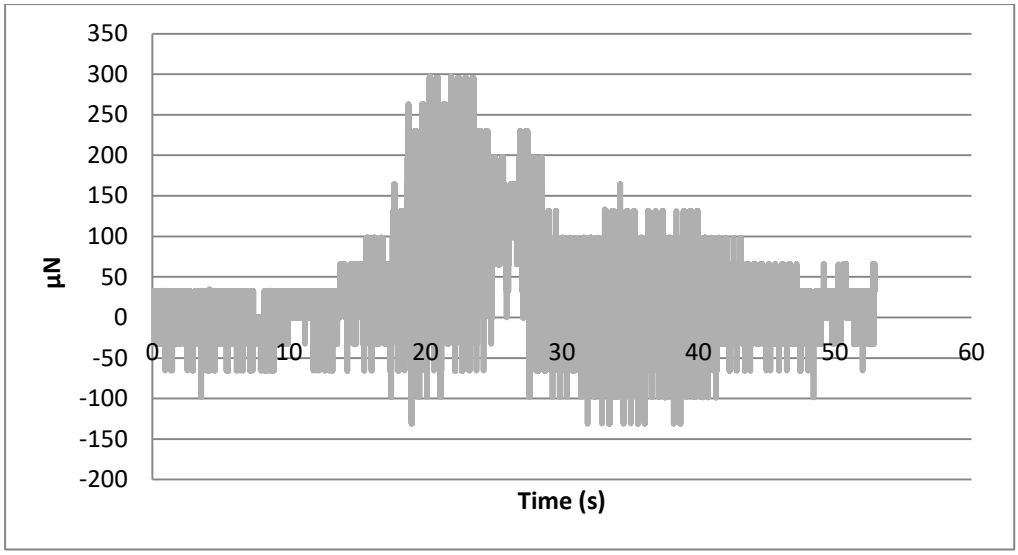

Figure 0-4 Micro newton conversion rate for 60µl/min flowrate experiment

8.2.4 Step 4:

Now, Noise reduction was performed on the data shown in Figure 0-4 to convert it into smoothed data. Out of 100, 250, 350, 450, 500 and 1000 moving point average methods, 500 moving point average gave better smoothness, and hence used for all the calculations. The comparison of 400 and 500 moving point averages is shown in Figure 0-5 and Figure 0-6 respectively.

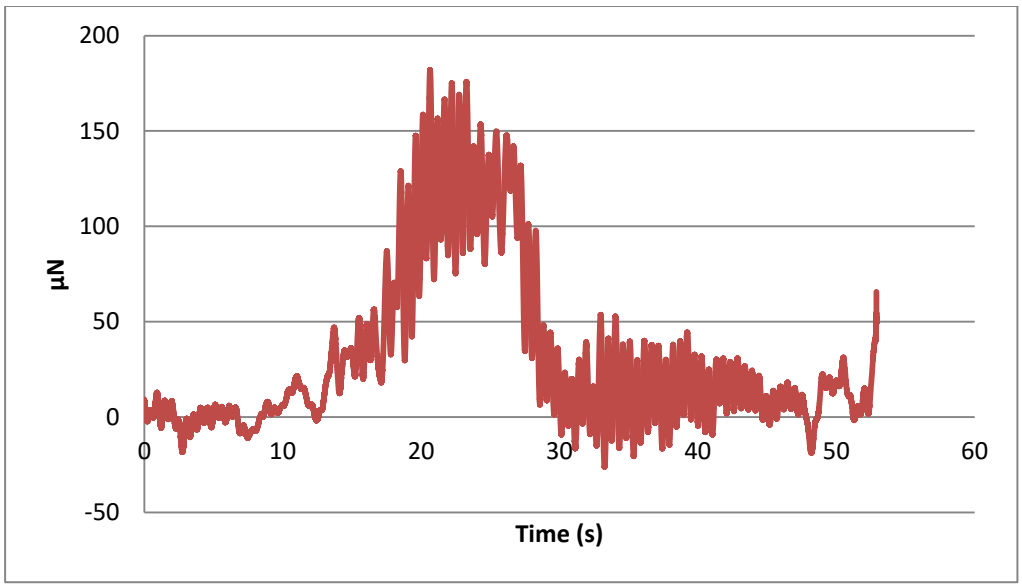

Figure 0-5 400 Moving point average

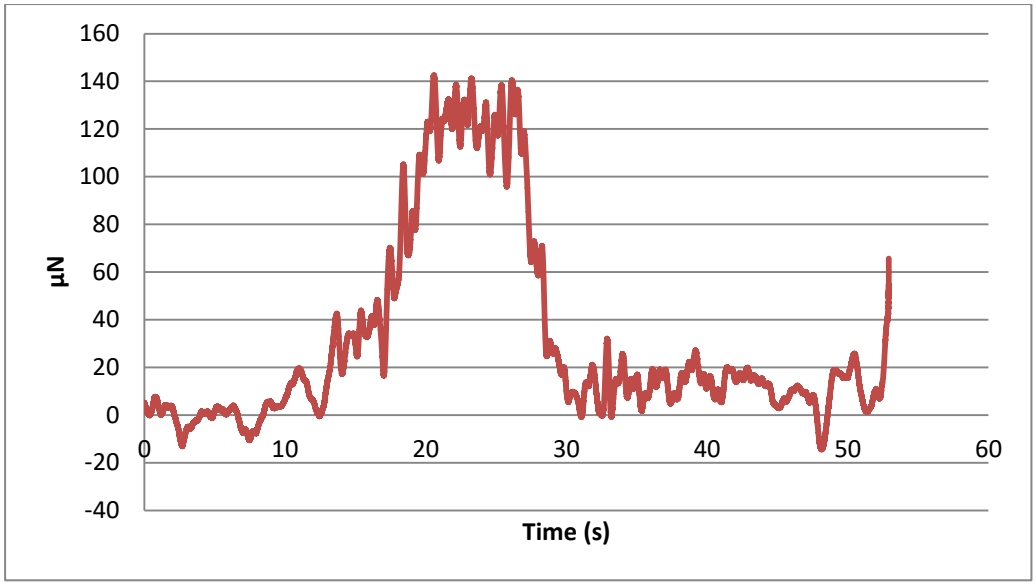

Figure 0-6 500 moving point average

8.2.5 Step 5:

Now, the area under the curve between 20s and 30s was calculated by integration by trapezoid rule in Microsoft Excel. This integration range was selected because of the smooth decomposition and thrust of the propellant in this region. The specific impulse calculation on the Figure 0-6 is shown in Table 0-4.

Table 0-4 Specific impulse calculation

Sum:	1392346	µn
Dt	0.001	S
Mg To µn	1392346	µn
Fuel Rate	60	µl/min
Fuel Rate/S	1	µl/s
Total Fuel	26.2	Mg
Density	1.31	Mg/µl
µn To N	1.392346	N

Area Under The Curve:	0.001392	Ns
Run Time	20	S
Fuel In Kg	2.62E-05	Kg
Specific Impulse	53.14299	NS/kg